Correlation of Ice Recrystallization Inhibition Activity to Hydration Parameters and Effect of the C-3 Hydroxyl Group

Jatinder Saini Singh

B.Sc. Honours Chemistry – University of Ottawa, 2018

Thesis submitted to the University of Ottawa
in partial fulfillment of the requirements for the
M.Sc. degree in Chemistry

Department of Chemistry and Biomolecular Sciences
Faculty of Science
University of Ottawa

Candidate	Supervisor
_____	_____
Jatinder Saini Singh	Robert N. Ben

Acknowledgments

I would like to first acknowledge Dr. Robert Ben for accepting me and guiding me throughout this journey. I would like to say thank you for teaching me life lessons and techniques that will direct me in the future, as well as an appreciation for the sophisticated taste of whiskey. Thank you to my thesis committee, Dr. John Pezacki and Dr. André Beauchemin. Dr. Beauchemin, thank you for your support and guidance in my seminar.

I would like to thank Ben Lab group members, both past and present: Dr. Jessica Poisson, Dr. Thomas Charlton, Dr. Madeline Adam, Julia Meyer, Anna Ampaw, Salma Alasmar-Abdou, Karishma Chopra, Leah McMunn, Marcus Diamante, Romeo Junior El Issa, Sophia Mangan, all the undergraduate students, and the Durst Lab members. I would like the thank Romeo Junior El Issa and Leah McMunn for their help with editing and proofreading this thesis, with special thanks to Leah for helping me with the intensive editing process. I would like to thank my parents for their love and support. Thank you, mom, dad, and my brother. The support you gave to me was tremendous and thank you for the home-cooked meals I bought for lunch, dad.

Summary

The use of cryoprotective agents (CPAs) in the storage of cells and tissues is essential for transfusion medicine and food storage. Currently, cryoprotectants such as glycerol and DMSO are ineffective at preventing ice recrystallization during freezing and thawing. Ice recrystallization is a significant contributor to cellular injury because ice growth can cause mechanical damage to cells. Modified CPAs that inhibit ice recrystallization are advantageous for improving cell recovery and viability following cryopreservation. Over the years, the Ben Lab has developed ice recrystallization inhibitors (IRIs) inspired by natural biological antifreezes. Further research has led to the discovery of small carbohydrate-based molecules that can be used as active IRIs.

The Ben Lab has previously shown that hydration parameters can be used to estimate IRI activity. Hydration parameters such as hydration number, hydration index, and partial molar compressibility have been found to be positively correlated to IRI activity for simple carbohydrates. However, these parameters cannot accurately account for the hydrophobic nature of functionalized carbohydrate derivatives. Therefore, a predictive hydration parameter for IRI activity must be able to describe carbohydrates that have both hydrophobic and hydrophilic regions. It is hypothesized that the partition coefficient could be used to assess the activity of functionalized carbohydrates because it provides a quantitative measure of a compound's hydrophilicity and hydrophobicity.

The first part of this thesis will look at several hydration parameters and their correlation to half-maximal inhibitory concentration (IC_{50}) values obtained from the 5-minute modified "splat-cooling" assay. These parameters have previously correlated to percent mean

grain size (%MGS) values (obtained from the 30-minute modified “splat-cooling” assay) and will act as a point of comparison for the IC_{50} activity data. In addition to the previously tested parameters, the log of the partition coefficient (logP) relationship with IRI activity will be explored. The correlations between hydration parameters and IRI activity measured using IC_{50} values are not the same as those measured with %MGS values. The logP hydration parameter displays a negative correlation with IRI activity measured using IC_{50} values in which high IRI activity is associated with low logP values.

The second part of this thesis will examine the impact of functionalization at the C-3 hydroxyl position of glucosides on IRI activity. The C-1 and C-6 hydroxyl positions have been extensively analyzed for their effects on IRI activity, but the C-3 position has been left primarily uninvestigated. C-3 functionalized compounds are synthesized and compared to their corresponding C-1 functionalized compounds. The results from the study illustrate the C-3 functionalized compounds have poor solubility compared to the C-1 compounds, which emphasizes the importance of the C-2 and C-4 positions in the hydration of carbohydrates. The range of IRI activity for the C-3 position is of interest because this position is more sensitive to functionalization than the C-1 position. Collectively, these results illustrate that logP can be used as a potential predictor of IRI activity and the importance of the C-2 and C-4 positions for hydration and solubility following investigation into modifications of the C-3 position. The C-3 position has a unique characteristic of being receptive to functionalization and is essential for the rational future design of IRIs.

Table of Contents

List of Figures

List of Tables

List of Schemes

List of Abbreviations

α	Alpha
β	Beta
1-OMG	1-*O*-Methyl-α-D-glucose
2DG	2-Deoxy-glucose
3-OMG	3-*O*-Methyl-D-glucose
AFC	Atom/fragment contribution
AFGP(s)	Antifreeze glycoprotein(s)
AFP(s)	Antifreeze protein(s)
BA(s)	Biological antifreeze(s)
$BF_3{\cdot}OEt_2$	Boron trifluoride diethyl etherate
$CDCl_3$	Deuterated Chloroform
CPA(s)	Cryoprotective agent(s)
$Cu(OTf)_2$	Copper (II) triflate
d	doublet
dd	doublet of doublets
dt	doublet of triplets
dq	doublet of quartets
ddd	doublet of doublets of doublets
ddt	doublet of doublets of triplets
DMSO	Dimethyl sulfoxide
DMSO-d_6	Deuterated Dimethyl sulfoxide
HES	Hydroxyethyl starch
I_c	Cubic ice
IC_{50}	Half-maximal inhibitory concentration
I_h	Hexagonal ice
IIF	Intracellular ice formation
IRI	Ice recrystallization inhibition
IRIs	Ice recrystallization inhibitors
LRMS	Low-resolution mass spectrometry
m	multiplet
MGS	Mean grain size
P	Partition coefficient
PBS	Phosphate-buffered saline
PMC	Partial molar compressibility
PMV	Partial molar volumes
q	quartet
QLL	Quasi-liquid layer
%SEM	Percent standard error of the mean
SMILES	Simplified molecular-input line-entry system
t	triplet
TH	Thermal hysteresis
TLC	Thin-layer chromatography

UCB	human umbilical cord blood

Chapter 1: Principles of Cryopreservation

1.1.1 Introduction to Cryopreservation

Cryopreservation is the process by which cells and tissues are stored by being cooled to subzero temperatures (-78 °C or -196 °C).[1] Scholars in the field of cryobiology study the effects of subzero temperatures on cells and tissues. Cryopreservation offers the ability to extend the storage life of cells by slowing down their biological processes.[2] Other common techniques for cell/tissue storage are hypothermic storage and vitrification.[2] Hypothermic storage involves storage at temperatures above the freezing points of the cells/tissue being preserved. Vitrification is a method for the preservation of cells/tissues in a glass-like state without the formation of ice crystals using ultra-rapid cooling rates. Cryopreservation allows for the storage of cells and tissues for an extended period.[2] The disadvantage of cryopreservation stems from the loss of cell viability due to injury from intracellular and extracellular ice growth, as well as ice recrystallization. The use of small molecule IRI can improve cell viability after cryopreservation.[3] The synthesis of IRIs to investigate and predicate IRI activity is the focus of this thesis.

1.1.2 Injury During Cryopreservation

Cellular injury can occur during freezing and thawing and has been thoroughly investigated over the years.[1] In 1972, Mazur proposed his two-factor freezing injury hypothesis,[4] which is that cellular injury during freezing occurs due to two factors: (1) at slow cooling rates, cryoinjury arises due to solution effects, and (2) at high cooling rates, cryoinjury results from intracellular ice formation (IIF).[5] The spontaneous formation of extracellular ice occurs between the temperatures of -5 and -15 °C. Water exits the cell and enables an osmotic

gradient across the cell membrane in response to ice formation. As the cell continues to cool, it can proceed down three different routes based on the cooling rate being either slow, optimal, or fast (Figure 1.1.1)[5]

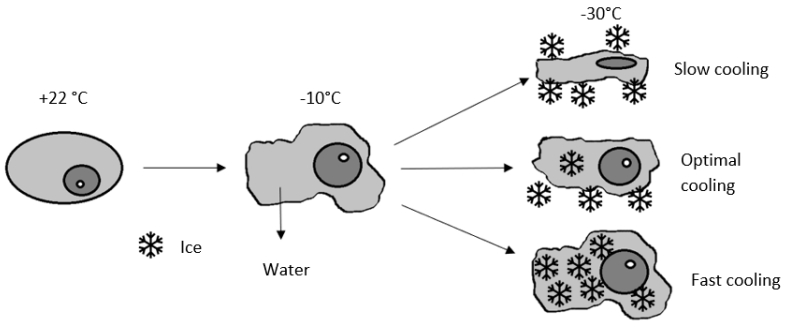

Figure 1.1 - Visual representation of the two-factor theory of freezing proposed by Dr. Mazur.[5]

If the cooling rate is slow, then the cell shrinks due to water loss as extracellular freezing occurs, causing the cell to dehydrate. Excess dehydration induces cellular injury resulting from a high extracellular ion concentration, this effect is referred to as the "solute effect."[5] In contrast, a high cooling rate produces IIFs because of the spontaneous freezing of the intracellular environment.[6] IIF can be deadly to the cell and arises due to the cooling rate being faster than the rate of water leaving the cell. This causes water to freeze while inside the cell and promotes cell damage. However, theories suggest that IIF can be innocuous and protect against further injuries during slow cooling.[6] Innocuous IIF prohibits further shrinkage of the cell because the osmotic equilibrium is controlled by the growth of ice in the cell instead of the osmotic water transport.[7]

The relationship between cooling rate and survival percentage forms an inverted U-shaped curve for different cells (Figure 1.2).[7] The optimal cooling rates can vary over a broad range depending on the membrane composition of the cell. For example, the optimal cooling rate for mouse stem cells is 1 °C/min, while for human red blood cells, it is 1,000 °C/min. Thus, different cells have unique optimal cooling rates where cell viability is at its maximum.[8]

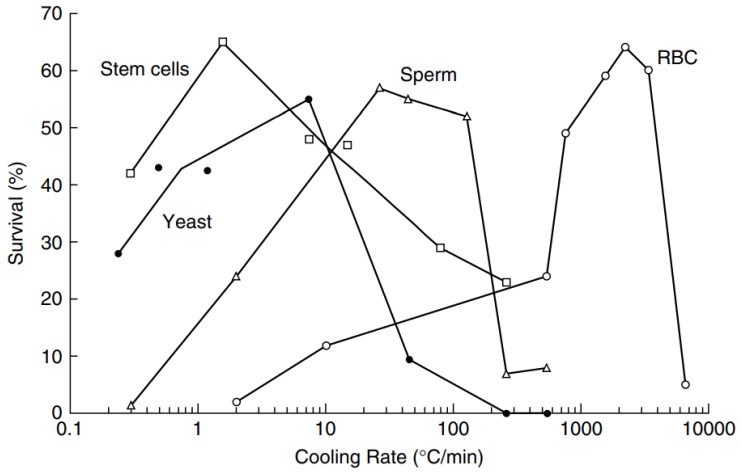

Figure 1.2 - Relationship between cooling rate and cell survival for different cell types.[7,9]

The damages associated with cryopreservation are primarily attributed to cell death during freezing and thawing.[10] Osmotic rupturing and IIF are two drivers of cell death.[5] The osmotic rupture hypothesis is that damage occurs to the cell's plasma membrane due to the solute effect and a high extracellular ion concentration. This damage allows extracellular ice to enter the cell and propagate intercellular ice formation.[11]

Ice recrystallization occurs during thawing, which leads to the growth of ice crystals that can damage the cell.[12] Studies show that cellular damage has a direct relationship with the size of ice crystals.[10] With this, recrystallization is regarded as a significant factor in cell death due to the injuries caused by ice crystal growth.[13] The use of fast or slow thawing rates impacts

survivability, alongside the freezing rate. Fast thawing rates prevent ice crystals from merging and forming the larger ice crystals that result in cell damage.[5] A slow thawing rate reduces death in slowly cooled cells because these cells are not affected by IIF. This benefit is not considered to be substantial with rapidly-cooled cells because it is presumed that the majority of cell death occurs during the cooling phase.[14] As such, there is a U-shaped curve for the optimal thawing rate, depending on the cooling rate, to explain the two factors that affect this, (1) IIF formation and (2) exposure to extracellular ions in slow cooling.[14]

1.2 Ice Recrystallization

1.2.1 Structure of Ice

To understand ice recrystallization, it is crucial to explain the structure of ice. The structure of ice at temperatures below 0 °C and atmospheric pressure is hexagonal (I_h) or metastable cubic ice (I_c).[15] At these temperatures and pressures, hexagonal ice is the most abundant.[16] Hexagonal ice consists of four axes labeled as a1, a2, a3, and c with six prism planes and two basal faces that are normalized to the c-axes, as visualized in Figure 1.3.[12] As the ice crystals grow, they will expand along the a-axes, producing hexagonal sheets of ice.[17]

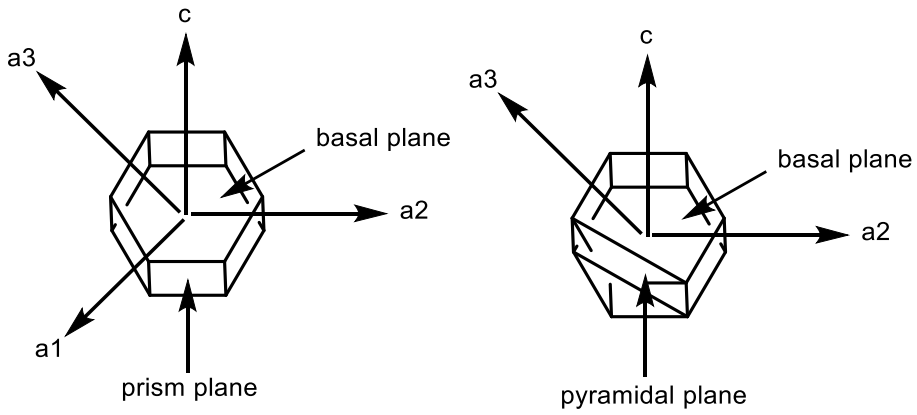

Figure 1.3 - Schematic of hexagonal ice (I_h) with axis and planes labeled.[18]

The surface of ice is covered by a thin layer of ice/water known as the quasi-liquid layer (QLL). It is theorized that the QLL is related to ice recrystallization and the process by which ice recrystallization inhibitors function.[19] Figure 1.4 shows a visualization of the QLL located between the ice lattice and bulk water. The QLL controls the surface properties of melting ice just below its freezing point, which is essential for the growth of ice crystals.[20] In 1842, Faraday first identified the existence of the QLL.[21] It was later discovered that the thickness of the QLL increases with temperature, and the thickness is typically between 10 and 15 Å. The QLL was experimentally measured as being ~9 Å at 205 K, ~10 Å at 215 K, and ~12 Å at 227 K.[19] Recent studies show that the QLL exists in two forms, round liquid-like droplets (α-QLLs) or thick liquid-like layers (β-QLLs).[20]

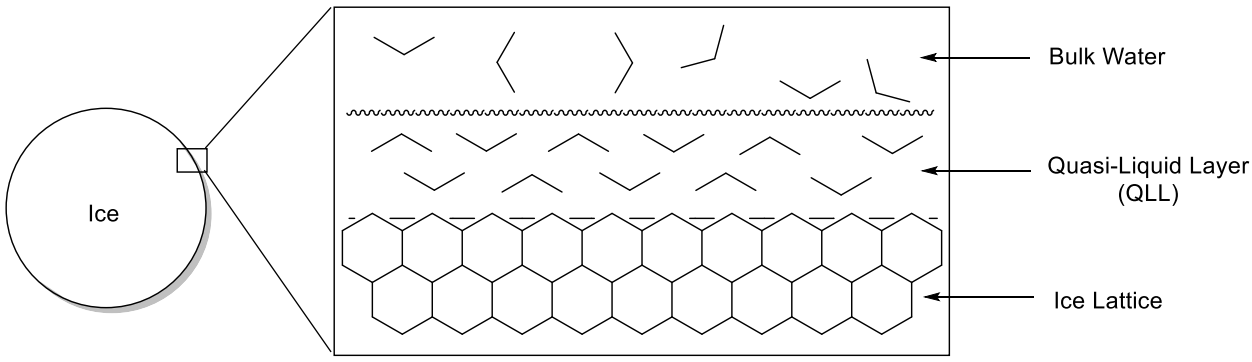

Figure 1.4 - Visualization of the liquid water-ice lattice interface of an ice crystal, with the intermediate quasi-liquid layer.[22]

1.2.2 Mechanism of Ice Recrystallization

Ice recrystallization occurs via two mechanisms, (1) grain boundary migration[23] and (2) Ostwald ripening.[24] Boundary migration causes large ice crystals to grow at the expense of smaller ones. The principle is similar to grain migration in metals.[23] The driving force instigating boundary migration is the formation of one large ice crystal, which will lead to an increased

surface area of the ice crystal. Large crystals have a concave boundary while smaller crystals are convex. Figure 1.5 shows the large concave boundary migrating into the small convex boundary.[25] This occurs because the high-energy curvatures are transferred to low-energy curvatures.[25]

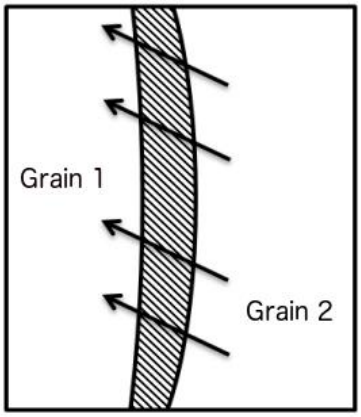

Figure 1.5 - Illustration of boundary migration with the shaded portion showing the space between two grains. The large concave is shown as grain 2, while the small convex is shown as grain 1. The arrows indicate the direction of the migration.[25]

Ostwald ripening occurs when large ice crystals grow at the expense of smaller ones, resulting in a small number of ice crystals and is a thermodynamically driven process.[26] This differs from boundary migration because Ostwald ripening considers water and the QLL and suggests there is a decrease in energy associated with the migration. This theory is that small water crystals will migrate to larger water crystals to be absorbed and decrease the surface area to volume ratio.[24] This occurs because small crystals have a larger surface-area-to-volume ratio than large crystals, resulting in an overall energy decrease following migration. This is commonly seen in slurry ice mixtures because of the high liquid water fraction.[27] For these

reasons, Ostwald ripening is the most accepted theory for the mechanisms of ice recrystallization.

1.2.3 Cryoprotective Agents (CPAs)

The steps of cryopreservation are as follows: (1) cryoprotective agents (CPAs) are added before cooling the cell or tissue, (2) the cell or tissue is cooled to the desired temperature for storage, (3) the cell or tissue is warmed, and (4) the CPA is removed.[5] A CPA is an additive that, when administered, can lead to the increased post-thaw viability of cells and tissues.[28] There are two types of CPAs: permeating and non-permeating CPAs. Examples of permeating CPAs are glycerol and dimethyl sulfoxide (DMSO), which can cross the cell membrane and reduce ice growth, cell dehydration, and mitigate osmotic injury. Non-permeating CPAs, such as polyvinylpyrrolidone and hydroxyethyl starch (HES), cannot cross the cell membrane.[29] Non-permeating CPAs prevent IIF because they assist the cell in becoming dehydrated by promoting water to leave the cell due to the increased osmolality of the extracellular solution. Non-permeating CPAs are generally less toxic than permeating CPAs at the same concentration.[30] The disadvantage of using CPAs is the cellular injury that occurs due to their toxicity.[8] The relationship between the concentration of CPA and cell viability is a U-shaped curve because high and low concentrations have low cell viability.[30] The introduction of CPAs leads to the shrinking of the cell and chemical disruption of the cytoskeleton.[5] Damage from toxicity is caused by the CPA disturbing the cellular membrane, producing adverse effects on enzyme function and hindering the development of cells.[8]

1.2.4 Inhibiting Ice Recrystallization

The inhibition of ice recrystallization is essential in preserving cells and tissues[29] because cell death can occur after freezing due to the recrystallization of ice.[5] Biological antifreezes (BAs) has evolved in many organisms that inhabit subzero environments.[31] This includes a class of molecules called antifreeze proteins (AFPs) and antifreeze glycoproteins (AFGPs).[31] These proteins can be found in organisms that inhabitant cold climates, such as the wood frog, which employs glycerol and urea as natural cryoprotectants to limit ice formation.[32]

One of the characteristics of AFPs is that they can cause a localized freezing point depression, known as thermal hysteresis (TH).[33] AFPs are peptides or glycopeptides that can irreversibly bind to the surface of ice crystals and inhibit ice growth.[34] AFP can be categorized into four groups (I-IV).[35] It is known that type I AFP can inhibit ice growth on the pyramidal plane.[36] The mechanism has not been entirely elucidated, but it is theorized that growth is arrested by a step-growth facet mechanism or the "stones on a pillow model."[37] The "stones on the pillow model" proposed by Knight suggests that the AFPs bind to the smooth curved surfaces of ice crystals, and growth must be budded between the attachment sites.[38] The freezing point is then depressed due to the Gibbs–Thompson effect, whereby curved surfaces have lower freezing points than flat surfaces.[34] This results in it being less favorable to add water molecules to the curve surface, resulting in the inhibition of ice growth (i.e., the Kelvin effect) along the pyramidal plane.[33]

BAs have been extensively studied and are found in animals and organisms that live in freezing temperatures.[37] The purpose of BAs is to inhibit ice growth to help the organisms survive freezing conditions and mediate damage associated with freezing.[39] They can also

inhibit ice recrystallization; antifreeze glycoproteins (AFGP) possess this trait.[39] However, BAs are not practically useful for cryopreservation due to the negative effect of TH at preservation temperatures. Ice crystals can grow into needles that can puncture and harm the cell wall, and this is called dynamic ice shaping.[40]

The structure of antifreeze glycoproteins (AFGP) is an alanine-alanine-threonine tripeptide repeat with a carbohydrate base.[41] AFGPs are categorized from 1–8 according to weight and range from 2.6 to 34 kDa.[42] AFGPs 1–4 consist of 20–33 kDa while 5–8 are less than 20 kDa, and AFGP-8 (Figure 1.6) is the smallest AFGP.[43] AFGPs have been demonstrated to be effective cryoprotectants by DeVries and colleagues in 1994.[44] However, AFGPs also have negative qualities like promoting changes in ice crystal morphology due to TH.[45] Therefore, AFGPS can be detrimental to cells.

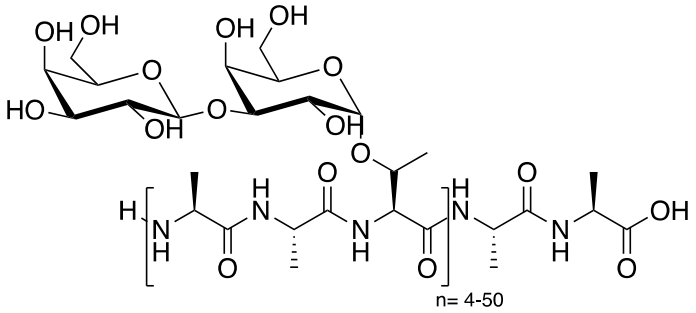

Figure 1.6 - Structure of AFGP-8, a disaccharide moiety with a β-(1-3) linkage.

It was discovered that synthetic AFGP analogs could possess cryoprotectant abilities without the negative effects of TH.[46] This contributed to the discovery of *C*-linked AFGPs that effectively inhibit ice recrystallization without the negative effects of TH, specifically dynamic ice shaping.[45] In addition, small molecules were also found to be effective at inhibiting ice

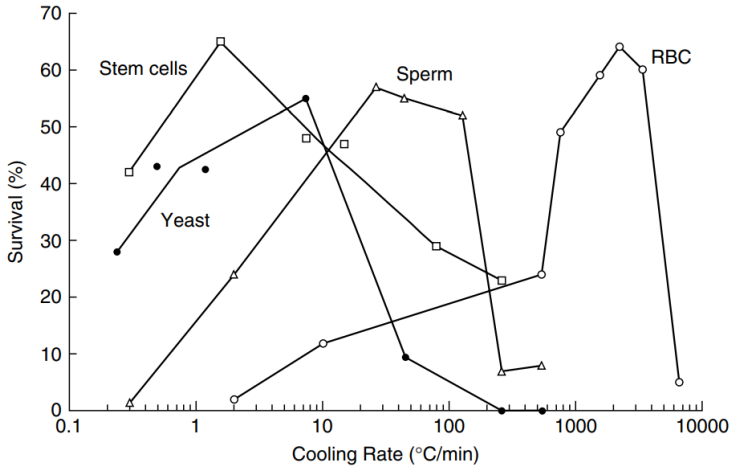

recrystallization.[46] Over the years, the Ben Lab has worked on the synthesis of small molecule IRIs.[45]

1.3 Introduction to Hydration Parameters

The hydration of compounds such as carbohydrates and proteins is a factor in their biological functions because water can form hydrogen bonds and stabilize active conformers.[47] The properties of carbohydrates enable them to form hydrogen bonds with other carbohydrate molecules and water. This is, in part, due to the amount and configuration of their hydroxyl groups. The hydroxyl groups can create an intramolecular network of hydrogen bonds and water bridges.[48]

1.3.1 Hydration Parameters

Hydration number is the number of water molecules closely bonded to a compound.[47] This is known as the primary hydration shell around the compound and is considered to be non-compressible.[47] This parameter is closely studied in the Ben Lab, and Czechura *et al*. identified a positive correlation between hydration number and IRI activity.[49] This result suggested that the orientation of the C-2 and C-4 hydroxyl groups of a carbohydrate affected the 3D hydrogen

bond network of water. The hydrogen bond network of water is a factor in the IRI potential of a compound.

Partial molar compressibility (PMC) is the ability of the solvent in the outer hydration shell to be compressed.[47] The compressibility of the solvent around a hydrophilic compound would be tighter because of the hydrogen bonds. The partial molar compressibility of water is 8.18 $cm^3 \cdot mol^{-1} \cdot bar^{-1}$.[47] Carbohydrates such as D-glucose and D-sucrose have PMC values of 111.7 cm^3 and 211.6 cm^3, respectively. Partial molar volume (PMV) is the volume of water displaced by a compound's hydrated shells. The outer boundary of the shell is where the outer boundary layer of water is analogous to bulk water regarding structure and properties. A positive correlation was identified between partial molar compressibility and IRI activity, with a low PMC value resulting in high IRI activity (see Figure 1.7).[49]

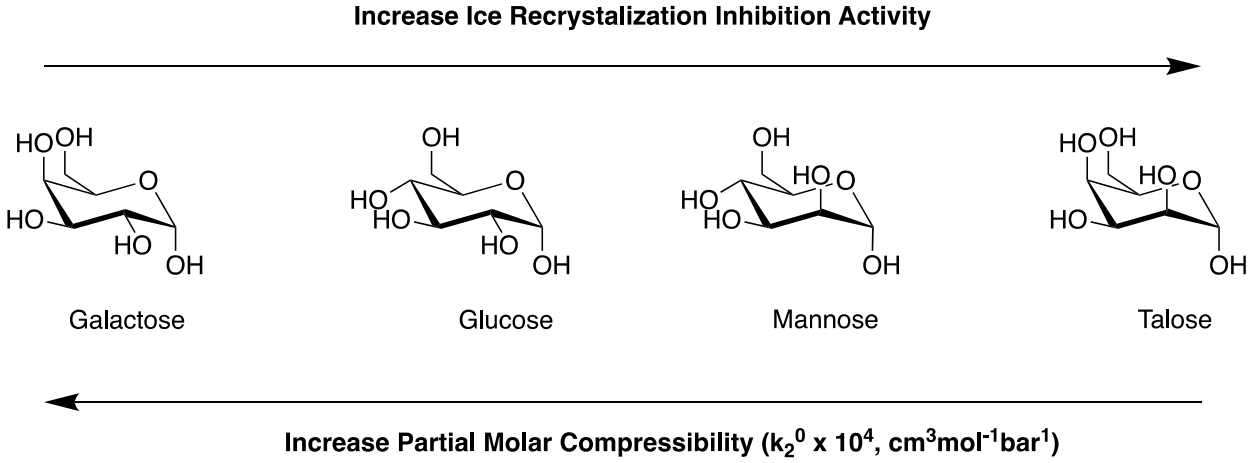

Figure 1.7 - Correlation between partial molar compressibility and IRI activity.[50]

The Ben Lab utilizes the hydration index parameter to account for the volume differences among carbohydrates for the comparison of monosaccharides versus disaccharides. The hydration index is the hydration number divided by the molar volume of the carbohydrate.

A correlation was identified between IRI activity and hydration number, as shown in Figure 1.8.[46] This figure displays a single correlation for a wide range of carbohydrates, and the water molecules per unit volume are important in determining IRI activity. The limitation of this metric is that it does not fully consider the importance of hydrophobic regions on IRI-active carbohydrate moieties. Work done by the Ben Lab with *N*-alkyl-aldonamides derivatives illustrated that as the hydrophobic region decreased in size, the IRI activity decreased as well.[9] The hydrophobic region is of importance because it contributes to IRI activity.

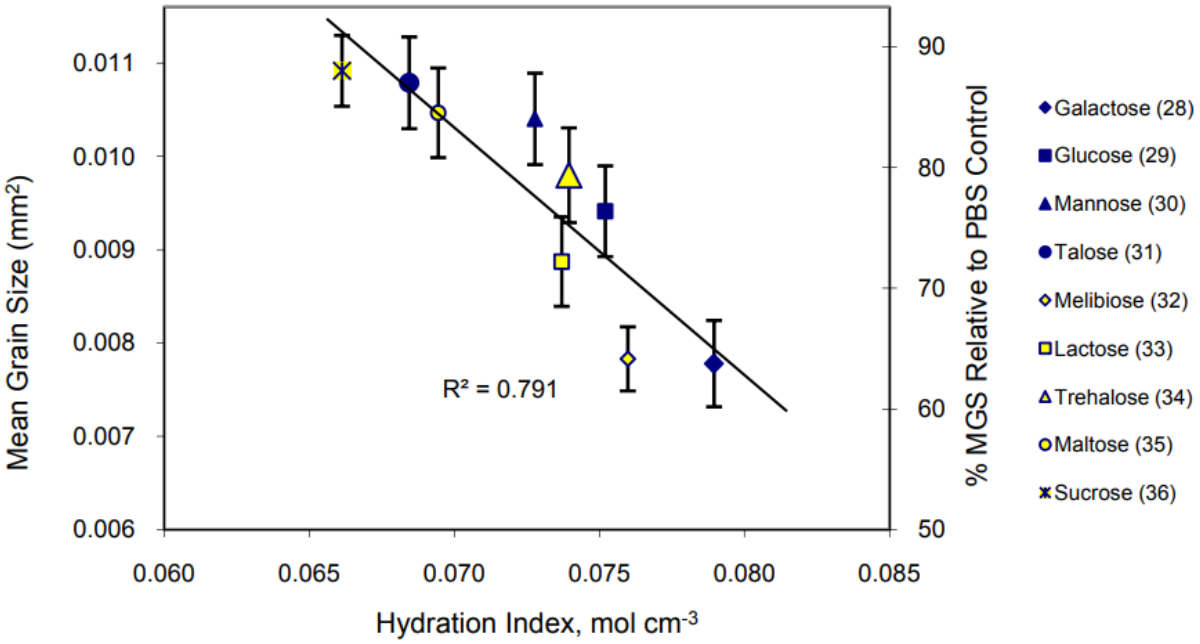

Figure 1.8 - IRI activity at 22 mM concerning hydration index of monosaccharides and disaccharides.[51]

1.3.2 The Partition Coefficient

The parameters previously discussed, are not sufficient to describe the IRI activity of carbohydrate analogs. The reason for this is that substituted carbohydrate derivatives contain

both hydrophilic and hydrophobic regions.[3] The hydrophobic region is believed to be essential for IRI activity, and the discussed parameters are unable to describe these regions. The partition coefficient (P) is a parameter that can be used to analyze the amphiphilic nature of carbohydrate derivatives.

The partition coefficient is a measure of how hydrophilic or hydrophobic a compound is.[52] This is important to understanding the permeability of compounds through the membrane and binding at receptor sites.[53] The coefficient is calculated by determining the solubility of a compound into water and 1-octanol.[54] The coefficient is the ratio of the compound in 1-octanol divided by the amount in water (see Eq. 1):

$$P = \frac{c_i^{oct}}{c_i^{W}} \text{ (Eq. 1)}$$

where c_i^{oct} and c_i^{W} are the solute concentrations in 1-octanol and water, respectively. The logarithm of this ratio is the logP.[55] The logP value is a measurement of the hydrophilicity of a compound.

Computational studies have been conducted to calculate logP and are preferred over the experimental method because they are time and cost-efficient.[56] The additive method is an example of a computational method used to calculate logP. In the additive method, a molecule is broken down into its functional groups or atoms, and the logP is calculated for each fragment and summed.[56] This method is improved upon by adding correction factors, such as those used by Rekkar and coworkers.[57] There are several software options used to compute logP, such as ALOGP,[58] SMILOGP,[61] and XLOGP.[56]

1.4 Ice Recrystallization Inhibition Activity

There are numerous methods used to measure IRI activity. The Ben Lab utilizes a modified splat-cooling assay introduced by Knight *et al*.[60] The "splat-cooling" assay involves dropping a 10-µL droplet of a compound dissolved in a phosphate-buffered saline (PBS) solution onto a polished aluminum block at -78 °C from a height of 2 meters. The droplet will land on the block and instantly freeze to form a wafer. The wafer is 1 cm in diameter and 20 µm thick and annealed at -6.4 °C in a cryostage. There are two methods for analyzing these wafers. The first is to anneal it for 30 minutes, and the other is to anneal it for 5 minutes. These two methods are known as the *30-minute modified splat-cooling assay* and the *5-minute modified splat-cooling assay*.

1.4.1 The 30-minute Modified "Splat-cooling" Assay

The 30-minute modified splat-cooling assay (30-minute assay) involves analyzing 12 random ice crystals on a single wafer. Afterwards, the IRI activity is determined by measuring the ice crystals' percent mean grain size (%MGS) relative to the PBS control.[61] The %MGS has an inverse correlation with IRI activity. Inactive compounds have %MGS values of less than 60%, and moderately active compounds have %MGS values of 60-80%.[61]

1.4.2 The 5-minute Modified "Splat-cooling" Assay

The change from a 30-minute assay to a 5-minute modified splat-cooling assay (5-minute assay) is based on the work done by previous Ben Lab member Stephanie Abraham.[61] It involves analyzing the growth of ice crystals over 60 minutes. Abraham showed that a compound's endpoint crystal growth does not represent the inhibition that occurs during the entire annealing timeframe.[52] The 30-minute assay is, therefore, not an accurate measure of IRI

activity because it only involves examining the ability of a compound to decrease the size of ice crystals at a specific time and concentration. Another shortcoming of this method is that it involves ignoring the heterogeneity of the size of the ice crystals and the time dependence of ice growth because only a selection of the ice crystals on the wafer is analyzed.

The 5-minute assay involves analyzing all the crystals in a picture. The crystals are categorized into size groups. The first category contains crystals that are 0.001 mm^2 in size, and each following category increases is 0.001 mm^2 larger than the previous one. This study determines that a dose-response curve better represents IRI activity over a series of concentrations. The dose-response curve with a four-parameter model outputs the best fit and can account for the top plateau, bottom plateau, slope, and IC_{50} value of IRI activity. The IC_{50} is the concentration of a compound required to achieve 50% inhibition of ice crystal growth relative to the negative control (PBS).[61]

1.5 Small Molecule Ice Recrystallization Inhibitors

1.5.1 Monosaccharides as Ice Recrystallization Inhibitors

Previous Ben Lab student Dr. Roger Tam found that various monosaccharides and disaccharides are moderately effective small-molecule IRIs, with D-galactose and D-melibiose being the most effective.[22] The importance of the hydration index regarding IRI activity is described.[49] A positive correlation was found between hydration index and the IRI activity of simple carbohydrates. With an increase in hydration index value, there is an increase in IRI activity. Figure 1.9 shows a comparison of the hydration index trend to the IRI activity of simple carbohydrates.[22]

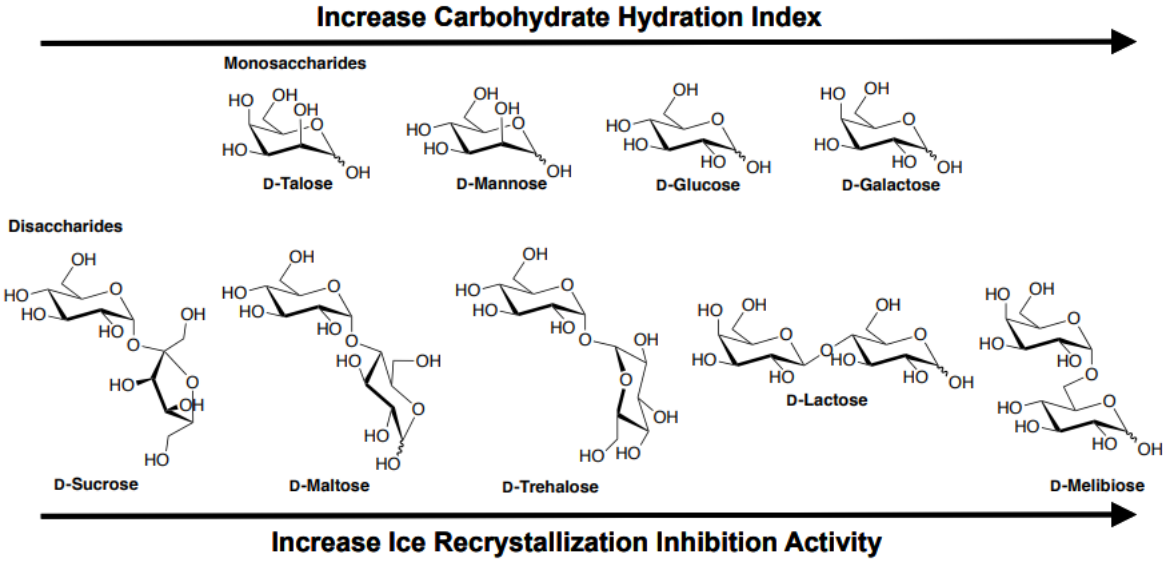

Studies show that the monosaccharides and disaccharides did not express TH activity or dynamic ice shaping. It is hypothesized that there is a disruption of the pre-ordering of water at the QLL-bulk water interface, which inhibits ice recrystallization.[46] It is proposed that the monosaccharides and disaccharides do not bind to the ice lattice because they are not observed to cause dynamic ice shaping,[62] and it is hypothesized that the carbohydrate would be

Figure 1.9 - Relationship between IRI activity and hydration Index.[22]

located between the two ice crystals (Figure 1.10).[22] It is not well known where the carbohydrate is located between the crystals because of limitations in our understanding of how the QLL behaves.[22] Water molecules in an ice crystal lattice are more organized than those in bulk water (which is disorganized), while the QLL is semi-organized. The addition of carbohydrates to the bulk water/QLL is more entropically favored than the addition of carbohydrates to the ice crystal lattice.[22]

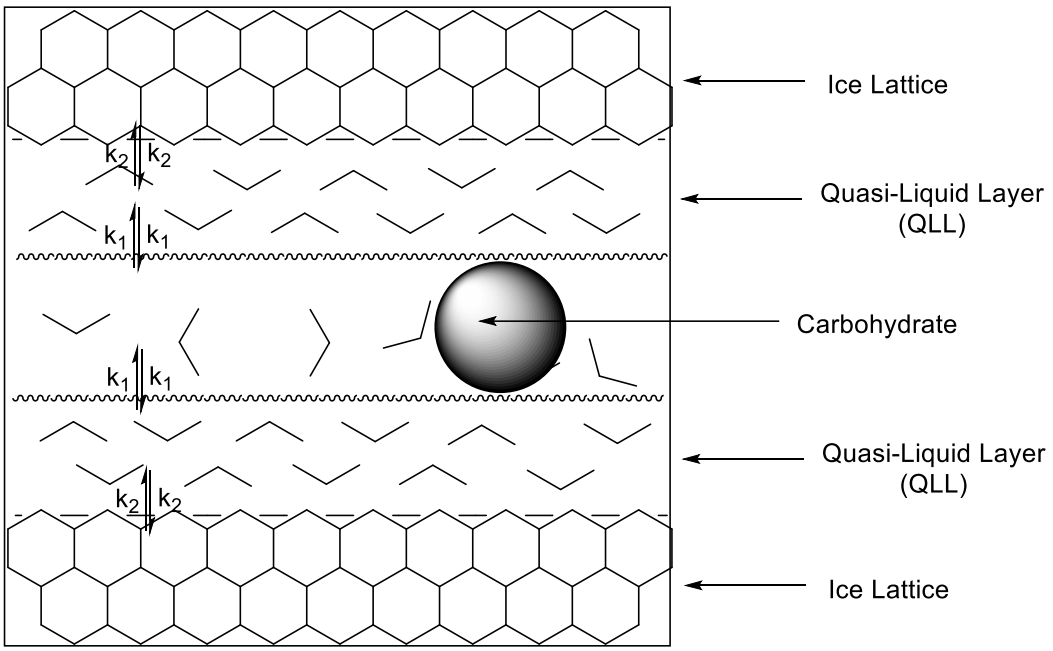

Figure 1.10 - Schematic of a carbohydrate, coloured in black, localized in the bulk water between two ice lattices. The proposed mechanism for ice recrystallization inhibition and shows hydration index is positively correlated to IRI activity.[22]

The hydration of carbohydrates will determine how well they will fit into a three-dimensional hydrogen-bonded network of bulk water.[47] Highly hydrated carbohydrates like D-galactose and D-melibiose have been shown to disturb the network, and it is thought that this

leads to higher IRI activity compared to relatively low hydrated carbohydrates like D-talose and D-sucrose (which showed inadequate IRI activity).[22]

1.5.2 Design of IRI Active Small Molecules

The use of carbohydrate derivatives is well documented in biological processes. *N*-Octyl-β-D-glycosides are primarily used as detergents for membrane protein stabilization, purification, and crystallization.[63] The IRI activity of this compound as a D-glucose and D-galactose derivative was tested using the 30-minute assay and displayed moderate activity at 22 mM, and the D-galactose derivative exhibited relatively higher activity (Figure 1.11).[3] It was concluded that long alkyl chains increase IRI activity because they function as hydrophobic moieties.[3]

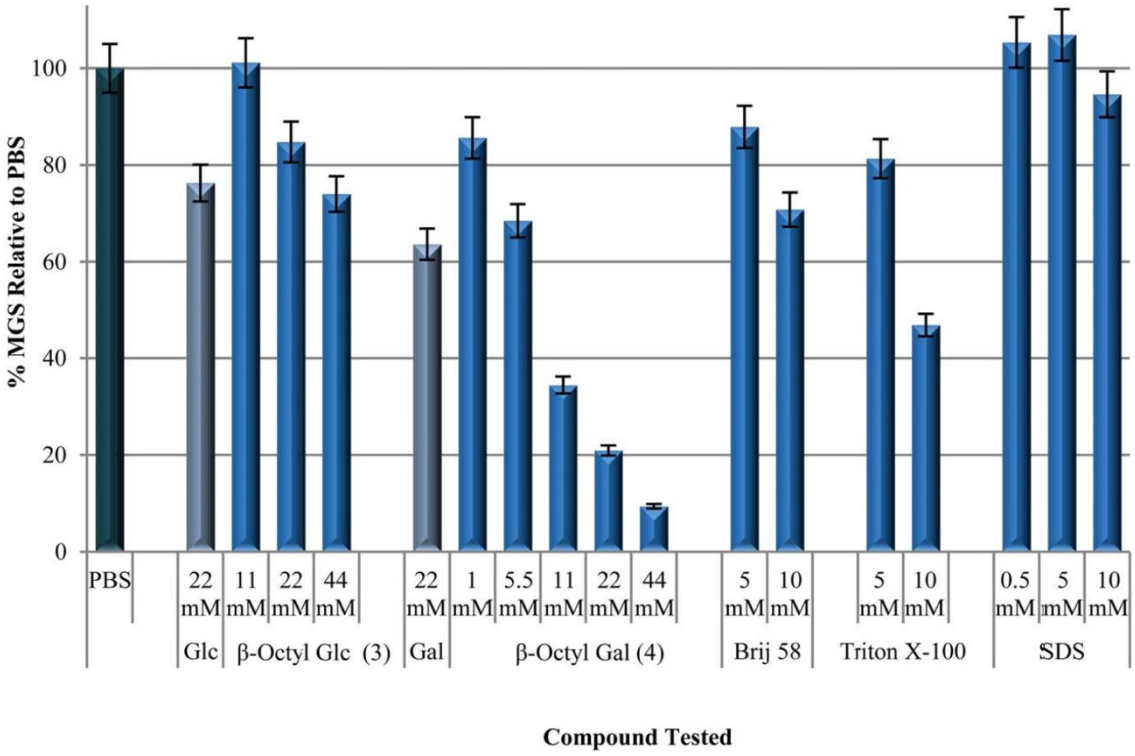

Figure 1.11 - IRI activity of *N*-Octyl-β-D-glycosides in relation to the parent glycoside.[3, 64]

Several carbohydrate derivatives have been investigated for their IRI activity, and aryl carbohydrate derivatives were found to be effective IRI molecules. Many derivatives were synthesized and tested for IRI activity by past Ben Lab member Dr. Capicciotti.[65] Replacing the hydrophobic alkyl chains with aryl derivatives showed moderate IRI activity.[65] It was determined that the para-substituted analogs had greater IRI activity than orth- and meta-substituted analogues (Figure 1.12).[65]

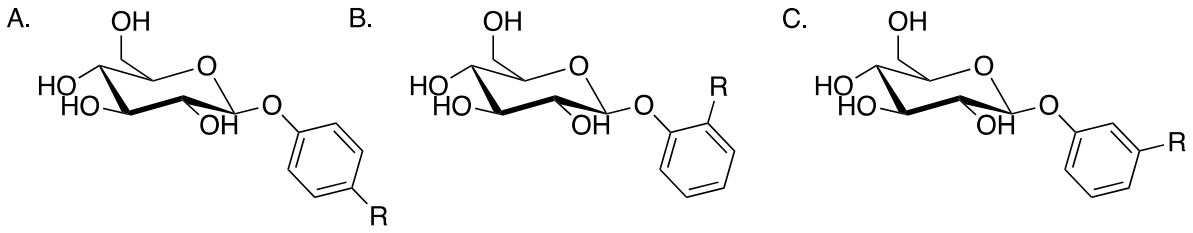

Figure 1.12 - Aryl substituted glucose (A) *para*-substituted (B) *ortho*-substituted (C) *meta*-substituted.

The Ben group has studied the effects of functionalization on various hydroxyl groups on carbohydrates with a gap in research for the C-3 hydroxyl group. Previous researchers reported that 3-*O*-Methyl-D-glucose (3-OMG) is an effective cryoprotectant, and its use is well documented in preserving primary rat hepatocytes.[66] 3-OMG is chemically similar to D-glucose, and the GLUT family of transporters regulates its uptake in mammalian cells, but it is a non-metabolized derivative of glucose.[67]

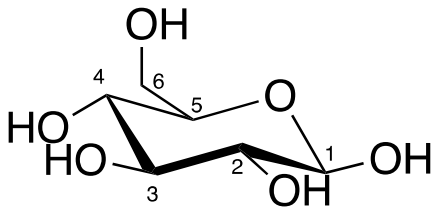

Figure 1.13 - Carbons labeled on a β-D-glucopyranose

The acetylation of β-D-glucopyranose shows the most chemically reactive hydroxyl groups as being C-1 and C-6, followed by the C-2 and C-3 groups. A labelled β-D-glucopyranose is seen in Figure 1.13. Bols and coworkers found that the C-3 hydroxyl group has the highest electron density and, therefore, is more reactive than C-2.[68] In addition, the antiperiplanar relationship between the C-2 hydroxyl and the ring oxygen reduces C-2's reactivity.[68] As such, it is hypothesized that functionalization at the C-3 position could dramatically influence IRI activity and this is worthy of further investigation as it has not been reported.

1.6 Goals and Objectives

1.6.1 Objective 1: The Use of Hydration Parameters to Predict the IRI Activity of Monosaccharides and Disaccharides

Hydration parameters (i.e., hydration number, hydration index, and PMC) have been found to be positively correlated to the IRI activity of simple monosaccharides and disaccharides.[5] The inability of these parameters to accurately predict IRI activity due to the factors discussed in Section 1.3 has resulted in the need to probe the relationship between IRI activity and additional parameters, such as the partition coefficient (P). This study aims to analyze the log of the partition coefficient (logP) of several monosaccharides and disaccharides and their relationship with IRI activity.

The two primary methods of acquiring logP values are experimental methods, such as enzymatic methods[8], the 1-octanol/water experiment,[9] single-entity electrochemistry,[10,] or computation using software that predicts the logP values.[11] Examples of computational software are Molinspiration's logP calculator (miLogP2.2), VCClab's ALOGPS 2.1,[12,] and ACD Labs' Partition Coefficient Calculation (ACD/LogP).[13] The predictions made in such software are performed using atom-, fragment- or knowledge-based methods.[11] The fragment-based method is used by software discussed in this thesis. Testing multiple computational software makes it possible to determine what software results in the closest predicted logP values to those calculated experimentally.

1.6.2 Objective 2: Determine the Importance of the C-3 Heteroatom of Aryl Glucosides for IRI Activity

Over the years, the Ben Group has synthesized an extensive library of C-1 *O*-linked aryl glucosides that exhibit IRI activity.[14] The position of the substitute on the aryl ring reflects a

difference in IRI activity, as seen in Figure 2.3. The IRI activity of these compounds is measured in percent mean grain size (%MGS) relative to the PBS control. The *para*-compound (**A**) has a % MGS of 23%, while the *meta*-compound (**B**) and *ortho*-compound (**C**) have %MGS values of 55% and 81% respectively.[14] The high IRI activity of **A** is attributed to properties such as a β-glycoside bond and a substituent in the *para*-position of the aryl ring.[3]

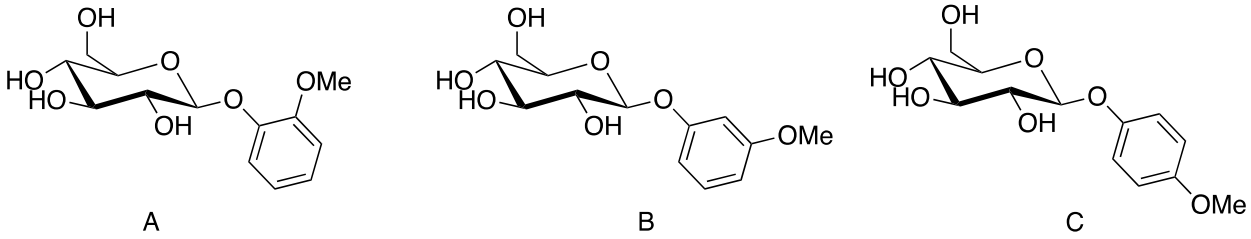

Figure 1.14 - Structure of ortho-, meta-, and para-methoxy-substituted glucoside derivatives[3]

The C-1 hydroxyl is the anomeric position on carbohydrates and has been researched by previous Ben group member Dr. Chantelle Capicciotti.[3] The ability of the anomeric position to form α or β linkages has been previously shown to influence IRI activity.[3] Other positions, such as C-6, have also been tested for their effect on IRI activity. The C-6 position of pyranose was studied by Dr. Capicciotti, [15] with the synthesis of 6-*O*-(4-methoxyphenyl)-β-D-glucopyranoside (**52,** Figure 2.4). The C-6 analog was found to be significantly less active than the C-1 functionalized β-PMP-Glc.[15] The %MGS value of **52** was 82% while **2** had a %MGS value of 23%.[15] These findings also reflect that the C-6 functionalized glycoside has a slightly lower IRI activity than D-glucose, which had a %MGS value of 77% at 22 mM. Therefore, the C-6 position is essential to IRI activity such that modifying this position would lead to decreased IRI activity.

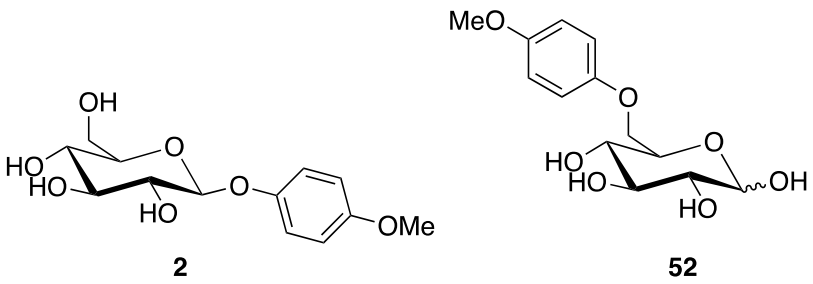

Figure 1.15 - C-1 functionalized glucose derivative **2** and C-6 functionalized glucose derivative **52**, investigated for the effect of functionalization at the C-6 position on IRI activity

However, researchers have not tested functionalization at the C-3 position because the complex synthetic pathway requires usage of protection group. The interest in the C-3 hydroxyl is due to it being the most chemically-reactive position following C-1 and C-6.[16] Thus, it is hypothesized that the hydroxyl at the C-3 position could be linked to IRI activity. Several C-3 functionalized compounds were synthesized and compared to their C-1 counterpart. The comparison to C-1 was done to form the basis for the functionalized C-3 compounds to assess solubility and IRI activity. Functional groups, such as alkanes, alkenes, and aryl rings, are substituted onto the C-3 position, as seen in Figure 2.6A. These compounds contain a β-glycoside bond, and the aryl rings are substituted in the *para*-position. The functional groups were chosen because they are primarily hydrophobic, and it has been shown that the presence of a hydrophobic region affects IRI activity.[15]

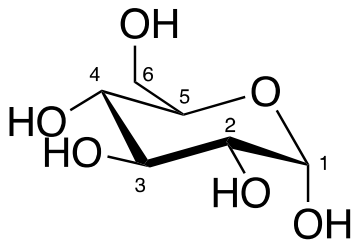

Figure 1.16 - Carbons labeled on an α-D-glucopyranose. The C-3 position is under investigation for its role in IRI activity and its effect on solubility.

The benzyl derivatives (**407** and **415)** were tested against the *para*-bromide and *para*-fluoride derivatives. It was hypothesized that the benzyl compound will have a low IRI activity level that will increase with the addition of the halogen groups. This is because their addition will lead to the increased polarity of the benzyl group, as shown in phenyl studies.[3] The allyl and methyl compounds (**410** and **417**) were also tested against their respective C-1 compounds. It was hypothesized that the methyl derivatives have higher solubility levels and are more IRI-active than the allyl compounds. This is due to the unsaturation of the allyl chain resulting in low solubility.[17] Unfortunately, due to time restrictions, the C-1 compound of **409** was unable to be synthesized.

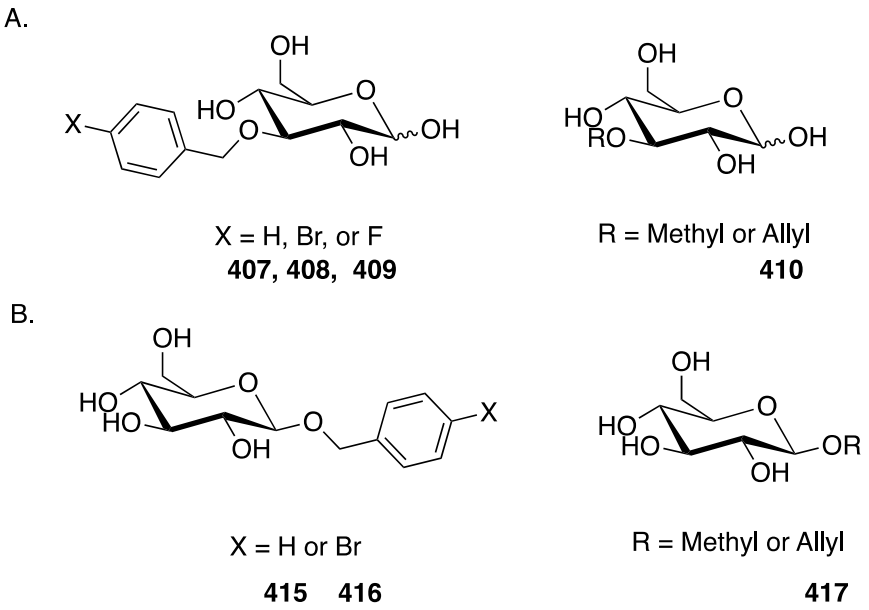

Figure 1.17 - Structure of (A) 3-*O* functionalized glucoside derivatives targets synthesized and assessed for IRI activity and (B) 1-*O* functionalized glucoside derivatives of A.

The C-3 functionalized compounds were tested against their corresponding C-1 compounds, as seen in Figure 2.6B. This involved assessing the difference in IRI activity between the C-1 and C-3 functionalized compounds and investigating the C-3 position.

1.7 Summary of Objectives:

(i) Calculate IRI activity for various commercially-available monosaccharides and disaccharides using the 5-minute assay method and determine an relationship between IRI activity and partition coefficient (P).

(ii) Synthesize novel IRI small molecules by functionalizing the C-3 position on D-glucose and comparison of IRI activity and solubility to their corresponding C-1 position analogs.

1.8 References

(1) Massie, I.; Selden, C.; Hodgson, H.; Fuller, B. Storage Temperatures for Cold-Chain Delivery in Cell Therapy: A Study of Alginate-Encapsulated Liver Cell Spheroids Stored at-80°C or-170°C for up to 1 Year. *Tissue Engineering - Part C: Methods* **2013**, *19* (3), 189–195. https://doi.org/10.1089/ten.tec.2012.0307.

(2) Baust, J. G.; Gao, D.; Baust, J. M. Cryopreservation: An Emerging Paradigm Change. *Organogenesis* **2009**, *5* (3), 90–96. https://doi.org/10.4161/org.5.3.10021.

(3) Capicciotti, C. J. The Rational Design of Potent Ice Recrystallization Inhibitors for Use as Novel Cryoprotectants, 2014.

(4) Mazur, P.; Leibo, S. P.; Chu, E. H. Y. A Two-Factor Hypothesis of Freezing Injury. Evidence from Chinese Hamster Tissue-Culture Cells. *Experimental Cell Research* **1972**, *71* (2), 345–355. https://doi.org/10.1016/0014-4827(72)90303-5.

(5) Gao, D.; Critser, J. K. Mechanisms of Cryoinjury in Living Cells. *ILAR Journal* **2000**, *41* (4), 187–196. https://doi.org/10.1093/ilar.41.4.187.

(6) Acker, J. P.; McGann, L. E. Protective Effect of Intracellular Ice during Freezing? *Cryobiology* **2003**, *46* (2), 197–202. https://doi.org/10.1016/S0011-2240(03)00025-7.

(7) Mazur, P. *Principles Of Cryobiology*; 2004. https://doi.org/10.1201/9780203647073.ch1.

(8) Best, B. P. Cryoprotectant Toxicity: Facts, Issues, and Questions. *Rejuvenation Research* **2015**, *18* (5), 422–436. https://doi.org/10.1089/rej.2014.1656.

(9) Ampaw, A.; Charlton, T. A.; Briard, J. G.; Ben, R. N. Designing the next Generation of Cryoprotectants–from Proteins to Small Molecules. *Peptide Science* **2019**, *111* (1). https://doi.org/10.1002/pep2.24086.

(10) He, X.; Park, E. Y. H.; Fowler, A.; Yarmush, M. L.; Toner, M. Vitrification by Ultra-Fast Cooling at a Low Concentration of Cryoprotectants in a Quartz Micro-Capillary: A Study Using Murine Embryonic Stem Cells. *Cryobiology* **2008**, *56* (3), 223–232. https://doi.org/10.1016/j.cryobiol.2008.03.005.

(11) Muldrew, K.; McGann, L. E. The Osmotic Rupture Hypothesis of Intracellular Freezing Injury. *Biophysical Journal* **1994**, *66* (2), 532–541. https://doi.org/10.1016/S0006-3495(94)80806-9.

(12) Bahr, M. M.; Amer, M. S.; Abo-El-Sooud, K.; Abdallah, A. N.; El-Tookhy, O. S. Preservation Techniques of Stem Cells Extracellular Vesicles: A Gate for Manufacturing of Clinical Grade Therapeutic Extracellular Vesicles and Long-Term Clinical Trials. *International Journal of Veterinary Science and Medicine* **2020**, *8* (1), 1–8. https://doi.org/10.1080/23144599.2019.1704992.

(13) *Life in the Frozen State*; Fuller, B. J., Lane, N., Benson, E. E., Eds.; CRC Press, 2004. https://doi.org/10.1201/9780203647073.

(14) Mazur, P. Freezing of Living Cells: Mechanisms and Implications. *The American journal of physiology* **1984**, *247* (3 Pt 1), 0–4. https://doi.org/10.1152/ajpcell.1984.247.3.C125.

(15) Malkin, T. L.; Murray, B. J.; Brukhno, A. v.; Anwar, J.; Salzmann, C. G. Erratum: Structure of Ice Crystallized from Supercooled Water (Proceedings of the National Academy of Sciences of the United States of America (2012) 109, 4 (1041-1045) DOI: 10.1073/Pnas.1113059109). *Proceedings of the National Academy of Sciences of the United States of America* **2012**, *109* (10), 4020. https://doi.org/10.1073/pnas.1201020109.

(16) Brill, R. The Structure of Ice. *Angewandte Chemie International Edition in English* **1962**, *1* (11), 563–567. https://doi.org/10.1002/anie.196205631.
(17) Fletcher, N. H. *The Chemical Physics of Ice*; Cambridge University Press, 1970. https://doi.org/10.1017/CBO9780511735639.
(18) Bahr, M. M.; Amer, M. S.; Abo-El-Sooud, K.; Abdallah, A. N.; El-Tookhy, O. S. Preservation Techniques of Stem Cells Extracellular Vesicles: A Gate for Manufacturing of Clinical Grade Therapeutic Extracellular Vesicles and Long-Term Clinical Trials. *International Journal of Veterinary Science and Medicine* **2020**, *8* (1), 1–8. https://doi.org/10.1080/23144599.2019.1704992.
(19) Kajima, Y.; Ogata, S.; Kobayashi, R.; Hiyama, M.; Tamura, T. Fluctuating Local Recrystallization of Quasi-Liquid Layer of Sub-Micrometer-Scale Ice: A Molecular Dynamics Study. *Journal of the Physical Society of Japan* **2014**, *83* (8), 4–7. https://doi.org/10.7566/JPSJ.83.083601.
(20) Asakawa, H.; Sazaki, G.; Nagashima, K.; Nakatsubo, S.; Furukawa, Y. Two Types of Quasi-Liquid Layers on Ice Crystals Are Formed Kinetically. *Proceedings of the National Academy of Sciences of the United States of America* **2016**, *113* (7), 1749–1753. https://doi.org/10.1073/pnas.1521607113.
(21) (1) Faraday. XXIV. On Regelation, and on the Conservation of Force. London, Edinburgh, Dublin Philos. Mag. J. Sci. **1859**, 17 (113), 162–169. https://doi.org/10.1080/14786445908642645.
(22) Tam, R. Y.; Ferreira, S. S.; Czechura, P.; Ben, R. N.; Chaytor, J. L. Hydration Index-a Better Parameter for Explaining Small Molecule Hydration in Inhibition of Ice Recrystallization. *Journal of the American Chemical Society* **2008**, *130* (51), 17494–17501. https://doi.org/10.1021/ja806284x.
(23) Montagnat, M.; Duval, P. Rate Controlling Processes in the Creep of Polar Ice, Influence of Grain Boundary Migration Associated with Recrystallization. *Earth and Planetary Science Letters* **2000**, *183* (1–2), 179–186. https://doi.org/10.1016/S0012-821X(00)00262-4.
(24) Inada, T.; Modak, P. R. Growth Control of Ice Crystals by Poly(Vinyl Alcohol) and Antifreeze Protein in Ice Slurries. *Chemical Engineering Science* **2006**, *61* (10), 3149–3158. https://doi.org/10.1016/j.ces.2005.12.005.
(25) Alley, R. B.; Perepezko, J. H.; Bentley, C. R. Grain Growth in Polar Ice: II. Application. *Journal of Glaciology* **1986**, *32* (112), 425–433. https://doi.org/10.3189/s0022143000012132.
(26) Budke, C.; Heggemann, C.; Koch, M.; Sewald, N.; Koop, T. Ice Recrystallization Kinetics in the Presence of Synthetic Antifreeze Glycoprotein Analogues Using the Framework of LSW Theory. *Journal of Physical Chemistry B* **2009**, *113* (9), 2865–2873. https://doi.org/10.1021/jp805726e.
(27) Flores, A. A.; Goff, H. D. Recrystallization in Ice Cream after Constant and Cycling Temperature Storage Conditions as Affected by Stabilizers. *Journal of Dairy Science* **1999**, *82* (7), 1408–1415. https://doi.org/10.3168/jds.S0022-0302(99)75367-1.
(28) Wilmut, I. The Effect of Cooling Rate, Warming Rate, Cryoprotective Agent, and Stage Ofdevelopment on Survival of Mouse Embryos during Freezing and Thawing. **1972**, *11* (22), 1071–1079.
(29) Fuller, B. J. Cryoprotectants: The Essential Antifreezes to Protect Life in the Frozen State. *Cryo-Letters* **2004**, *25* (6), 375–388.
(30) Fahy, G. M. The Relevance of Cryoprotectant "Toxicity" to Cryobiology. *Cryobiology* **1986**, *23* (1), 1–13. https://doi.org/10.1016/0011-2240(86)90013-1.

(31) Muchlisin, Z. A.; Nadiah, W. N.; Nadiya, N.; Fadli, N.; Hendri, A.; Khalil, M.; Siti-Azizah, M. N. Exploration of Natural Cryoprotectants for Cryopreservation of African Catfish, Clarias Gariepinus, Burchell 1822 (Pisces: Clariidae) Spermatozoa. *Czech Journal of Animal Science* **2015**, *60* (1), 10–15. https://doi.org/10.17221/115/2013-CJAS.

(32) Costanzo, J. P.; Lee, R. E.; Dcvries, A. L.; Wang, T.; Layne, J. R. Survival Mechanisms of Vertebrate Ectotherms at Subfreezing Temperatures: Applications in Cryomedicine. *The FASEB Journal* **1995**, *9* (5), 351–352. https://doi.org/10.1096/fasebj.9.5.7896003.

(33) Celik, Y.; Drori, R.; Pertaya-Braun, N.; Altan, A.; Barton, T.; Bar-Dolev, M.; Groisman, A.; Davies, P. L.; Braslavsky, I. Microfluidic Experiments Reveal That Antifreeze Proteins Bound to Ice Crystals Suffice to Prevent Their Growth. *Proceedings of the National Academy of Sciences of the United States of America* **2013**, *110* (4), 1309–1314. https://doi.org/10.1073/pnas.1213603110.

(34) Sander, L. M.; Tkachenko, A. v. Kinetic Pinning and Biological Antifreezes. *Physical Review Letters* **2004**, *93* (12), 12–15. https://doi.org/10.1103/PhysRevLett.93.128102.

(35) Sicheri, F.; Yang, D. ~S. ~C. Ice-Binding Structure and Mechanism of an Antifreeze Protein from Winter Flounder. *Nature* **1995**, *375* (6530), 427–431. https://doi.org/10.1038/375427a0.

(36) Davies, P. L.; Hew, C. L. Biochemistry of Fish Antifreeze Proteins. *The FASEB Journal* **1990**, *4* (8), 2460–2468. https://doi.org/10.1096/fasebj.4.8.2185972.

(37) Vries, A. L. de. Antifreeze Peptides and Glycopeptides in Cold-Water Fishes. *Ann. Rev. Physiol* **1983**, *45* (16), 245–260.

(38) Knight, C. A.; Wierzbicki, A. Adsorption of Biomolecules to Ice and Their Effects upon Ice Growth. 2. A Discussion of the Basic Mechanism of "Antifreeze" Phenomena. *Crystal Growth and Design* **2001**, *1* (6), 439–446. https://doi.org/10.1021/cg015532l.

(39) Biggs, C. I.; Stubbs, C.; Graham, B.; Fayter, A. E. R.; Hasan, M.; Gibson, M. I. Mimicking the Ice Recrystallization Activity of Biological Antifreezes. When Is a New Polymer "Active"? *Macromolecular Bioscience* **2019**, *19* (7), 1–9. https://doi.org/10.1002/mabi.201900082.

(40) Kristiansen, E.; Zachariassen, K. E. The Mechanism by Which Fish Antifreeze Proteins Cause Thermal Hysteresis. *Cryobiology*. 2005, pp 262–280. https://doi.org/10.1016/j.cryobiol.2005.07.007.

(41) Harding, M. M.; Anderberg, P. I.; Haymet, A. D. J. "Antifreeze" Glycoproteins from Polar Fish. *European Journal of Biochemistry* **2003**, *270* (7), 1381–1392. https://doi.org/10.1046/j.1432-1033.2003.03488.x.

(42) Graham, B.; Bailey, T. L.; Healey, J. R. J.; Marcellini, M.; Deville, S.; Gibson, M. I. Polyproline as a Minimal Antifreeze Protein Mimic That Enhances the Cryopreservation of Cell Monolayers. *Angewandte Chemie - International Edition* **2017**, *56* (50), 15941–15944. https://doi.org/10.1002/anie.201706703.

(43) Takago, S.; Matsumoto, I.; Kato, H.; Saito, N.; Ueda, H.; Iino, K.; Kimura, K.; Takemura, H. Hypothermic Preservation of Rat Hearts Using Antifreeze Glycoprotein. *Physiological Research* **2020**, *69* (6), 1029–1038. https://doi.org/10.33549/physiolres.934473.

(44) Eniade, A.; Purushotham, M.; Ben, R. N.; Wang, J. B.; Horwath, K. A Serendipitous Discovery of Antifreeze Protein-Specific Activity in C-Linked Antifreeze Glycoprotein Analogs. *Cell Biochemistry and Biophysics* **2003**, *38* (2), 115–124. https://doi.org/10.1385/CBB:38:2:115.

(45) Liu, S.; Ben, R. N. C -Linked Galactosyl Serine AFGP Analogues as Potent Recrystallization Inhibitors. *Organic Letters* **2005**, *7* (12), 2385–2388. https://doi.org/10.1021/ol050677x.

(46) Tam, R. Y.; Rowley, C. N.; Petrov, I.; Zhang, T.; Afagh, N. A.; Woo, T. K.; Ben, R. N. Solution Conformation of C-Linked Antifreeze Glycoprotein Analogues and Modulation of Ice Recrystallization. *Journal of the American Chemical Society* **2009**, *131* (43), 15745–15753. https://doi.org/10.1021/ja904169a.
(47) Galema, S. A.; Høiland, H. Stereochemical Aspects of Hydration of Carbohydrates in Aqueous Solutions. 3. Density and Ultrasound Measurements. *Journal of Physical Chemistry* **1991**, *95* (13), 5321–5326. https://doi.org/10.1021/j100166a073.
(48) Moulik, S. P.; Gupta, S.; Das, A. R. Hydration Studies on Some Polyhydroxy Non-Electrolytes and Non-Ionic Surfactants. *Canadian Journal of Chemistry* **1989**, *67* (2), 356–364. https://doi.org/10.1139/v89-058.
(49) Czechura, P.; Tam, R. Y.; Dimitrijevic, E.; Murphy, A. v.; Ben, R. N. The Importance of Hydration for Inhibiting Ice Recrystallization with C-Linked Antifreeze Glycoproteins. *Journal of the American Chemical Society* **2008**, *130* (10), 2928–2929. https://doi.org/10.1021/ja7103262.
(50) Takeo, K.; Kitamura, S.; Murata, Y. Synthesis of Nigero-Oligosaccharides. *Carbohydrate Research* **1992**, *224* (C), 111–122. https://doi.org/10.1016/0008-6215(92)84098-D.
(51) Yang, H. J. Nonfluorous, Highly CO_2-Soluble Chelating Ligands for ScCO 2 Metal Ion Extraction. *Chemistry Letters* **2006**, *35* (9), 1000–1001. https://doi.org/10.1246/cl.2006.1000.
(52) Ramløv, H.; Friis, D. S. *Contents of Volume 2-Antifreeze Proteins: Biochemistry, Molecular Biology, and Application*; 2020; Vol. 2. https://doi.org/10.1007/978-3-030-41948-6_1.
(53) Mazzobre, M. F.; Román, M. v.; Mourelle, A. F.; Corti, H. R. Octanol–Water Partition Coefficient of Glucose, Sucrose, and Trehalose. *Carbohydrate Research* **2005**, *340* (6), 1207–1211. https://doi.org/10.1016/j.carres.2004.12.038.
(54) Sangster, J. M. *Octanol-Water Partition Coefficients: Fundamentals and Physical Chemistry*; John Wiley & Sons, 1997; Vol. 1.
(55) Comer, J.; Tam, K. Lipophilicity Profiles: Theory and Measurement. In *Pharmacokinetic Optimization in Drug Research*; Verlag Helvetica Chimica Acta: Zürich; pp 275–304. https://doi.org/10.1002/9783906390437.ch17.
(56) Wang, R.; Gao, Y.; Lai, L. Calculating Partition Coefficient by Atom-Additive Method. *Perspectives in Drug Discovery and Design* **2000**, *19*, 47–66. https://doi.org/10.1023/A:1008763405023.
(57) Mannhold, R.; Rekker, R. F. The Hydrophobic Fragmental Constant Approach for Calculating Log P in Octanol/Water and Aliphatic Hydrocarbon/Water Systems. *Perspectives in Drug Discovery and Design* **2000**, *18*, 1–18. https://doi.org/10.1023/A:1008782809845.
(58) Ghose, A. K.; Pritchett, A.; Crippen, G. M. Atomic Physicochemical Parameters for Three Dimensional Structure Directed Quantitative Structure-Activity Relationships III: Modeling Hydrophobic Interactions. *Journal of Computational Chemistry* **1988**, *9* (1), 80–90. https://doi.org/10.1002/jcc.540090111.
(59) Convard, T.; Dubost, J. -P; le Solleu, H.; Kummer, E. SmilogP: A Program for a Fast Evaluation of Theoretical Log P from the Smiles Code of a Molecule. *Quantitative Structure-Activity Relationships* **1994**, *13* (1), 34–37. https://doi.org/10.1002/qsar.19940130107.
(60) Knight, C. A.; Hallett, J.; DeVries, A. L. Solute Effects on Ice Recrystallization: An Assessment Technique. *Cryobiology* **1988**, *25* (1), 55–60. https://doi.org/10.1016/0011-2240(88)90020-X.
(61) Abraham, S.; Keillor, K.; Capicciotti, C. J.; Perley-Robertson, G. E.; Keillor, J. W.; Ben, R. N. Quantitative Analysis of the Efficacy and Potency of Novel Small Molecule Ice Recrystallization

Inhibitors. *Crystal Growth and Design* **2015**, *15* (10), 5034–5039. https://doi.org/10.1021/acs.cgd.5b00995.

(62) Uchida, T.; Nagayama, M.; Shibayama, T.; Gohara, K. Morphological Investigations of Disaccharide Molecules for Growth Inhibition of Ice Crystals. *Journal of Crystal Growth* **2007**, *299* (1), 125–135. https://doi.org/10.1016/j.jcrysgro.2006.10.261.

(63) Lorber, B.; Bishop, J. B.; DeLucas, L. J. Purification of Octyl β-d-Glucopyranoside and Re-Estimation of Its Micellar Size. *Biochimica et Biophysica Acta (BBA) - Biomembranes* **1990**, *1023* (2), 254–265. https://doi.org/10.1016/0005-2736(90)90421-J.

(64) Capicciotti, C. J.; Leclère, M.; Perras, F. A.; Bryce, D. L.; Paulin, H.; Harden, J.; Liu, Y.; Ben, R. N. Potent Inhibition of Ice Recrystallization by Low Molecular Weight Carbohydrate-Based Surfactants and Hydrogelators. *Chemical Science*. **2012**, pp 1408–1416. https://doi.org/10.1039/c2sc00885h.

(65) Capicciotti, C. J.; Mancini, R. S.; Turner, T. R.; Koyama, T.; Alteen, M. G.; Doshi, M.; Inada, T.; Acker, J. P.; Ben, R. N. O-Aryl-Glycoside Ice Recrystallization Inhibitors as Novel Cryoprotectants: A Structure-Function Study. *ACS Omega* **2016**, *1* (4), 656–662. https://doi.org/10.1021/acsomega.6b00163.

(66) Sugimachi, K.; Roach, K. L.; Rhoads, D. B.; Tompkins, R. G.; Toner, M. Nonmetabolizable Glucose Compounds Impart Cryotolerance to Primary Rat Hepatocytes. *Tissue Engineering* **2006**, *12* (3), 579–588. https://doi.org/10.1089/ten.2006.12.579.

(67) Storey, K. B.; Mommsen, T. P. Effects of Temperature and Freezing on Hepatocytes Isolated from a Freeze- Tolerant Frog. *American Journal of Physiology - Regulatory Integrative and Comparative Physiology* **1994**, *266* (5 35-5). https://doi.org/10.1152/ajpregu.1994.266.5.r1477.

(68) Pedersen, C. M.; Olsen, J.; Brka, A. B.; Bols, M. Quantifying the Electronic Effects of Carbohydrate Hydroxy Groups by Using Aminosugar Models. *Chemistry - A European Journal* **2011**, *17* (25), 7080–7086. https://doi.org/10.1002/chem.201100020.

Chapter 2: Correlations between Hydration Parameters and the Ice Recrystallization Inhibition Activity of Carbohydrates and Carbohydrate Derivatives

The number and configuration of hydroxyl groups on carbohydrates give them a unique hydration characteristic.[1] The ratio of axial to equatorial hydroxyl groups, hydration number, and anomeric effect are all factors that have been used to describe the hydration state of carbohydrates.[2] Galema and Engberts utilized parameters to assess the hydration of carbohydrates.[1] The Ben Lab has examined various hydration parameters, such as hydration number, hydration index, PMCs, and PMVs, and their correlations to IRI activity.

These parameters have been correlated to the mean grain size (%MGS) of various simple carbohydrates using a 30-minute modified splat-cooling assay (30-minute assay). This assaying method does not result in a comprehensive representation of what occurs during ice recrystallization, and the 5-minute modified splat-cooling assay (5-minute assay) results in a relatively better representation of what occurs during ice recrystallization. As discussed in Section 1.4.3, several issues with the 30-minute assay include the fact that the assaying method does not involve considering the heterogeneity of ice crystal size and the time dependence of ice growth. As such, analyzing a data point at one concentration and at a single time point was not representative of what occurred during overall ice recrystallization.

2.1 Ice Recrystallization Inhibition Activity of Simple Monosaccharides and Disaccharides

A 5-minute assay was used to measure the IRI activity of various monosaccharides and disaccharides. The monosaccharides tested included D-glucose, D-fructose, D-galactose, and D-mannose. The tested disaccharides were lactose, sucrose, and trehalose. These monosaccharides were chosen because they are readily accessible and have usages as cryoprotectants for perseverations of cells and tissue (i.e., human umbilical cord blood (UCB)).[3]

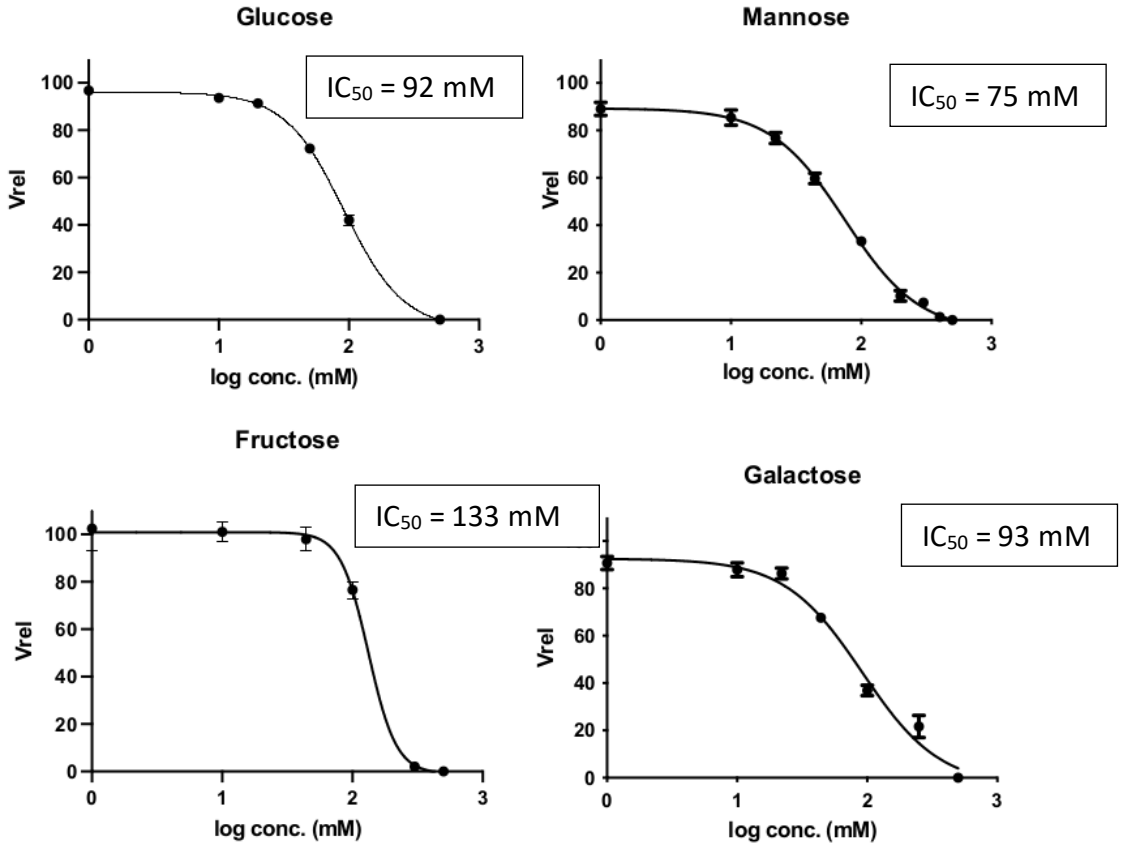

Figure 2.1 - Dose-response curve for IRI activity of monosaccharides. The average crystal growth rate (V_{rel}) was normalized to PBS. The standard error of the mean (SEM) is represented by the error bars. A four-parameter sigmoidal curve was fit to the data.

The compounds were tested using the 5-minute assay that defines IRI activity as the IC_{50} value from the dose-response curve.[4] The IC_{50} value is the concentration required to achieve 50% inhibition of ice crystal growth relative to the negative control (PBS). All these compounds were tested by the author of the thesis, except D-glucose. Which was tested by Romeo Junior El Issa, an MSc candidate in the Ben Lab, who generously supplied the data. The monosaccharides were measured for IRI activity, and their IC_{50} values were calculated to be 92 mM, 133 mM, 93 mM, and 75 mM for D-glucose, D-fructose, D-galactose, and D-mannose, respectfully.

The IC_{50} values of D-glucose and D-galactose were calculated to be 92 mM and 93 mM, respectively, using the 5-minute assay. These results were not expected because studies that were conducted using the 30-minute assay showed that D-galactose was the more active compound. D-Galactose has a %MGS of 64%, and D-glucose has a %MGS of 83% at 22 mM when measured using the 30-minute assay.[5] The higher activity of D-galactose was attributed to the axial hydroxyl group at C-4, giving D-galactose a lower PMC than D-glucose.[5] PMC is the measurement of a solute to fit in or disturb a solvent's three-dimensional arrangement. It was theorized that a low PMC is positively correlated with high IRI activity.[5] The correlation between IRI activity and PMC shows that the ability of a sugar to arrange itself in solvent is inversely proportional to its IRI activity. The ice crystal growth rate is similar for the two sugars, and it was hypothesized that PMC cannot be used as a predictor for IRI activity, as determined using the 5-minute assay. D-Mannose being more IRI-active than D-glucose and D-galactose was also unexpected due to the finding from previous studies that D-mannose has a higher %MGS[5] and a higher PMC than D-glucose .

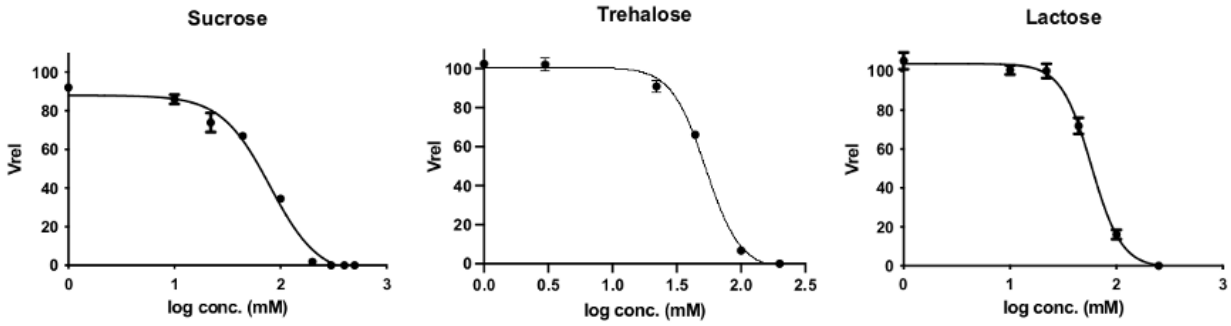

Figure 2.2 - Dose-response curve for IRI activity of disaccharides. The average crystal growth rate (V_{rel}) was normalized to PBS. The standard error of the mean (SEM) is represented by the error bars. A four-parameter sigmoidal curve was fit to the data.

The disaccharides have been selected for testing because they are readily available, and trehalose and sucrose are examples of non-permeating cryoprotectants.[6] As seen in Figure 3.2, the IC50 sucrose, trehalose, and lactose were found to be 80 mM, 53 mM, and 58 mM, respectively. The similarity in the IRI activity of trehalose and lactose is in agreement with previously-determined IRI activity levels using the 30-minute assay. Sucrose has not been tested for its IRI activity using the 30-minute assay.

IC_{50} = 80 mM

IC_{50} = 53 mM

IC_{50} = 58 mM

Table 2.1 IC_{50} values of various *monosaccharides* and disaccharides

	Sugar	IC_{50} (mM)
Monosaccharides	D-Glucose	92
	D-Fructose	133
	D-Galactose	93
	D-Mannose	75
Disaccharides	Sucrose	80
	Lactose	58
	Trehalose	53

The IC_{50} values of all carbohydrates tested are shown in Table 3.1. Overall, the disaccharides have a lower IC_{50} than the monosaccharides, with trehalose having the lowest IC_{50} value of 53 mM. The disaccharides are more hydrated than the monosaccharides due to the higher count of hydroxyl groups than monosaccharides, and this is a possible cause of their low overall IC_{50} values.[7]

As stated earlier, the results for the monosaccharides from the 5-minute assay conflicted with those in earlier work from the 30-minute assay. The differences in the IRI activity of carbohydrates such as D-galactose resulted in previous correlations conflicting. This reinforces the hypothesis that the 30-minute assay does not accurately capture what occurs during ice recrystallization compared to the 5-minute assay. The 30-minute assay involves neglecting the heterogeneity of the size of ice crystals and the time dependence of ice growth and measuring the compound's endpoint, which is not representative of inhibition during the timeframe. The 5-minute assay is more informative than the 30-minute assay about what transpires during ice recrystallization because it involves testing at multiple concentrations and measuring the ice crystal growth rate. Previous correlations of carbohydrates to hydration parameters must be re-examined with the differences in IRI activity for the simple monosaccharides.

2.2 Hydration Parameters and Ice Recrystallization Inhibition Activity

2.2.1 Precedent for Correlation Between Hydration Parameters and IRI Activity

The hydration parameters (i.e., hydration number, hydration index, and PMC) were previously found to be positively correlated to IRI activity by past Ben Lab member Dr. Roger Tam.[7] The 30-minute assay was utilized with the percent mean grain size (%MGS) as an indicator of IRI activity. In this section, these parameters will be reinvestigated and their relationship to IRI activity determined using the 5-minute assay.

2.2.2 Investigating a Correlation Between Hydration Number and IRI Activity

As discussed in Section 1.3.2, the hydration number is the number of water molecules closely bound to a carbohydrate molecule.[8] The correlation between hydration number and IRI activity (IC_{50} values) from the 5-minute assay is shown in Figure 3.3.

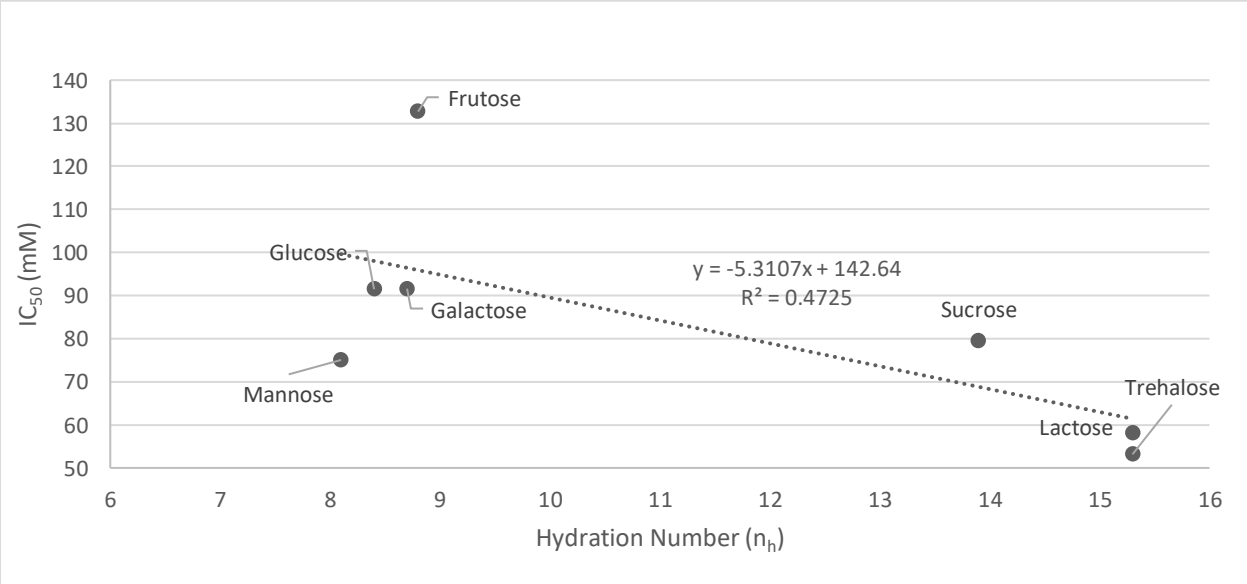

Figure 2.3 - Correlation of hydration number (n_h) of various monosaccharides and disaccharides values to IRI activity (IC_{50}).

The line of best fit has an R^2 of 0.4725, which is a poor correlation between IRI activity and hydration number. This is consistent with data shown by Dr. Roger Tam and is attributed to the differences in size between the carbohydrates and improves by categorizing the carbohydrates by their size, monosaccharides, and disaccharides (Figure 3.4).[7]

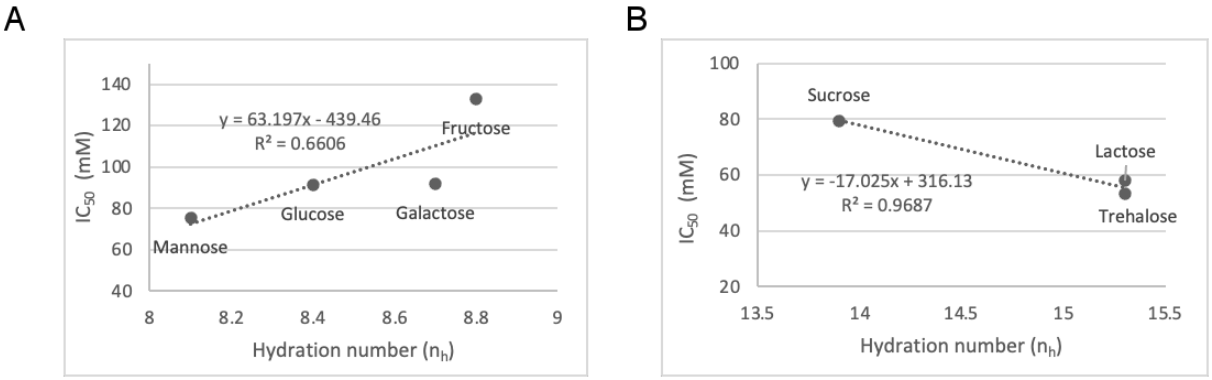

Figure 2.4 - Correlation of hydration number (n_h) with IRI activity (IC_{50}) for (A) monosaccharides and (B) disaccharides.

As seen in Figure 3.4, there is a poor correlation between IRI activity and hydration number with monosaccharides (R^2 = 0.6606). One of the contributing factors to the poor line of best fit is that D-galactose has a similar IRI activity level as D-glucose but possesses a higher hydration number. This was not predicted because it was theorized that a high hydration number is positively correlated with high IRI activity. For the disaccharides, the correlation cannot be justified due to there being essentially two points resulting from the IRI activity levels and hydration numbers of lactose and trehalose being similar in value. Additional disaccharides will need to be tested to determine if a correlation between hydration number and IRI activity exists. The line of best fit differs from a positive slope with monosaccharides to a negative slope

with disaccharides. This is a change from the previous studies, where monosaccharides and disaccharides exhibited a negative slope of best fit with %MGS.[5] This change was hypothesized to be a consequence of using IC_{50} values to measure IRI activity. The IC_{50} values represent the ice crystal growth rate, and %MGS is a measure of the size difference between the ice crystals. The hydration number is not consistent with previously-found correlations using IRI activity from the 5-minute assay. It can be hypothesized that the hydration number is not predictive of IRI activity measured by the rate of ice crystal growth.

2.2.3 Assessment of the Correlation between Hydration Index and IRI Activity

The hydration index is a hydration parameter utilized by the Ben Lab to describe the hydration of mono- and disaccharides simultaneously.[7] The hydration index is calculated as the hydration number divided by the molar volume of the carbohydrate.[7] Thus, the larger volume of disaccharides than monosaccharides is accounted for.

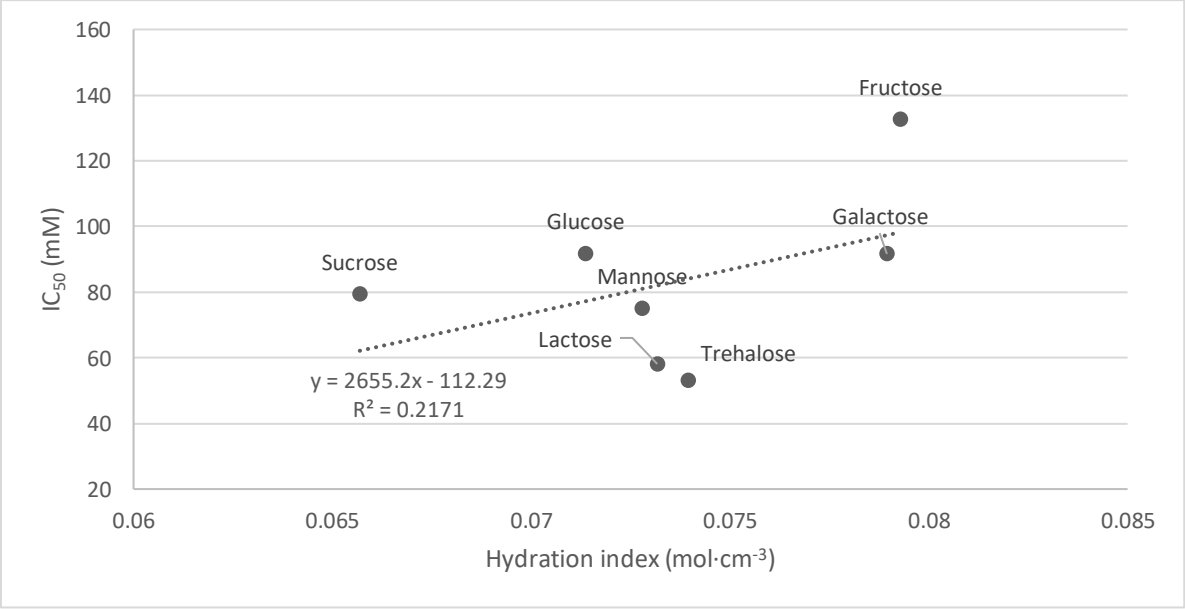

Figure 2.5 - Correlation of hydration index (hydration number/partial molar volume, mol·cm^{-3}) to IRI activity (IC_{50}) for various monosaccharides and disaccharides.

The correlation between hydration index and IRI activity of both monosaccharides and disaccharides calculated by Dr. Roger Tam illustrates a positive slope of best fit between hydration index and IRI activity.[7] When determining the correlation obtained using IC_{50} values, a negative slope is observed with a very poor line of best fit of $R^2 = 0.2171$ (Figure 3.5). The poor fit is attributed to several causes, the first being that the IRI activity of D-glucose and D-galactose are relatively similar in value to one another. There is a significant difference in hydration index between the two sugars that are not reflected in their IRI activity. The second reason is the high hydration index and IC_{50} value of fructose as it is an outlier. Trehalose also has a middling hydration index and the lowest IC_{50} value. As such, these alterations from previous work result in a poor correlation between IRI activity and hydration index.

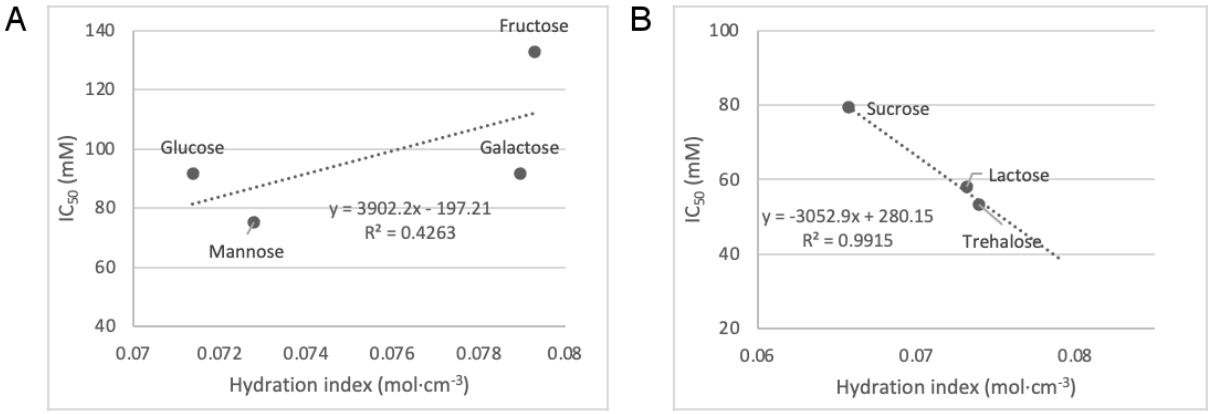

Figure 2.6 - Correlation of hydration index (hydration number/partial molar volume, mol·cm^{-3}) to IRI activity (IC_{50}) for various (A) monosaccharides and (B) disaccharides.

An improved fit (Figure 3.6) between hydration index and IRI activity is observed when monosaccharides ($R^2 = 0.4263$) and disaccharides ($R^2 = 0.9915$) are separated. The disaccharides have a good fit compared to the monosaccharides. The monosaccharides have a negative correlation with a poor line of best fit because of changes in IRI activity. This was not expected

because it was previously shown that both monosaccharides and disaccharides had positive correlations with hydration index to IRI activity.[7] For disaccharides, there is a positive correlation between hydration index and IRI activity whereby a high hydration index corresponds to high IRI activity, which is in line with the results of previous work. However, the hydration index can show a positive correlation with the IRI activity of both monosaccharides and disaccharides measured with %MGS, but this is not seen with IRI activity measured using IC_{50} values.[7] The hydration index is not an appropriate parameter to use with IC_{50} values because it cannot qualify monosaccharides and disaccharides in the same dataset due to the weak correlation for monosaccharides between IRI activity and hydration index. As such, it can be stated that the hydration index is not predictive of IRI activity for monosaccharides measured by the rate of ice crystal growth.

2.2.4 Assessment of the Correlation Between Partial Molar Compressibility and IRI Activity

PMC is the ability of the solvent in the outer hydration shell of a compound to compress.[9] Researchers have shown a poor correlation between the *C*-linked AFGP derivatives of D-mannose, D-galactose, D-glucose, and D-talose[5] and IRI activity, as seen in Section 1.3.2 and Figure 1.7. The conclusions from this study indicate the importance of the configuration of hydroxyl groups on carbohydrates and their effect on IRI activity.[10] This is theorized as to why D-galactose is observed as being more IRI active than D-glucose, as D-galactose's C-2 and C-4 hydroxyl groups are equatorial and axial, respectively. Using IC_{50} values instead of %MGS (Figure 3.7) illustrates differences in activity between the two assay methods. The IRI activities of D-galactose and D-glucose are similar in value, and D-mannose and fructose have IC_{50} values

that are not in agreement with those of the other carbohydrates. Thus, PMC is a poor predictor of IRI activity using the 5-minute assay.

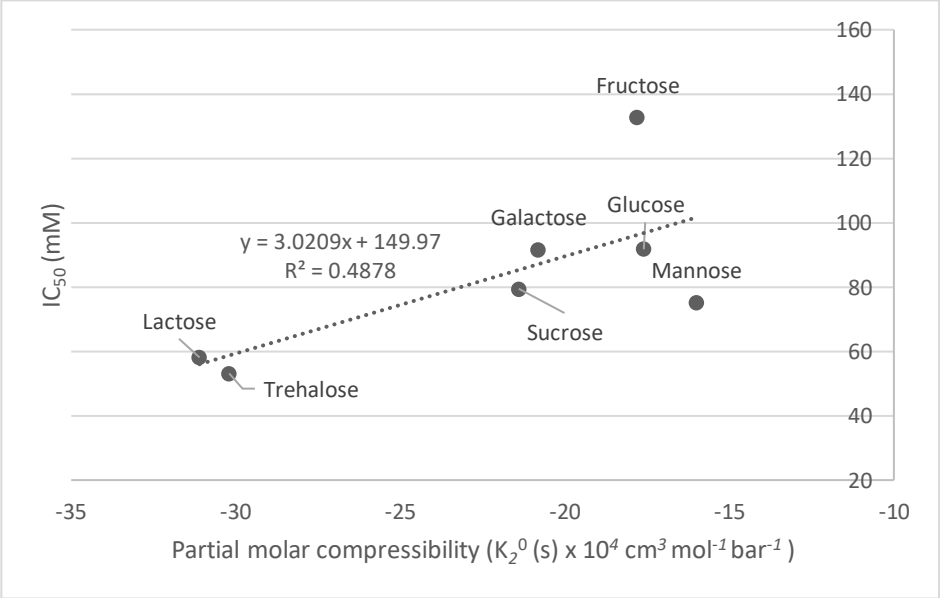

Figure 2.7 - Correlation between partial molar compressibility (K_2^0 (s) x 10^4 $cm^3 \cdot mol^{-1} \cdot bar^{-1}$) and IRI activity ($IC_{50}$) of various monosaccharides and disaccharides.

The hydration parameters (i.e., hydration number, hydration index, and PMC) are evaluated using IC_{50} values, and differences in correlation are seen compared to %MGS. The changes in IRI activity, especially for D-glucose and D-galactose, revealed that these hydration parameters are poorly correlated to IRI activity. These parameters are not ideal predictors for assessing IRI activity using IC_{50} as a measurement, and alternative parameters are needed.

2.3 Partition Coefficient Relationship to IRI Activity

2.3.1 Measurement of the Partition Coefficient (P)

The partition coefficient (P) is a measure of how hydrophilic or hydrophobic a compound is. The logarithm of this ratio is the logP.[11] This parameter is not well researched for carbohydrates, with only a few carbohydrates being investigated for their logP values. Because carbohydrates have been used to stabilize foods and biomolecules,[12] logP values can be utilized to determine the hydrophilicity/hydrophobicity of carbohydrates and their effects on IRI activity. IRI activity was previously found to be significantly positively correlated to the amphiphilic nature of carbohydrate derivatives.[13]

The experimental values for several carbohydrates have been previously calculated and used as benchmarks for computationally-derived logP values. The use of computational software is time- and cost-efficient in contrast to experimental methods. Experimentally-derived values will aid in determining the efficiency of software because carbohydrates cannot be investigated well using computational software. Mazzobre *et al.* experimentally calculated the logP values of various carbohydrates.[12] The logP values for D-glucose, sucrose, and trehalose were calculated to be -2.82 ± 0.04, -3.30 ± 0.03, and -3.77 ± 0.05 logP, respectively, at 20 °C (Table 3.2).[12]

Table 2.2 Experimentally calculated logP values of carbohydrates at 20 °C[12]

Carbohydrate	LogP value	Error
D-glucose	-2.82	± 0.04
sucrose	-3.30	± 0.03
trehalose	-3.77	± 0.05

Previous experiments on D-glucose and sucrose were conducted using 1-octanol and various aqueous mediums, such as a 0.05 M phosphate buffer. Radiochemical experiments done on D-glucose resulted in experimental logP values of -3.00 and -3.10, and for sucrose, they resulted in a range from -2.70 to -3.67. The range of values for sucrose is a result of temperatures not being cited in original papers and differences in the aqueous medium used. The logP of trehalose has not been previously reported experimentally. The logP values of glucose and sucrose obtained by Mazzobre[12] is in agreement with what was previously reported with accuracy to the temperature at which the test was performed. The experimental values calculated by Mazzobre[12] are used to determine the accuracy of the computational calculations.

2.3.2 Computational LogP Calculations

The computational calculation of logP values is advantageous due to costs and time efficiency. The computational methods grant convenient access to logP values for new drugs and large screening purposes.[14] The most commonly-used method is the "fractional constant" method, whereby a molecule is broken down into fragments, and the sum of the logP calculations from those fragments is to the logP value for the molecule.[15] The logP values for the fragments are determined by experimentally testing a small library of "training" molecules. Then they are used to predict the logP values of a "test" set of similar molecules.[12] The "fractional constant" method is limited to the molecules in the training library. The fractional constant may not represent the compound of interest if it includes "missing fragments" in the database.[16]

The "fractional constant" method was improved by the atom/fragment contribution (AFC) method that involves utilizing a correction factor.[15] The correction factor adjusts for bond angle, unsaturation versus saturation, conjugation, polar proximity, and other factors as necessary. AFC allows for the selection of simple atoms/fragments to avoid being limited by missing fragments.[15] AFC is currently being used by logP calculators, such as ALOGPS.[14]

2.3.3 Analysis of Computational Software

Some popular logP computational software includes Molinspiration's logP calculator (miLogP2.2), VCC Lab's ALOGPS 2.1,[14] and ACD Labs' Partition Coefficient Calculation (ACD/LogP).[17] This software uses similar fragment-based contributions and correction factors for calculating logP, and differences arise from specific training sets. For example, Molinspiration uses a training set of 12,000 drug-like molecules, VCC Labs' ALOGPS 2.1 uses 12,908 molecules from the PHYSPROP database,[18] and the ACD/LogP calculator uses a combination of three training set algorithms. The first is a >12,000 drug-like molecule set using a classic algorithm, the second is an 11,000-molecule set using an internally developed GALAS algorithm (which is a proprietary set that can be manipulated according to specific needs), and the third combines the first two to produce a complete >23,000 molecule training set.[19]

The logP values calculated in all three computational software programs were compared to the experimental values for D-glucose, trehalose, and sucrose (calculated by Mazzobre in Table 3.3) to identify the most accurate software.[12] The Molinspiration logP calculator was removed from consideration because of its calculation of trehalose and sucrose as being more lipophilic than experimentally calculated. The differences between the computational and experimental numbers from ACD Labs for D-glucose, trehalose, and sucrose were -0.94, -0.5,

and +0.18, respectively. The differences in ALOGPS 2.1 between the computational and experimental numbers for D-glucose, trehalose, and sucrose were -0.25, -0.81, and -0.67, respectively. Both ACD and VCC's computational software generally underestimate the affinity for the aqueous layer of the monosaccharides and disaccharides.

Table 2.3 LogP calculations using computational software Molinspiration's miLogP2.2, VCClab's ALOGPS,[17] ACD Lab's Partition Coefficient Calculation (ACD/LogP), and logP values obtained experimentally.[12]

Carbohydrate	logP Molinspiration	logP ALOGPS	logP ACD/Labs	Experimental[12]
D-Glucose	-2.64	-2.57	-1.88	-2.82
D-Fructose	-2.78	-1.79	-1.79	N/A
Trehalose	-4.30	-2.98	-3.29	-3.79
D-Galactose	-2.64	-2.57	-1.88	N/A
Sucrose	-3.75	-2.63	-3.48	-3.3
D-Mannose	-2.64	-2.57	-1.88	N/A
Lactose	-4.46	-3.01	-3.41	N/A

The differences between the software stem from the use of their algorithm and training sets. VCClab's ALOGPS was chosen as the computational software for sue in this study because it produces the most accurate experimental D-glucose, trehalose, and sucrose values. These are the computational calculated logP values that were used in the study.

2.4 Assessment of Log of Partition Coefficient Correlation to IRI Activity

The logP values of the monosaccharides and disaccharides were calculated using VCClab's program ALOGPS.[14] The simplified molecular-input line-entry system (SMILES) of the compounds is inputted into the Java-based software to receive the logP values for each compound (Table 3.4).

Table 2.4 Calculated LogP values of monosaccharides and disaccharides using VCClab's program ALOGPS.[18]

Carbohydrate	logP
D-Glucose	-2.57
D-Fructose	-1.79
D-Galactose	-2.57
D-Mannose	-2.57
Trehalose	-2.98
Sucrose	-2.63
Lactose	-3.01

The relationship between logP values calculated with VCClab's ALOGPS17 program and IRI activity is shown in Figure 3.8. There is a strong positive correlation between logP and IRI activity with an R^2 value of 0.9465. The correlation indicates that a low logP value positively corresponds to a low IC_{50} and, therefore, high IRI activity. Because a low logP equates to a high affinity for the aqueous phase, it can be hypothesized that IRI activity increases with an affinity for the aqueous phase. The disaccharides trehalose and lactose have the lowest logP values and highest IRI activities, with fructose having the highest logP values and the lowest determined IRI activity. Fructose is more highly-soluble than the other carbohydrates, and it can be theorized that it is well incorporated into bulk water.[20] Therefore, it cannot disrupt the QLL to the same

extent as the other carbohydrates.[10] As discussed in Section 1.5.1, it was hypothesized that carbohydrates reside in the bulk water layer and disrupt the QLL to inhibit ice recrystallization.[7]

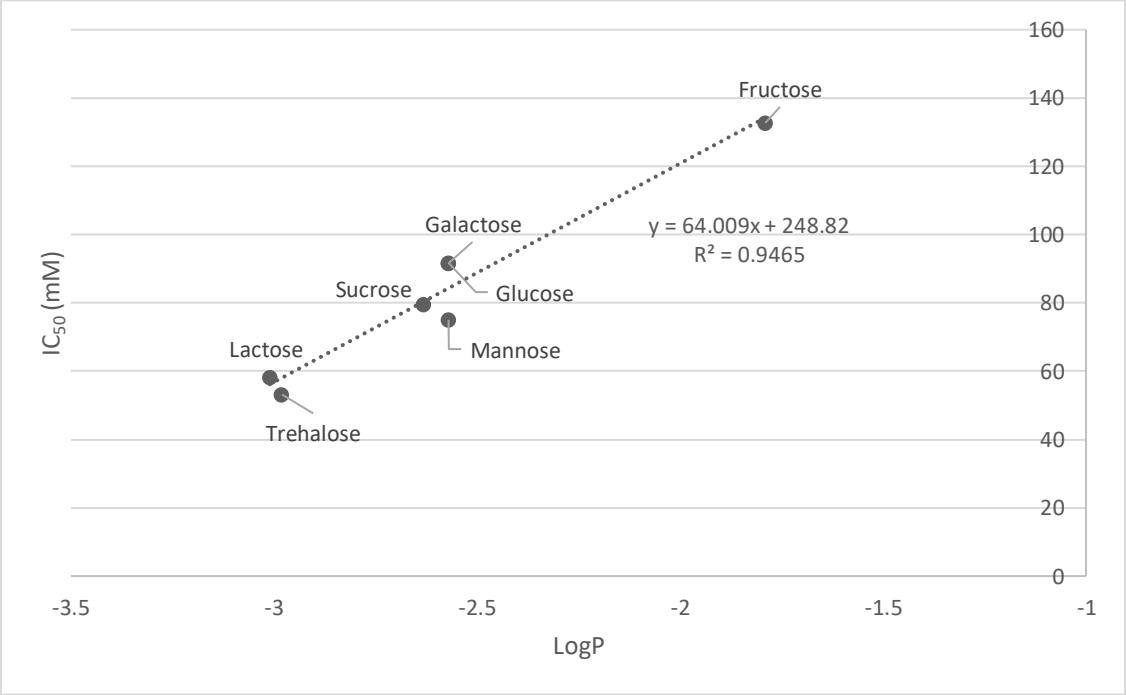

Figure 2.8 - Correlation of LogP calculated using VCClab's ALOGPS with IRI activity (IC_{50}) of monosaccharides and disaccharides.

Analyzing monosaccharides and disaccharides separately (Figure 3.9), it became evident that D-galactose, D-glucose, and D-mannose have the same logP value. This is caused by the program's inability to distinguish between axial/equatorial hydroxyl groups, resulting in carbohydrates sharing the same logP values. This is a complication because modifying axial/equatorial hydroxyl groups results in chemical, biological differences and and also differences in IRI activity independent of the method used to evaluate IRI activity. The inability of the software to distinguish between small configuration changes also applies to

disaccharides (i.e., lactose and trehalose) because lactose has a 1,4 β-linkage between a D-galactose and a D-glucose unit, and trehalose has a 1,1 α-linkage between two D-glucose units, but they have similar logP values (i.e., a difference of 0.03). The insensitivity to changes in linkage and hydroxyl positions was expected because computational software has not been well used with carbohydrates to study logP values.

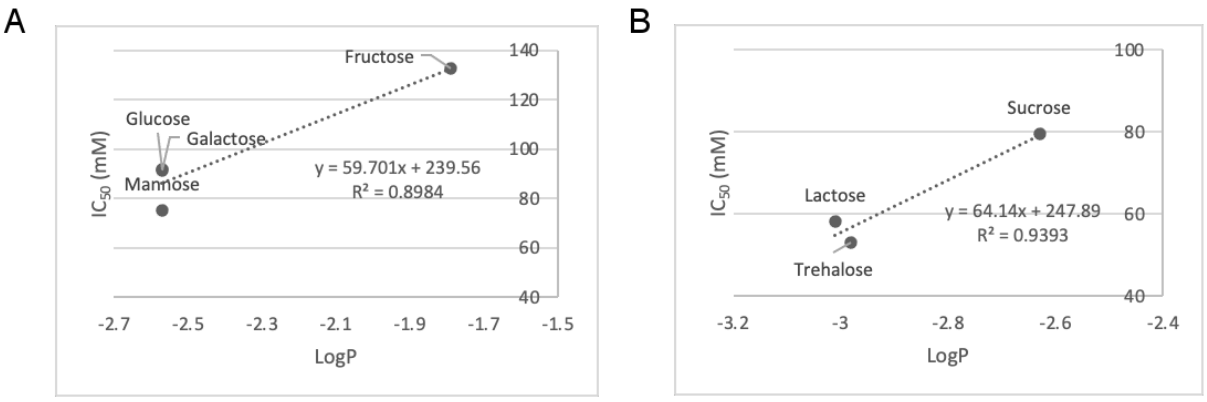

Figure 2.9 – Correlation of LogP calculated using VCClab's ALOGPS 2.1 to IRI activity (IC_{50}) of (A) monosaccharides and (B) disaccharides.

An R^2 value of 0.7884 was obtained through the incorporation of experimentally-derived logP values for D-glucose, sucrose, and trehalose (Figure 3.8) into the computational data. This was done because D-glucose would not have the same logP value as D-galactose and D-mannose. The inclusion of experimental logP values results in a lower fit than Figure 3.9 due to the mixture of experimentally- and computationally-derived logP values. The computationally-derived values are not accurate compared to the experimental values because of the factors discussed earlier, such as the inability to distinguish between axial and equatorial hydroxyl groups. As such, including both values results in one set of logP values that accounts for this difference.

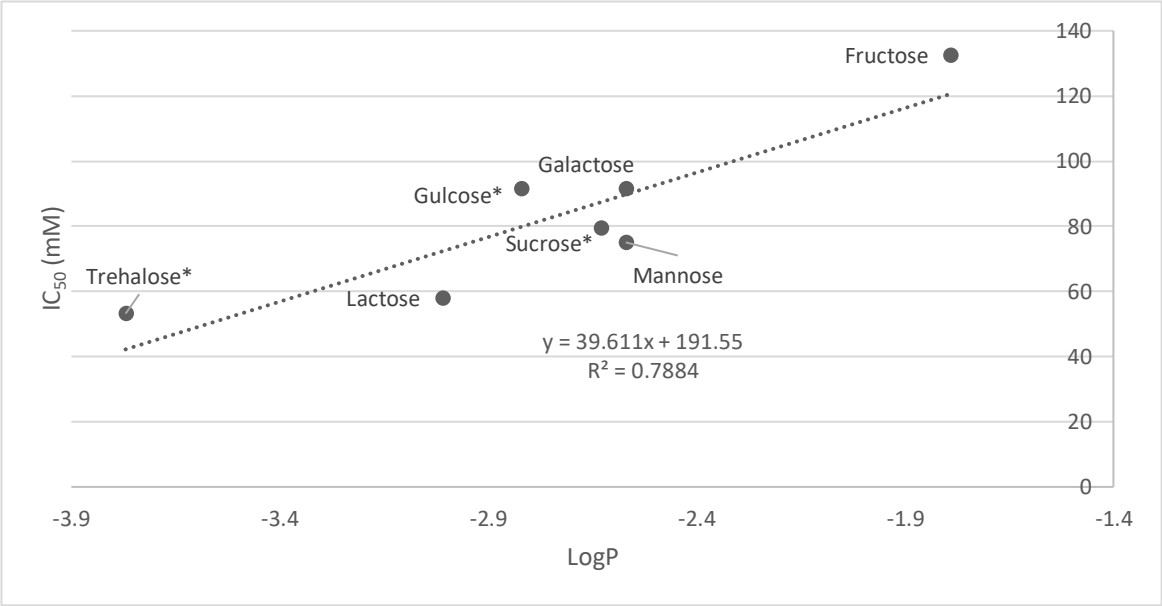

Figure 2.10 - Correlation of LogP calculated using VCClab's ALOGPS 2.1 to IRI activity (IC_{50}) of monosaccharides and disaccharides using experimental values for D-glucose, trehalose, and sucrose. Experimental values are indicated by *.

With the separation of carbohydrates into groups based on size, the fit between IRI activity and logP is similar to that in Figure 3.8. For the monosaccharides, the $R^2 = 0.7601$, and for disaccharides, the $R^2 = 0.7394$. The correlation between the carbohydrates grouped or separated by size remains consistent. This shows that it is possible to compare the logP and IRI activity of monosaccharides and disaccharides on the same axis, which is one advantage of using the hydration index. However, the hydration index did not display a strong positive correlation to IRI activity measured with the 5-minute assay.

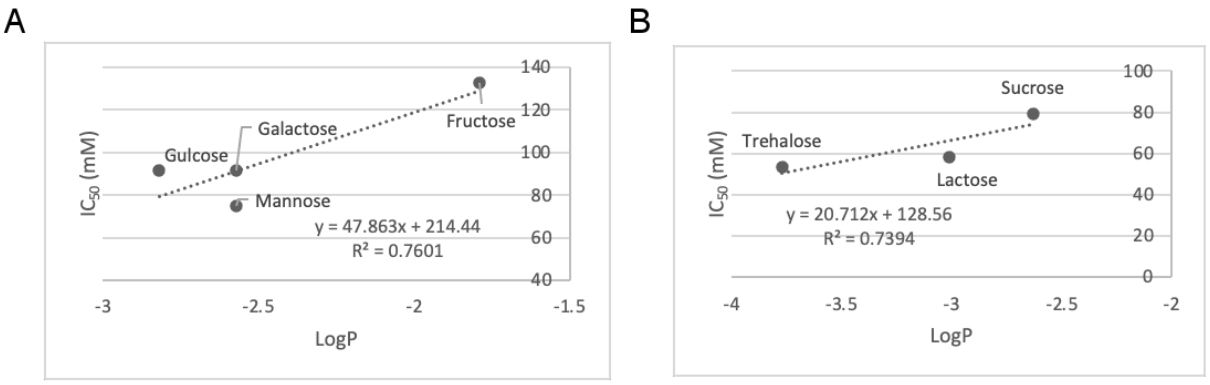

Figure 2.11 - Correlation of LogP calculated using VCClab's ALOGPS 2.1 to IRI activity (IC_{50}) of (A) monosaccharides and (B) disaccharides using experimental values for D-glucose, trehalose, and sucrose. Experimental values are indicated by *.

As both monosaccharides and disaccharides can be analyzed on the same axis, logP is the desired hydration parameter. LogP exhibited a stronger correlation to IRI activity from the 5-minute assay than the previously-correlated hydration parameters (i.e., hydration number, hydration index, and PMC). Thus, the rate of ice crystal growth can be hypothesized to have a strong correlation to logP.

The inaccuracy of computational logP calculations is a challenge that needs to be addressed before computational studies can be utilized with carbohydrates. The current training sets used by computational software are not suitable for use for carbohydrates. The training sets cannot distinguish between differences in stereochemistry of hydroxyl groups from axial to equational or changes in the linkage between carbohydrates for disaccharides. There is a general overestimate of the lipophilicity of carbohydrates that results in high logP values. Computational software gives a range of logP values for carbohydrates, such as ACD/LogP assigning D-glucose a logP of -1.88 while VCClab's ALOGPS[18] assigns it a logP of -2.57.

Computational software does not agree with the experimental logP values for carbohydrates, and there is a need for additional experimental data to enable researchers to make accurate calculations. As of now, it is not possible to use logP as a predicator of IRI activity due to insufficient experimental data.

2.5 Chapter Summary

In summary, the correlation between IRI activity and hydration parameters (hydration number, hydration index, PMC, and logP) was explored. The IRI activity measured using IC_{50} values was found to have a poor correlation with hydration number, hydration index, and PMC compared to logP. The fit of specific hydration parameters (i.e., hydration number and hydration index) did not correlate with IRI activity to the same degree as the 30-minute assay, displaying a poor correlation when using the 5-minute assay. The change to using IC_{50} as a measure of IRI activity results in past correlation data being unrepresentative and unable to accurately predict activity. It was hypothesized that ice crystal growth rate is positively correlated to logP, and further research is required. Additional work is necessary in this field because experimental logP values are missing in the literature for several carbohydrates. Currently, computational software cannot account for differences in hydroxyl group positioning and linkages. Further experimental data can allow for complete training sets to be created that can be used to predict logP values for complex and substituted carbohydrate derivatives.

2.6 References

(1) Corzana, F.; Busto, J. H.; Jiménez-Osés, G.; de Luis, M. G.; Asensio, J. L.; Jiménez-Barbero, J.; Peregrina, J. M.; Avenoza, A. Serine versus Threonine Glycosylation: The Methyl Group Causes a Drastic Alteration on the Carbohydrate Orientation and on the Surrounding Water Shell. *Journal of the American Chemical Society* **2007**, *129* (30), 9458–9467. https://doi.org/10.1021/ja072181b.

(2) Franks, F. Solute—Water Interactions: Do Polyhydroxy Compounds Alter the Properties of Water? *Cryobiology* **1983**, *20* (3), 335–345. https://doi.org/10.1016/0011-2240(83)90022-6.

(3) Yang, G.; Zhang, A.; Xu, L. X. Experimental Study of Intracellular Ice Growth in Human Umbilical Vein Endothelial Cells. *Cryobiology* **2009**, *58* (1), 96–102. https://doi.org/10.1016/j.cryobiol.2008.10.123.

(4) Abraham, S.; Keillor, K.; Capicciotti, C. J.; Perley-Robertson, G. E.; Keillor, J. W.; Ben, R. N. Quantitative Analysis of the Efficacy and Potency of Novel Small Molecule Ice Recrystallization Inhibitors. *Crystal Growth and Design* **2015**, *15* (10), 5034–5039. https://doi.org/10.1021/acs.cgd.5b00995.

(5) Czechura, P.; Tam, R. Y.; Dimitrijevic, E.; Murphy, A. v.; Ben, R. N. The Importance of Hydration for Inhibiting Ice Recrystallization with C-Linked Antifreeze Glycoproteins. *Journal of the American Chemical Society* **2008**, *130* (10), 2928–2929. https://doi.org/10.1021/ja7103262.

(6) Stoll, C.; Holovati, J. L.; Acker, J. P.; Wolkers, W. F. Synergistic Effects of Liposomes, Trehalose, and Hydroxyethyl Starch for Cryopreservation of Human Erythrocytes. *Biotechnology Progress* **2012**, *28* (2), 364–371. https://doi.org/10.1002/btpr.1519.

(7) Tam, R. Y.; Ferreira, S. S.; Czechura, P.; Ben, R. N.; Chaytor, J. L. Hydration Index-a Better Parameter for Explaining Small Molecule Hydration in Inhibition of Ice Recrystallization. *Journal of the American Chemical Society* **2008**, *130* (51), 17494–17501. https://doi.org/10.1021/ja806284x.

(8) Galema, S. A.; Høiland, H. Stereochemical Aspects of Hydration of Carbohydrates in Aqueous Solutions. 3. Density and Ultrasound Measurements. *Journal of Physical Chemistry* **1991**, *95* (13), 5321–5326. https://doi.org/10.1021/j100166a073.

(9) Galema, S. A.; Høiland, H. Stereochemical Aspects of Hydration of Carbohydrates in Aqueous Solutions. 3. Density and Ultrasound Measurements. *Journal of Physical Chemistry* **1991**, *95* (13), 5321–5326. https://doi.org/10.1021/j100166a073.

(10) Tam, R. Y.; Rowley, C. N.; Petrov, I.; Zhang, T.; Afagh, N. A.; Woo, T. K.; Ben, R. N. Solution Conformation of C-Linked Antifreeze Glycoprotein Analogues and Modulation of Ice Recrystallization. *Journal of the American Chemical Society* **2009**, *131* (43), 15745–15753. https://doi.org/10.1021/ja904169a.

(11) Johnson, M. E.; Blankschtein, D.; Langer, R. Evaluation of Solute Permeation through the Stratum Corneum: Lateral Bilayer Diffusion as the Primary Transport Mechanism. *Journal of Pharmaceutical Sciences* **1997**, *86* (10), 1162–1172. https://doi.org/10.1021/js960198e.

(12) Mazzobre, M. F.; Román, M. v.; Mourelle, A. F.; Corti, H. R. Octanol–Water Partition Coefficient of Glucose, Sucrose, and Trehalose. *Carbohydrate Research* **2005**, *340* (6), 1207–1211. https://doi.org/10.1016/j.carres.2004.12.038.

(13) Capicciotti, C. J. The Rational Design of Potent Ice Recrystallization Inhibitors for Use as Novel Cryoprotectants, 2014.

(14) Tetko, I. v.; Bruneau, P. Application of ALOGPS to Predict 1-Octanol/Water Distribution Coefficients, LogP, and LogD, of AstraZeneca in-House Database. *Journal of Pharmaceutical Sciences* **2004**, *93* (12), 3103–3110. https://doi.org/10.1002/jps.20217.
(15) Meylan, W. M.; Howard, P. H. Atom/Fragment Contribution Method for Estimating Octanol–Water Partition Coefficients. *Journal of Pharmaceutical Sciences* **1995**, *84* (1), 83–92. https://doi.org/10.1002/jps.2600840120.
(16) Leo, A. J. Hydrophobic Parameter: Measurement and Calculation; **1991**; pp 544–591. https://doi.org/10.1016/0076-6879(91)02027-7.
(17) Kolovanov, E. ACD / Log P Method Description ACD / Log P Method Description. **2014**, No. May, 99–116.
(18) Tetko, I. v.; Tanchuk, V. Y. Application of Associative Neural Networks for Prediction of Lipophilicity in ALOGPS 2.1 Program. *Journal of Chemical Information and Computer Sciences* **2002**, *42* (5), 1136–1145. https://doi.org/10.1021/ci025515j.
(19) Walker, M. J. Training ACD/LogP with Experimental Data. *QSAR and Combinatorial Science* **2004**, *23* (7), 515–520. https://doi.org/10.1002/qsar.200410010.
(20) Gharsallaoui, A.; Rogé, B.; Génotelle, J.; Mathlouthi, M. Relationships between Hydration Number, Water Activity and Density of Aqueous Sugar Solutions. *Food Chemistry*. **2008**, pp 1443–1453. https://doi.org/10.1016/j.foodchem.2007.02.047.

Chapter 3: Investigating the Importance of Functionalizing the C-3 Position on Glucosides and the Effect of Doing so on IRI Activity

3.1 Introduction

The position of substituents on carbohydrate derivatives plays an essential role in determining their IRI activity levels.[1] The hydrogen bond donating and accepting abilities of the hydroxyl groups are considered to be necessary for determining IRI activity.[2] The positions of C-2, C-3, C-4, and C-6 (Figure 4.1) were investigated by previous Ben Lab student Dr. Jennifer Chaytor for their role in hydrogen bonding and effects on IRI activity.[3] The hydroxyl groups on an α-*C*-allyl galactose were methylated. The methyl groups are hydrogen bond acceptors but not hydrogen bond donors.[4]

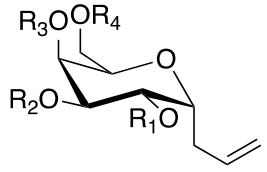

14: R_1= H R_2=R_3=R_4= H
28: R_1= Me R_2=R_3=R_4= H
29: R_2= Me R_1=R_3=R_4= H
30: R_3= Me R_1=R_2=R_4= H
31: R_4= Me R_1=R_2=R_3= H

Figure 3.1 - Methylated α-*C*-allyl derivatives tested for IRI activity.

The study described above concluded that methylated *C*-allyl galactose derivatives are less active IRIs than the parent *C*-allyl derivative.[5] The derivatives (**28**-**31**) have a %MGS that is relative to PBS between 85 and 90%, which is high compared to 60% of the parent *C*-allyl derivative (**14**) at 22 mM and illustrates the importance of hydrogen bonding on IRI activity.[5]

The Ben Lab has also investigated how the functionalization of hydroxyl groups on D-glucose affects IRI.[6] There has been an emphasis at the C-1 hydroxyl position with frequent modifications occurring at C-6.[7] Functionalization at C-6 results in poor IRI activity compared to the D-glucose and C-1 derivative. Dr. Capicciotti investigated the C-1 and C-6 positions (Figure 4.2) with the synthesis of 6-*O*-(4-methoxyphenyl)-β-D-glucopyranoside (**2**), and the %MGS at 22 mM was calculated to be 82%, which is high compared to a %MGS of 23% for 4-methoxyphenyl-β-D-glucopyranoside (**52**). The *p*-methoxyphenyl (PMP) group was moved from the C-1 to the C-6 position, resulting in reduced IRI activity. The C-6 position is, therefore, important for IRI activity because modification leads to a reduction in IRI activity.

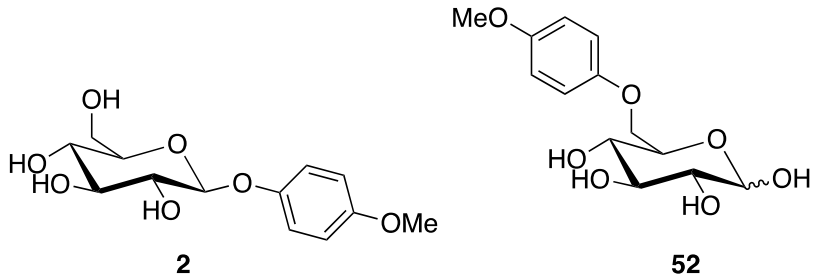

Figure 3.2 - C-1 functionalized glucose derivative **2** and C-6 functionalized glucose derivative **52**, investigated for the effect of functionalization at the C-6 position on IRI activity.

The C-3 and C-4 positions are of interest for potential functionalization. Bols and coworkers[8] reported that the C-3 hydroxyl group has the highest electron density and is more reactive than C-4. However, functionalization at C-3 has not been tested in past studies due to the complex synthetic pathway requiring protecting group manipulation to functionalize C-3 selectively compared to C-1 and C-6. The synthetic route is difficult for C-3. In contrast, the C-2 and C-4 synthetic routes are highly complex. We hypothesized that the C-3 position may influence IRI activity. Thus, we propose that the C-3 hydroxyl group will be functionalized and

compared to its counterpart C-1 functionalized derivatives, as seen in Figure 4.3. The comparison is required to form the basis for the functionalized C-3 compounds to assess solubility and IRI activity. The substituents added to C-1 will be identical to those added to C-3.

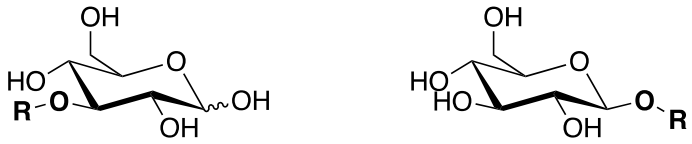

Figure 3.3–C-3 functionalized glucoside (left) and C-1 functionalized glucoside (right).

The objectives of this chapter are as follows:

1) Synthesize derivatives of D-glucose in which the C-3 position is functionalized and assess the effect of functionalization on IRI activity.
2) Synthesize derivatives of D-glucose in which the C-1 position is functionalized to compare solubility and IRI activity to the 3-*O* functionalized derivatives.

3.2 Influence of Functionalizing the C-3 Position on IRI Activity

Modifying the C-3 hydroxyl group is a challenge due to the reactivity of the C-1 and C-6 hydroxyl groups.[9] It is necessary to use protecting groups to facilitate selective functionalization of the C-3 position, as prepared in Figure 4.4.

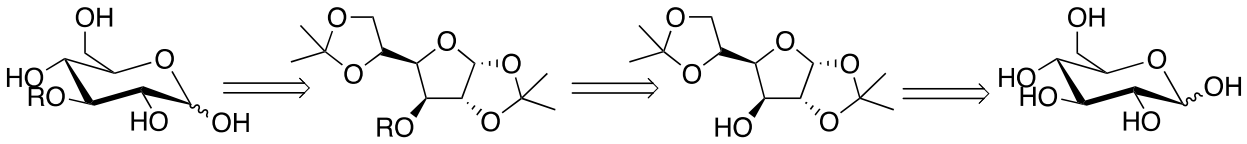

Figure 3.4 - Retrosynthesis of 3-*O*-glucoside analogs.

The substituents explored were benzyl, 4-bromobenzyl, 4-fluorobenzyl, propene, and methyl (Figure 4.5). These substituents were chosen because there is precedent in previous studies done by Dr. Capicciotti.[7] The benzyl derivative was previously shown to be moderately active, and there is a precedent for adding halogens for increased IRI activity.[7] The methyl derivative, 3-O-Methyl glucose (3-OMG), is used as a cryoprotectant in preserving primary rat hepatocytes.[10] 3-OMG and 1-*O*-methyl-α-D-glucose (1-OMG) are commercially available. The substituents will also be added to C-1 for comparison, except for 4-fluorobenzyl, because the synthesis could not be performed due to time restrictions.

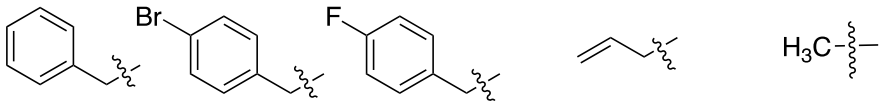

Figure 3.5 - Substituents to be added to C-3 and C-1.

3.2.1 Synthesis of 3-*O*-glucosides and 1-*O*-glucosides Analogs

The synthesis of the C-3 derivatives (see Scheme 4.1) starts with the D-glucose. Using anhydrous copper (II) sulfate and a catalytic amount of sulfuric acid dissolved in acetone leads

to diacetone glucose (**402**) in a 50% yield. Selective functionalization can then occur at the free hydroxyl at the C-3 position. Functionalization requires the use of a base (NaH) and the desired electrophiles (i.e., a benzyl bromide or an allyl bromide derivative). An S_N2-like reaction occurs, yielding the products **403**–**406**. Finally, the deprotection of the sugar by dissolving it in 10% acetic acid in water and heating it at 80 °C overnight produces the final deprotected products **407**–**410** with moderate yields of 68–80%. The methyl derivative 3-*O*-methyl-D-glucose (3-OMG) is readily available from commercial sources.

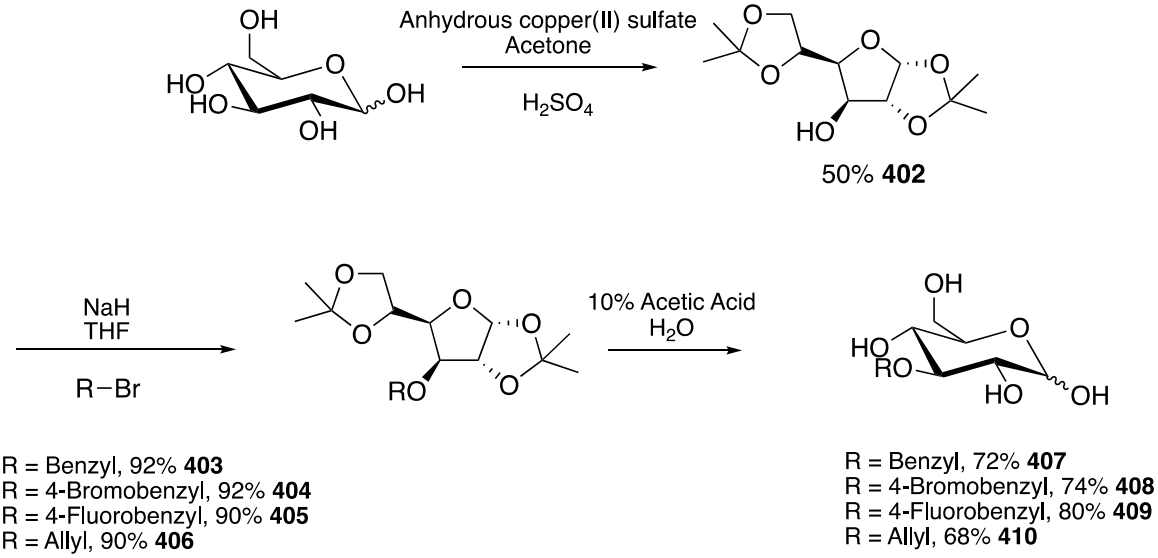

Scheme 3.1 Synthesis of 3-*O* functionalized glucosides (**407–409**).

The synthesis of the C-1 derivatives is based on the synthesis of the *O*-linked aryl glucosides (Scheme 4.2).[11] Starting with the peracetylated compound **401,** the addition of boron trifluoride diethyl etherate ($BF_3{\cdot}OEt_2$) and the desired benzyl alcohol or allyl alcohol to give **412**–**414** in low to moderate yields 32–60%. The final step is deprotection using Zemplén deacetylation conditions to produce **415**–**417** in good yields (i.e., 90–92%).[12] The methyl derivative 1-*O*-Methyl-α-D-glucose (1-OMG) is readily available from commercial sources.

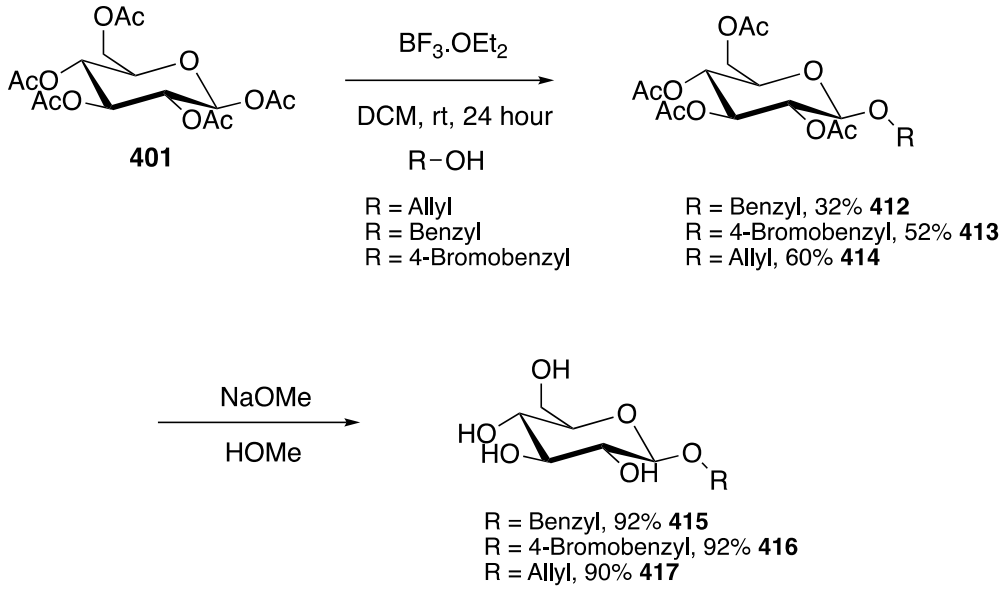

Scheme 3.2 Synthesis of 1-*O* glucoside compounds (**415–417**).

3.2.2 Assessment of Solubility and IRI Activity of 3-O-glucoside and 1-O-glucoside Analogs

The 3-*O* (Figure 4.6) and 1-*O* compounds (Figure 4.7) were assessed for solubility and IRI activity. The maximum solubility of the 3-*O* compounds (**407**, **408**, **409**, **410**) and 3-*O*-Methyl-D-glucose (3-OMG) were found to be 5 mM, 41 mM, 100 mM, 30 mM, and 500 mM, respectively. The maximum solubility levels of 1-*O* compounds (i.e., **415**, **416**, **417**) and 1-*O*-Methyl-α-D-glucose (1-OMG) were found to be 50 mM, 60 mM, 100 mM, and > 1,000 mM, respectively. Overall, the solubility values of compounds **407**–**410** and **415**–**417** are poor. Therefore, a proper dose-response curve that can produce IC_{50} values cannot be generated.

As such, the IRI activity of these compounds is assessed using the percent mean grain size (%MGS) relative to PBS using the 5-minute assay. The IC_{50} is the concentration of a compound required to achieve 50% activity, while the %MGS value is an assessment of the IRI activity at a single time point and concentration, as stated in Section 1.4. The IC_{50} is determined

using multiple concentrations. The %MGS describes the IRI activity of these compounds at their maximum concentration using the 5-minute assay.

The %MGS values of 3-*O* compounds **407**, **408**, **409**, and **410** were calculated to be 92%, 68%, 43%, and 57%, respectively, at their respective maximum solubilities (see Table 4.1). The IC_{50} value of 3-OMG was found to be 99 mM. The %MGS value of **415**, **416**, and **417** were calculated to be 59%, 66%, and 61%, respectively, at their respective maximum solubilities (see Table 4.1). The IC_{50} value of 1-OMG was found to be 194 mM.

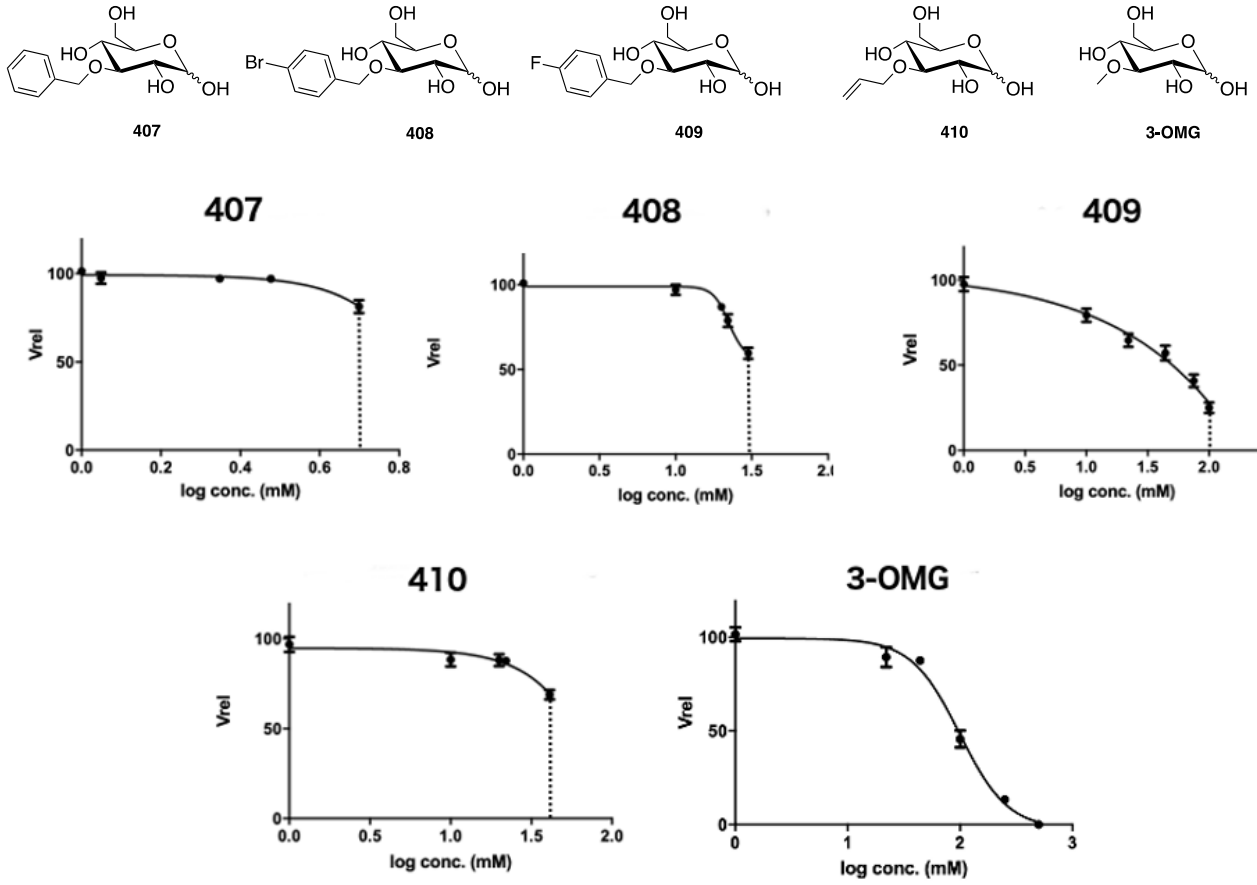

Figure 3.6 - Dose-response curve for IRI activity of 3-*O* glucosides analogs, the average crystal growth rate (V_{rel}) is normalized to PBS. The standard error of the mean (SEM) is represented by the error bars. A four-parameter sigmoidal curve is fit to the data. The dotted line represents maximum solubility.

Table 3.1 Comparison of maximum solubility and IRI activity of 3-*O* glucoside and 1-*O* glucoside compounds.

	3-*O*			1-*O*		
Functionalization		Maximum solubility	%MGS		Maximum solubility	%MGS
Benzyl	**407**	5 mM	92%	**415**	50 mM	59%
para-Bromo-benzyl	**408**	41 mM	68%	**416**	60 mM	66%
para-Fluoro-benzyl	**409**	100 mM	43%		N/A	N/A
Allyl	**410**	30 mM	57%	**417**	100 mM	61%
Methyl		500 mM	IC_{50} = 91		>1,000 mM	IC_{50} = 194

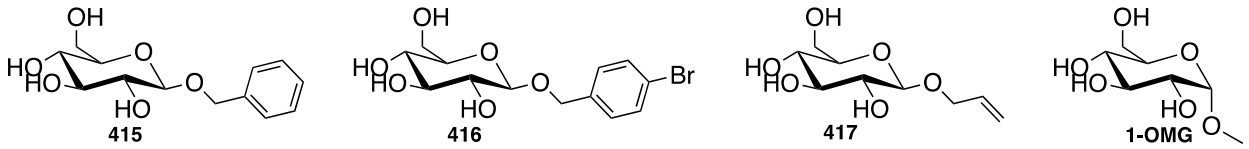

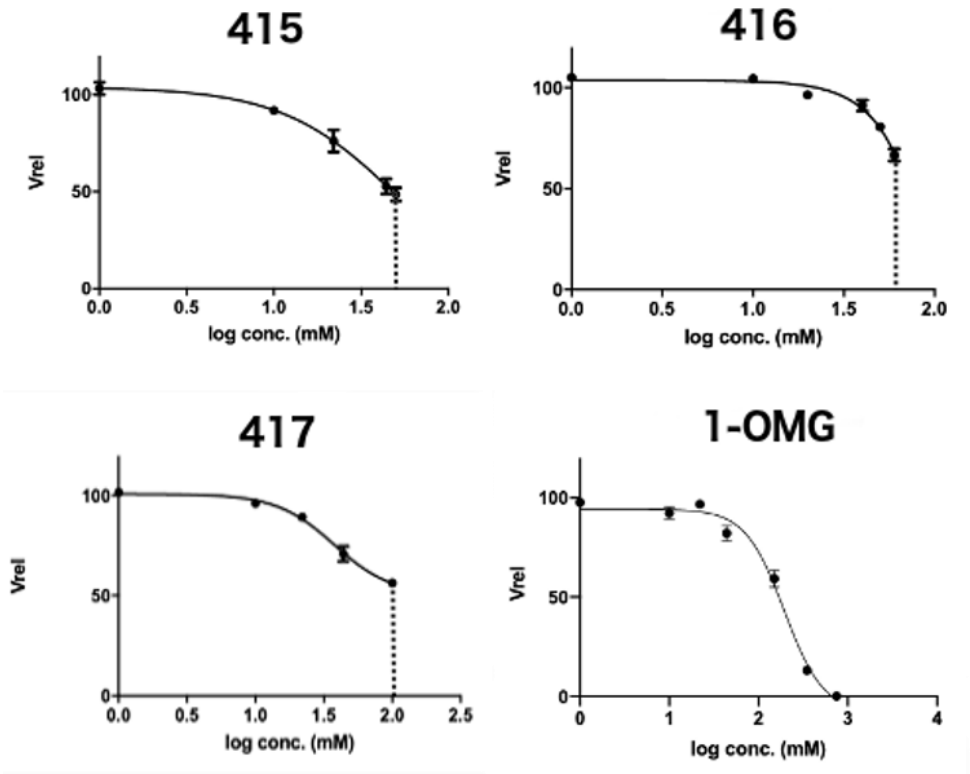

Figure 3.7 - Dose-response curve for IRI activity of 1-*O* glucoside compounds, the average crystal growth rate (V_{rel}) is normalized to PBS. The standard error of the mean (SEM) is represented by the error bars. A four-parameter sigmoidal curve is fit to the data. The dotted line represents max solubility.

The 3-O and 1-O compounds tested are all ineffective inhibitors of ice recrystallization and poorly soluble. The solubility of 3-*O* benzyl derivative **407** is poor and has insufficient IRI activity with a %MGS of 92% at its maximum solubility of 5 mM. The low solubility of **407** is hypothesized to be due to steric hindrance affecting the hydrogen bonding of the C-2 and C-4 hydroxyl groups. The ability of the C-2 and C-4 hydroxyl groups to hydrogen bond is essential in hydration and the three dimensional fit of carbohydrates in water.[1]

The functionalized 3-*O* benzyl derivatives **408** and **409** consist of a *para*-halogen (bromide and fluoride, respectively) on the benzyl ring. With the addition of a halogen, the solubility of both compounds increases compared to that of **407**. The change in solubility was not expected because a similar effect is not seen with phenyl-β-D-glucopyranoside with the addition of the halogen.[11] The %MGS values (at the maximum solubility) of **408** and **409** are 68% at 41 mM and 43% at 100 mM, respectively. The IRI activity values of the two halogens cannot be directly compared because the %MGS values are calculated at different concentrations. The change in solubility with **408** and **409** is thought to be linked to the increase in electronegativity of the halogens. A similar effect is seen with C-1 phenyl derivatives.[13] The halogens (i.e., bromide, fluoride, and iodide) attached to the para-position of the phenyl have increased solubility with increased electronegativity. 4-fluorophenyl-β-D-glucopyranoside, 4-bromophenyl-β-D-glucopyranoside, and 4-iodophenyl-β-D-glucopyranoside have maximum solubilities of 100 mM, 55 mM, and 10 mM, respectively (Table 4.2).[14] However, this trend was not expected because it is thought that increasing electronegativity will result in a reduction in solubility because the lone pairs of the halogens are held closely to the nucleus.[15]

Therefore, it is hypothesized that the hydrogen bonding of halogens is correlated with electronegativity and that high electronegatively results in high hydrogen bonding.[15]

Table 3.2 - Solubilities of halogen substituents on 3-*O* benzyl compared to 1-*O* phenyl

Halogen	3-*O* (Benzyl)	1-*O* (Phenyl)
F	100 mM	100 mM
Cl	N/A	75 mM
Br	41 mM	55 mM
I	N/A	10 mM

The 3-*O* allyl compound **410** has a %MGS of 57% at its maximum solubility of 30 mM. The unsaturated substitution at the hydroxyl of C-3 results in a poorly soluble compound and poor IRI activity. β-*C*-allyl glucose has a %MGS of 76% at 22 mM and similar IRI activity to **410**. The maximum solubility of β-*C*-allyl glucose has not been tested. The similarity in IRI activity at 22 mM reflects that the activity is not significantly changed by shifting the allyl substituent from C-1 to C-3.

The short allyl chain is hypothesized to be inadequate in length to benefit from the hydrophobic characteristics, and a longer chain could improve the IRI activity. The partition coefficient parameter is valuable in quantifying the hydrophilicity and hydrophobicity of a compound, as discussed in Chapter 3.[16] IRI active compounds with long alkyl chains, such as *N*-octyl-β-D-galactoside,[17] have computational logP values of 1.13 when calculated using ALOGPS 2.1 software,[18] which is high in contrast to the logP of compound **410** of -1.60.

3-OMG has an IC_{50} of 99 mM and a maximum solubility of 500 mM. The relatively high solubility could result from the lower hindrance of C-2 and C-4 hydrogen bonding due to the smaller volume of the methyl group compared to the other tested substituents. 3-OMG has an

IRI activity level similar to D-glucose, with IC_{50} values of 91 mM and 92 mM, respectively. These results indicate that the methylation of C-3 does not result in a drastic change in IRI activity. The methyl groups act as hydrogen bond acceptors but not hydrogen bond donors. The similarity in activity could mean that hydrogen bond donating at the C-3 position is unnecessary for IRI activity.

The 1-*O* benzyl derivative **415** has a maximum solubility of 55 mM with a %MGS of 59%. This is the least soluble compound of the 1-*O* compounds and is hypothesized to have poor IRI activity for the same reasons as the 3-*O* compound. The solubility does not improve with the addition of the bromide at the *para*-position because **416** has a maximum solubility of 60 mM. Compound **416** has a %MGS of 66% at its maximum concentration and similar IRI activity to **415**. This was not expected because we theorized that the addition of the bromide would increase solubility and change IRI activity, as was seen with the 3-*O* compounds.

The 1-*O* allyl compound **417** had a maximum solubility of 100 mM but could not produce a dose–response curve as with the 3-*O* allyl compound **410**. The poor IRI activity of **417** is thought to be due to similar reasons as the low IRI activity of **410**. β-*C*-allyl glucose has a %MGS of 76% at 22 mM and is more IRI-active than the *O*-linked compound **417**. *C*-linked compounds have been previously shown to be IRI active molecules due to their ability to result in micelle formation.[2] 1-OMG has an IC_{50} of 194 mM and maximum solubility of >1,000 mM. 1-OMG has lower IRI activity than D-glucose, which has an IC_{50} of 92 mM. The methylation of the C-1 position resulted in low IRI activity, and it is evident that the C-1 position is vital in determining IRI activity from previous studies.[7] The C-1 position is anomeric oxygen and is essential for activity.[7] The modification of this position could lead to a reduction in IRI activity,

depending on the substituent. It was previously shown with *N*-octyl-β-D-galactoside[17] that long alkyl chains result in sufficient IRI active compounds with poor solubility.

3.2.3 Comparison of Solubility and IRI Activity of 3-O-glucoside and 1-O-glucoside Analogs

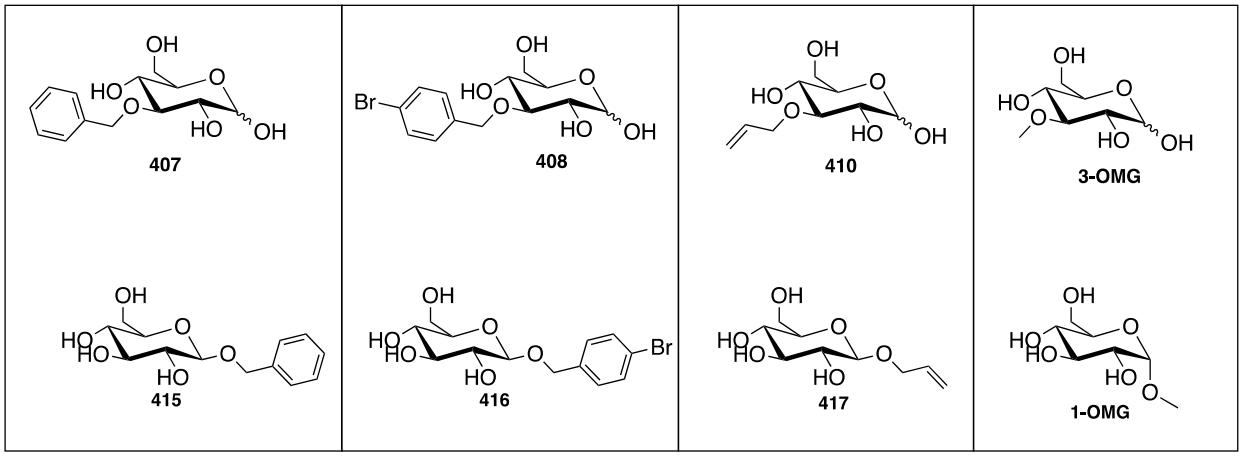

Figure 3.8 - Structure of 3-*O* compounds and 1-*O* compounds for comparison of their IRI activity and solubility.

The least active of the 3-*O* glucoside compounds is 3-*O*-benzyl-D-glucopyranoside (**407**), with a %MGS of 92%, and the most active is 3-*O*-*para*-fluorobenzyl-D-glucopyranoside (**411**), with a %MGS of 43% (Table 4.3). This was not reflected with the 1-*O* glucosides because the (4-bromophenyl)methyl-β-D-glucopyranoside (**416**) was the least active compound, with a %MGS of 66%, and benzyl-β-D-glucopyranoside (**415**) was the most active compound, with a %MGS of 59%. The range of activities for the 3-*O* compounds is notable compared to the range of the 1-*O* compounds. The 3-*O* compounds vary significantly in IRI activity with %MGS values of 66–92%, while the 1-*O* compound %MGS values vary between 59 and 66%. This suggests that the 3-*O* position is more sensitive to change than the 1-*O* compounds.

Table 3.3 - Comparison of solubilities between 3-*O* and 1-*O* glucosides

	3-*O*		1-*O*	
Functionalization		Maximum solubility		Maximum solubility
Benzyl	**407**	5 mM	**415**	50 mM
para-Bromo-benzyl	**408**	41 mM	**416**	60 mM
para- fluoro-benzyl	**409**	100 mM		N/A
Allyl	**410**	30 mM	**417**	100 mM
Methyl		500 mM		>1,000 mM

407–**410** and 3-OMG exhibited lower solubility than their corresponding 1-*O* compounds (**415**–**417** and 1-OMG), as seen in Table 4.3. There is a magnitude of difference between the solubilities, except for the *para*-bromo benzyl derivatives. The C-2 and C-4 hydroxyl groups are essential in hydration for the fit of the carbohydrate in solution.[1] The C-3 functionalization was hypothesized to hinder the hydrogen bonding of these hydroxyl groups, resulting in poor solubility.[1]

The benzyl derivatives for the 3-*O* and 1-*O* compounds followed the same trend of the solubilities increasing with the addition of the halogen onto the benzyl ring. The 3-*O* benzyl compound **407** has a maximum solubility of 5 mM, and the *para*-bromo-benzyl derivative **408** has a maximum solubility of 41 mM. This value was compared to 50 mM for the 1-*O* benzyl **415** and 60 mM for the 1-*O* *para*-bromo benzyl **416**. The change in solubility is greater in the 3-*O* compounds than the 1-*O* compounds, further illustrating the sensitivity of the C-3 hydroxyl group to IRI activity.

When comparing the 3-O and 1-O allyl, it can be seen that the 3-*O* derivative **410** has a maximum solubility of 30 mM. The C-1 derivative **417** has a maximum solubility of 100 mM due to the C-2 C-4 hydrogen bonding hindrance reducing the solubility of **410**. The IRI activity of the two compounds is within the same range because the 3-*O* derivative has a %MGS value of 57%,

and the 1-*O* derivative has a %MGS value of 61% at maximum solubility. This similarity in IRI activity was also observed with the *para*-bromo-benzyl derivatives.

The comparison of the 1-*O*-benzyl compounds to 1-*O*-phenyl compounds is of interest because the substituents are related in structure. The benzyl compounds **415** and **416** have weaker IRI activity than phenyl-β-D-glucopyranoside and 4-bromophenyl-β-D-glucopyranoside.[11] The phenyl compounds reach a rate of zero at their maximum concentration, produce full dose-response curves, and are hypothesized to result from the direct linkage of the C-1 oxygen to the aryl ring.[5] The 1-*O*-benzyl compounds and 1-*O*-phenyl compounds also have differences in solubilities. 4-bromophenyl-β-D-glucopyranoside has a maximum solubility of 55 mM, and phenyl-β-D-glucopyranoside has a maximum of 140 mM.[11] For **415** and phenyl-β-D-glucopyranoside, the change in solubility is 50 mM to 140 mM. The difference for **416** and 4-bromophenyl-β-D-glucopyranoside is 60 mM to 55 mM. The increase in solubility between **416** and the phenyl derivative was not expected because adding an extra carbon is theorized to increase hydrophobicity and, thus, decrease solubility.

The comparison of 3-OMG and 1-OMG shows that the 3-*O* compound has relatively lower solubility and greater IRI activity. This reinforces the theory that the solubility of a compound is decreased when substituents are moved from C-1 to C-3. This is also the first example of the IRI activity discussed in this chapter being quantitatively comparable. It is not accurate to compare the %MGS of compounds measured at different concentrations, but the IC_{50} of the 1-OMG and 3-OMG can be directly compared. The IC_{50} was lower for 3-OMG compared to 1-OMG, which was not hypothesized. The small volume of the methyl group could

not interfere with C-2 and C-4 hydrogen bonding to the same extent as the benzyl derivative and, therefore, has less of an effect on solubility and IRI activity.

The low solubility of the C-3 compounds is not detriment to IRI activity. Low soluble compounds such as aryl aldonamides are IRI active with max solubility of >15 mM. The aryl aldomaides compound, *N*-(2-fluorophenyl)-D-gluconamide has an IC_{50} of 3 mM.[6] The low solubility of the C-3 compounds results in potentially active concentrations not being measurable. With further modifications of the C-3 compounds, the solubility could be improved and the potentially active concentrations measured. Modifications such as further functionalization or the introduction of an ionic species to improve solubility.[6]

3.3 Summary

In conclusion, this chapter analyzed substituents' solubility and IRI activity differences on the hydroxyl at the C-3 position compared to their C-1 modified counterparts. The 1-*O* glucoside compounds are more soluble than the 3-*O* glucoside compounds, but the IRI activity for both is varied. It is theorized that the volume of the substituents on C-3 hinders hydrogen bonding of the C-2 and C-4 hydroxyl groups, leading to poor solubility. The C-3 compound that has potential as an IRI is 3-*O*-*para*-fluorobenzyl-D-glucopyranoside, as the compound was the most active. The 3-*O* compounds vary significantly in IRI activity with %MGS values of 66–92% and are unique as the C-1 modifications were closer in range compared to the C-3 functionalized compounds. This reflects the sensitivity of the C-3 position and is essential for the future rational design of IRIs.

3.4 References

(1) Galema, S. A.; Høiland, H. Stereochemical Aspects of Hydration of Carbohydrates in Aqueous Solutions. 3. Density and Ultrasound Measurements. *Journal of Physical Chemistry* **1991**, *95* (13), 5321–5326. https://doi.org/10.1021/j100166a073.

(2) Czechura, P.; Tam, R. Y.; Dimitrijevic, E.; Murphy, A. v.; Ben, R. N. The Importance of Hydration for Inhibiting Ice Recrystallization with C-Linked Antifreeze Glycoproteins. *Journal of the American Chemical Society* **2008**, *130* (10), 2928–2929. https://doi.org/10.1021/ja7103262.

(3) Chaytor, J. L.; Ben, R.; Basu, A.; Beauchemin, A.; Willmore, W.; Boddy, C.; Slater, G. W. Examining the Role of Carbohydrate Hydration and Structure in Preventing Ice-Recrystallization, 2010.

(4) Yang, X.; Gérczei, T.; Glover, L.; Correll, C. C. Crystal Structures of Restrictocin-Inhibitor Complexes with Implications for RNA Recognition and Base Flipping. *Nature Structural Biology* **2001**, *8* (11), 968–973. https://doi.org/10.1038/nsb1101-968.

(5) Tam, R. Y.; Rowley, C. N.; Petrov, I.; Zhang, T.; Afagh, N. A.; Woo, T. K.; Ben, R. N. Solution Conformation of C-Linked Antifreeze Glycoprotein Analogues and Modulation of Ice Recrystallization. *Journal of the American Chemical Society* **2009**, *131* (43), 15745–15753. https://doi.org/10.1021/ja904169a.

(6) Ampaw, A.; Charlton, T. A.; Briard, J. G.; Ben, R. N. Designing the next Generation of Cryoprotectants–from Proteins to Small Molecules. *Peptide Science* **2019**, *111* (1). https://doi.org/10.1002/pep2.24086.

(7) Capicciotti, C. J. The Rational Design of Potent Ice Recrystallization Inhibitors for Use as Novel Cryoprotectants, 2014.

(8) Pedersen, C. M.; Olsen, J.; Brka, A. B.; Bols, M. Quantifying the Electronic Effects of Carbohydrate Hydroxy Groups by Using Aminosugar Models. *Chemistry - A European Journal* **2011**, *17* (25), 7080–7086. https://doi.org/10.1002/chem.201100020.

(9) Capon, B. Mechanism in Carbohydrate Chemistry. *Chemical Reviews* **1969**, *69* (4), 407–498. https://doi.org/10.1021/cr60260a001.

(10) Storey, K. B.; Mommsen, T. P. Effects of Temperature and Freezing on Hepatocytes Isolated from a Freeze- Tolerant Frog. *American Journal of Physiology - Regulatory Integrative and Comparative Physiology* **1994**, *266* (5 35-5). https://doi.org/10.1152/ajpregu.1994.266.5.r1477.

(11) Capicciotti, C. J.; Mancini, R. S.; Turner, T. R.; Koyama, T.; Alteen, M. G.; Doshi, M.; Inada, T.; Acker, J. P.; Ben, R. N. O-Aryl-Glycoside Ice Recrystallization Inhibitors as Novel Cryoprotectants: A Structure-Function Study. *ACS Omega* **2016**, *1* (4), 656–662. https://doi.org/10.1021/acsomega.6b00163.

(12) Ágoston, K.; Dobó, A.; Rákó, J.; Kerékgyártó, J.; Szurmai, Z. Anomalous Zemplén Deacylation Reactions of α- and β-d-Mannopyranoside Derivatives. *Carbohydrate Research* **2001**, *330* (2), 183–190. https://doi.org/10.1016/S0008-6215(00)00283-4.

(13) Abraham, S.; Keillor, K.; Capicciotti, C. J.; Perley-Robertson, G. E.; Keillor, J. W.; Ben, R. N. Quantitative Analysis of the Efficacy and Potency of Novel Small Molecule Ice Recrystallization Inhibitors. *Crystal Growth and Design* **2015**, *15* (10), 5034–5039. https://doi.org/10.1021/acs.cgd.5b00995.

(14) Hine, J.; Brader, W. H. The Effect of Halogen Atoms on the Reactivity of Other Halogen Atoms in the Same Molecule. III. The SN^2 Reactivity of Ethylene Halides 1. *Journal of the American Chemical Society* **1953**, *75* (16), 3964–3966. https://doi.org/10.1021/ja01112a026.
(15) Zhou, P.-P.; Qiu, W.-Y.; Liu, S.; Jin, N.-Z. Halogen as Halogen-Bonding Donor and Hydrogen-Bonding Acceptor Simultaneously in Ring-Shaped H3N·X(Y)·HF (X = Cl, Br and Y = F, Cl, Br) Complexes. *Physical Chemistry Chemical Physics* **2011**, *13* (16), 7408. https://doi.org/10.1039/c1cp00025j.
(16) Banerjee, S.; Yalkowsky, S. H.; Valvani, S. C. Water Solubility and Octanol/Water Partition Coefficients of Organics. Limitations of the Solubility-Partition Coefficient Correlation. *Environmental Science and Technology* **1980**, *14* (10), 1227–1229. https://doi.org/10.1021/es60170a013.
(17) Capicciotti, C. J.; Leclère, M.; Perras, F. A.; Bryce, D. L.; Paulin, H.; Harden, J.; Liu, Y.; Ben, R. N. Potent Inhibition of Ice Recrystallization by Low Molecular Weight Carbohydrate-Based Surfactants and Hydrogelators. *Chemical Science*. **2012**, pp 1408–1416. https://doi.org/10.1039/c2sc00885h.
(18) Kujawski, J.; Bernard, M. K.; Janusz, A.; Kuźma, W. Prediction of Log P: ALOGPS Application in Medicinal Chemistry Education. *Journal of Chemical Education* **2012**, *89* (1), 64–67. https://doi.org/10.1021/ed100444h.

Chapter 4: Experimental Procedures and Characterization Data

4.1 Analysis of Ice Recrystallization Inhibition activity

A modified "splat cooling" assay was used to quantify IRI activity.[1] The sample is dissolved in a PBS solution, and 10 µL dropped from a height of 2 meters onto a polished aluminum block cooled to -78 °C. The droplet freezes instantly to form a wafer, which is transferred using pre-cooled tools to a glass coverslip (Fisherbrand, 12-545-80) and placed in a cryostage held at -6.4 °C. The cryostage temperature is controlled by a programmable Peltier unit (S3 Series 800 temperature controller, Alpha Omega Instruments). The wafer is annealed for 5-minutes before being placed under a microscope and photographed by a digital camera (Nikon CoolPix 5000) fitted to the microscope. Three droplets are tested for each concentration. The images are then analyzed with ImageJ[2] (Image Processing and Analysis in Java, version 1.51s) to circle well-defined ice crystal borders, and the area of each crystal is calculated. The ice crystal areas are sorted based on size (bin size increases in increments of 0.001 mm^2) and can be used to calculate the initial rate of ice recrystallization (v). The rate is then normalized to PBS, and a normalized rate (v_{norm}) for each concentration is calculated. A dose-response curve is generated in GraphPad[3] by plotting the normalized rate values by the log concentration that was tested. A four-parameter sigmoidal curve is fitted to the data, and error bars represent the percent standard error of the mean (SEM).

4.2 General experimental

All experiments were performed in flame-dried glassware under argon, where necessary. The reagents were transferred using air-sensitive techniques, such as transferring with oven-dried syringes or cannulae. Chemical reagents were used without further purification when obtained from commercial sources. Column chromatography was performed using E. Merck silica gel 60 (230-400 mesh), and thin-layer chromatography (TLC) was performed on 0.2 mm pre-coated silica gel aluminum plates (60 F_{254} E. Merck). TLC plates were visualized using short-wavelength (254 nm) ultra-violet light or through staining (*p*-anisaldehyde stain). The solvents used for dry reactions were distilled. *N*,*N*-Dimethylformamide was kept under argon with 4Å molecular sieves. ^{1}H (300 or 400 MHz) and ^{13}C (101 or 125 MHz) were used for NMR spectra at room temperature using a Bruker Avance 300 or Bruker Avance 400. The NMR solvents that were used were deuterated dimethyl sulfoxide (DMSO-d_6) and chloroform ($CDCl_3$). The chemical shifts were adjusted to the solvent peak and measured in ppm. The splitting patterns are singlet (s), doublet (d), triplet (t), quartet (q), multiplet (m), doublet of doublets (dd), doublet of triplets (dt), doublet of quartets (dq), doublet of doublet of doublets (ddd), and doublet of doublet of triplets (ddt). Low-resolution mass spectrometry (LRMS) was performed using a Micromass Q-TOF mass spectrometer in positive electrospray ionization mode (ESI+) at the John L. Holmes Mass Spectrometry Facility (University of Ottawa).

1,2:5,6-Di-*O*-isopropylidene-α-D-glucofuranose (**402**)

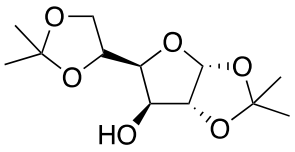

Commercial D-glucose (5.0 g, 27.78 mmol) was added to dry acetone (150 mL) in a flame-dried flask under argon, and anhydrous copper(II) sulfate (8.86 g, 55.5 mmol) was added to the mixture. While stirring at room temperature, concentrated sulfuric acid (0.73 mL) was added dropwise. The reaction was stirred at room temperature for 72 hours. The reaction mixture was neutralized with solid sodium bicarbonate, and the inorganic solids were removed by filtration. The residue was recrystallized from hexane (3.8 g, 50%). All spectra data were consistent with that in the literature.[4]

1,2:5,6-Di-*O*-isopropylidene-α-D-3-*O*-Benzyl-glucofuranose (**403**)

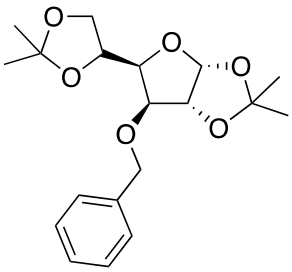

402 (0.5 g, 1.92 mmol) was added to dry *N,N*-dimethylformamide (2 mL) in a flame-dried flask under argon. NaH (0.2257 g, 5.509 mmol, 60% dispersion in mineral oil) was slowly added at 0 °C. After the gas formation stopped, the flask was warmed to room temperature, and benzyl bromide (0.274 mL, 2.304 mmol) was added at room temperature and stirred for 20 minutes. The reaction was quenched by adding methanol, and the organic layer was collected. The aqueous layer was extracted with ethyl acetate and combined with the organic layer. The organic layer was dried over magnesium sulfate ($MgSO_4$), filtered, and concentrated. The resulting residue was purified via column chromatography using ethyl acetate:hexanes (1:5) as an eluent to make the final product a colorless oil (0.62 g, 92% yield).[5]
^{1}H-NMR (300 MHz, $CDCl_3$): δ 7.35-7.26 (m, 5H), 5.90 (d, J= 3.7, 1H), 4.70-4.58 (m, 3H), 4.39-4.34 (m, 1H), 4.16-4.10 (m, 2H), 4.02-3.99 (m, 2H), 1.49 (s,3H), 1.43 (s,3H), 1.37 (s,3H), 1.31 (s,3H) ppm
^{13}C-NMR(101 MHz, $CDCl_3$): δ 137.7, 128.4, 127.9, 127.7, 111.8, 109.0, 105.3, 82.7, 81.7, 81.4, 72.5, 72.4, 67.4, 26.9(2C), 26.3, 25.5 ppm

1,2:5,6-Di-*O*-isopropylidene-α-D-3-*O*-Bromobenzyl-glucofuranose (**404**)

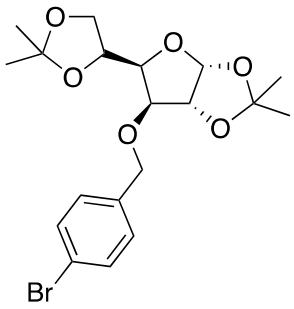

402 (1 g, 4 mmol) was added to dry THF (7 mL) in a flame-dried flask under argon. NaH (0.171 g, 7.125 mmol 60% dispersion in mineral oil) was slowly added at 0 °C. After the gas formation stopped, the flask was warmed to room temperature, and 4-bromobenzyl bromide (1 g, 4 mmol) was added at room temperature and stirred for 20 minutes. The reaction was quenched with the addition of methanol, and the organic layer was collected. The aqueous layer was extracted with ethyl acetate and combined with the organic layer. The organic layer was dried over $MgSO_4$, filtered, and concentrated. The resulting residue was purified by column chromatography using ethyl acetate:hexanes (1:20) as eluent to make the final product a colorless oil (1.58 g, 92% yield).[5]

.

^{1}H-NMR (300 MHz, $CDCl_3$): δ 7.46 (m, 2H), 7.22 (m, 2H), 5.88(d, J= 3.7 Hz, 1H), 4.65-4.56 (m, 3H), 4.37-4.31 (m, 1H), 4.13-4.01 (m, 2H), 4.01-3.97 (m, 2H), 1.49 (s, 3H), 1.42 (s, 3H), 1.36 (s, 3H), 1.31 (s, 3H) ppm

^{13}C-NMR(101 MHz, $CDCl_3$): δ 136.7, 131.5(2C), 129.3(2C), 121.7, 111.9, 109.1, 105.3, 82.7, 81.8, 81.3, 72.4, 71.6, 67.5, 26.8(2C), 26.3, 25.5 ppm

1,2:5,6-Di-*O*-isopropylidene-α-D-3-*O*-Fluorobenzyl-glucofuranose (**405**)

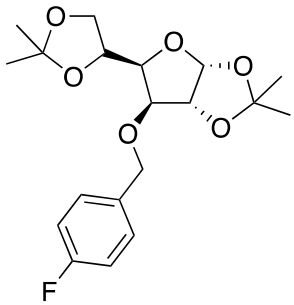

402 (1 g, 4.0 mmol) was added to dry THF (7 mL) in a flame-dried flask under argon. NaH (0.228 g, 9.5 mmol, 60% dispersion in mineral oil) was slowly added at 0 °C. After the gas formation stopped, the flask was warmed to room temperature, 4-fluorobenzyl bromide (0.5 mL, 4.02 mmol) was added, and the mixture was stirred for 24 hours. The reaction was quenched with water, and the organic layer was collected. The aqueous layer was extracted with ethyl acetate, and the organic layers were combined. The organic layer mixture was dried over $MgSO_4$, filtered, and concentrated. The resulting residue was purified by column chromatography using

ethyl acetate:hexanes (1:2) as an eluent to make the final product a colorless oil (1.33 g, 90% yield).[5]

^{1}H-NMR (300 MHz, $CDCl_3$): δ 7.33-7.30 (m, 2H), 7.04-6.99 (m, 2H), 5.89 (d, J= 3.7 Hz, 1H), 4.66-4.56 (m, 3H), 4.36-4.31 (m, 1H), 4.13-4.08 (m, 2H), 4.00-3.97 (m, 2H), 1.49 (s, 3H), 1.42 (s, 3H), 1.36 (s, 3H), 1.31 (s, 3H) ppm.

^{13}C-NMR(101 MHz, $CDCl_3$): δ 137.7, 128.4, 127.8, 127.7, 111.8, 109.0, 105.3, 82.7, 81.7, 81.3, 72.5, 72.4, 67.4, 26.8 (2C) 26.3, 25.5 ppm

1,2:5,6-Di-*O*-isopropylidene-α-D-3-*O*-allyl-glucofuranose (**406**)

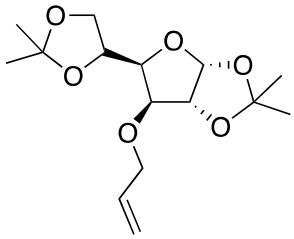

402 (0.5 g, 1.92 mmol) was added to dry DMF (2 mL) in a flame-dried flask under argon. NaH (0.2257 g, 5.509 mmol 60% dispersion in mineral oil) was slowly added at 0 °C. After the gas formation stopped, the flask was warmed to room temperature, benzyl allyl (0.274 mL, 2.304 mmol) was added, and the mixture was stirred for 20 minutes. The reaction was quenched through the addition of methanol, and the organic layer was collected. The aqueous layer was extracted with ethyl acetate, and the organic layers were combined. The organic layer mixture was dried over $MgSO_4$, filtered, and concentrated. The resulting residue was purified by column chromatography using ethyl acetate:hexanes (1:5) as an eluent to make the final product a white solid (0.39 g, 68% yield).

^{1}H-NMR (300 MHz, $CDCl_3$): δ 5.92-5.83 (m, 2H), 5.29 (dq, J= 17.2, 1.6 Hz, 1H), 5.18 (dq, J= 10.6, 1.6 Hz, 1H), 4.53 (d, J= 3.7 Hz, 1H), 4.32-4.28 (m,1H), 4.13-4.06 (m, 4H), 4.00-3.93 (m, 2H), 1.48 (s, 3H), 1.41 (s, 3H), 1.34 (s, 3H), 1.30 (s, 3H).

^{13}C-NMR(101 MHz, $CDCl_3$): δ 134.2, 117.27, 111.7, 108.9, 105.2, 82.8, 81.4, 81.2, 72.5, 71.3, 67.2, 26.8(2C), 26.2, 25.4 ppm.

3-*O*-Benzyl-D-glucopyranoside (**407**)

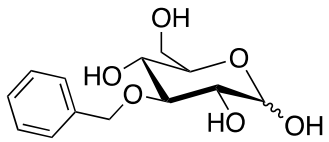

403 (0.1 g, 0.789 mmol) was dissolved in 1.0 mL of water. Amberlite® IR120 H^+ resin was added until the pH level was equal to 11, and the mixture was stirred until finished by TLC. The mixture was filtered through celite, and the filtrate was concentrated. After recrystallization from ethyl acetate, the final product was formed as a mixture of anomers (0.15 g, 72% yield).[6]

^{1}H-NMR (300 MHz, DMSO-d_6): δ 7.39-7.20 (m, 5H), 6.65 (d, J= 6.4 Hz, 1H), 5.04 (t, J= 10.3 Hz, 2H), 4.77 (m, 1H), 4.49 (m, 1H), 4.30 (t, J= 14.1 Hz, 1H), 3.66 (dd, J= 10.7, 3.2 Hz, 1H), 3.45-3.39 (m, 1H), 3.24-3.02(m, 4H) ppm.
^{13}C-NMR(101 MHz, DMSO-d_6): δ 144.4, 136.0, 134.7, 125.2, 102.1, 90.6, 81.9, 80.0, 78.0, 75.0, 66.2 ppm.
LRMS (ESI): m/z calcd. For $C_{13}H_{18}NaO_6$ [M+Na]+ 292.1; found, 292.0

3-*O-para*-Bromobenzyl-D-glucopyranoside (**408**)

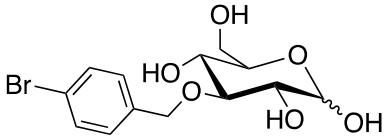

405 (1.0 g, 2.86 mmol) was dissolved in 10% acetic acid (20 mL) and stirred at 80 °C overnight. The mixture wad concentrated, and the final product was formed as a mixture of anomers (0.66 g, 80% yield) after recrystallization from ethyl acetate.

^{1}H-NMR (300 MHz, DMSO-d_6): δ 7.50 (d, J= 8.4 Hz, 2H), 7.37 (d, J= 8.4 Hz, 2H), 6.68 (d, J= 6.4 Hz, 1H), 5.09 (t, J= 12.1 Hz, 2H), 4.76 (d, J= 28.1, 3.6 Hz, 2H), 4.52 (t, J= 5.8 Hz, 1H), 4.31 (t, J= 14.1 Hz, 1H), 3.69-3.65 (m, 1H), 3.47-3.41 (m, 1H), 3.24-3.03 (m, 4H)
^{13}C-NMR(101 MHz, DMSO-d_6): δ 139.6, 131.3, 130.0, 120.4, 97.3, 85.9, 77.1, 75.2, 73.2, 70.2, 61.5
LRMS (ESI): m/z calcd For $C_{13}H_{17}NaO_6Br$ [M+Na]+ 371.0, 373.0; found, 371.1,373.0.

3-*O*-*para*-Fluorobenzyl-D-glucopyranoside (**409**)

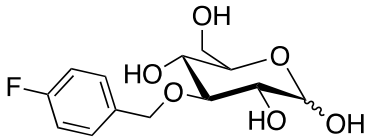

405 (1.0g, 2.86mmol) was dissolved in 10% acetic acid (20 mL) and stirred at 80°C overnight. The mixture wad concentrated, and the final product was formed as a mixture of anomers (0.66 g, 80% yield) after recrystallization from ethyl acetate.

^{1}H-NMR (300 MHz, DMSO-d_6): δ 7.46-7.42 (m, 2H), 7.15-7.11 (m, 2H), 6.70 (d, J= 6.3 Hz, 1H), 5.10 (m, 2H), 5.44 (d, J= 14.4 Hz, 2H), 4.54 (t, J= 5.7 Hz, 2H), 4.32 (t, J= 13.8 Hz, 1H), 3.69-3.65 (m, 1H), 3.47-3.41 (m, 1H), 3.23-3.02 (m, 4H)
^{13}C-NMR(101 MHz, DMSO-d_6): δ 136.4 (d, J_{C-F}= 3.0 Hz), 136.3, 129.9 (d, J_{C-F}= 8.0 Hz), 115.2 (d, J_{C-F}= 3.2 Hz), 115.0 (d, J_{C-F}= 3.3 Hz), 97.3, 85.8, 77.1, 75.2, 73.3, 72.7, 72.6, 70.3
LRMS (ESI): m/z calcd For $C_{13}H_{17}NaO_6F$ [M+Na]+ 311.1; found, 311.1.

3-*O*-allyl-D-glucopyranoside (**410**)

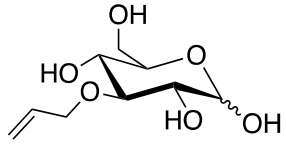

406 (1 g, 4.54 mmol) was dissolved in 10 mL of water. 10 g of Amberlite® IR120 H^+ resin was added, and the mixture was stirred at 60 °C for 7 hours. The mixture was filtered through celite, and the filtrate was concentrated. After recrystallization from ethyl acetate, the final product was formed as a mixture of anomers (0.68 g, 68% yield).

^{1}H-NMR (300 MHz, DMSO-d_6): δ 6.43 (d, J= 6.4 Hz, 1H), 5.94 (m, 1H), 5.25-5.20 (m, 1H), 5.07-5.04 (m,1H), 4.96 (dd, J= 5.2, 1 Hz, 2H), 4.49 (m, 1H), 4.30-4.23 (m, 3H), 3.67-3.62 (m, 1H), 3.44-3.38 (m, 1H), 3.17-2.95 (m, 4H)
^{13}C-NMR(101 MHz, DMSO-d_6): δ 137.1, 115.8, 97.4, 85.3, 77.1, 75.1, 73.3, 70.2, 61.5
LRMS (ESI): m/z calcd. For $C_9H_{16}NaO_6$ [M+Na]+ 243.1; found, 243.1.

Benzyl-2,3,4,6-tetra-*O*-acetyl-β-D-glucopyranoside (**412**)

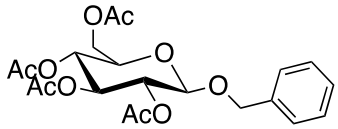

1,2,3,4,6-Penta-*O*-acetyl-β-D-glucopyranose (1 g, 2.56 mmol) was added to dry DCM (10 mL) with 4 Å molecular sieves in a flame-dried flask under argon. The mixture was cooled to 0 °C, and boron trifluoride diethyl etherate (0.5 mL, 4.08 mmol) was added dropwise. Benzyl alcohol (0.27 ml, 0.27 mmol) was added at room temperature, and the mixture was stirred for 24 hours, after which it was quenched with sodium carbonate at 0 °C. The organic layer was separated and washed with water and brine. The combined organic layer wasd dried over $MgSO_4$, filtered, and concentrated. The residue wad purified via column chromatography using 4:6 to 5:5 ethyl acetate:hexanes as the eluent to produce a white solid (0.37 g, 32% yield).[7]

^{1}H-NMR (300 MHz, $CDCl_3$): δ 7.36-7.27 (m, 5H), 5.20-5.03 (m, 3H), 4.89 (d, J= 12.3 Hz, 1H), 4.63 (d, J= 12.3 Hz, 1H), 4.56 (d, J= 7.8 Hz, 1H), 4.89 (dd, J= 12.3, 4.7 Hz, 1H), 4.18-4.03 (m, 2H), 3.70-3.65 (m, 1H), 2.09 (s, 3H), 2.01 (s, 3H), 2.00 (s, 3H), 1.99 (s, 3H).
^{13}C-NMR(101 MHz, $CDCl_3$): δ 170.6, 170.2, 169.3, 169.2, 136.7, 128.4, 128.0, 127.7, 99.3, 72.8, 71.8, 71.3, 70.7, 68.4, 62.0, 60.3, 20.7, 20.6, 20.6, 20.6

4-Bromobenzyl-2,3,4,6-tetra-*O*-acetyl-β-D-glucopyranoside(**413**)

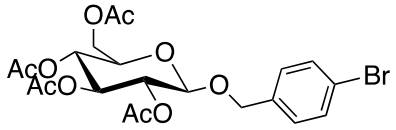

1,2,3,4,6-Penta-*O*-acetyl-β-D-glucopyranose (1 g, 2.56 mmol) was added to dry DCM (10 mL) with 4 Å molecular sieves in a flame-dried flask under argon. The mixture was cooled to 0 °C, and boron trifluoride diethyl etherate (0.5 mL, 4.08 mmol) was added dropwise. 4-bromo benzyl alcohol (1.1 g, 3.1 mmol) was added at room temperature, and the mixture was stirred for 24 hours, after which it was quenched with sodium carbonate at 0 °C. The organic layer was separated and washed with water and brine. The combined organic layer was dried over $MgSO_4$, filtered, and concentrated. The residue was purified via column chromatography using a 3:1 ethyl acetate:hexanes as the eluent to produce a white solid (0.75 g, 52% yield).[7]

^{1}H-NMR (300 MHz, $CDCl_3$): δ 7.47-7.45 (m, 2H), 7.16-7.14 (m, 2H), 5.20-5.03 (m, 3H), 4.83 (d, J= 12.4 Hz, 1H), 4.63 (d, J= 12.3 Hz, 1H), 4.57-4.53 (m, 2H), 4.28-4.13 (m, 2H), 3.69-3.64 (m, 1H), 2.08 (s, 3H), 2.00 (s, 3H), 2.00 (s, 3H), 1.99 (s, 3H).
^{13}C-NMR(101 MHz, $CDCl_3$): δ 170.6, 170.2, 169.3, 169.4, 169.2, 135.7, 131.6, 128.0, 128.3, 121.9, 99.5, 72.8, 71.9, 71.3, 70.0, 68.4, 61.9, 20.7, 20.6, 20.6, 20.6

Allyl-2,3,4,6-tetra-*O*-acetyl-β-D-glucopyranoside(**414**)

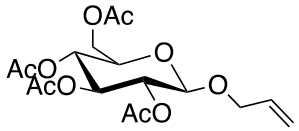

1,2,3,4,6-Penta-*O*-acetyl-β-D-glucopyranose (1 g, 2.56 mmol) was added to dry DCM (10 mL) with 4 Å molecular sieves in a flame-dried flask under argon. The mixture was cooled to 0 °C, and boron trifluoride diethyl etherate (0.5 mL, 4.08 mmol) was added dropwise. Allyl alcohol (0.25 mL, 3.32 mmol) was added at room temperature, and the mixture was stirred for 24 hours, after which it was quenched with sodium carbonate at 0 °C. The organic layer was separated and washed with water and brine. The combined organic layer was dried over $MgSO_4$, filtered, and concentrated. The residue was purified by column chromatography using a 3:1 hexanes:ethyl acetate as the eluent to produce a white solid (0.60 g, 60% yield).[8]

^{1}H-NMR (300 MHz, $CDCl_3$): δ 5.89-5.79 (m, 1H), 5.87 (dq, 1H, J= 1.6, 17.2 Hz), 5.23-5.18 (m, 2H), 5.11-4.99 (m, 2H), 4.55 (d, J= 7.9 Hz, 1H), 4.33 (ddt, J= 13.3, 4.8, 1.5 Hz, 1H), 4.14 (dd, J= 12.2, 2.4 Hz, 1H), 4.10 (ddt, J= 13.2, 6.2, 1.5 Hz, 1H), 3.68 (ddt, J= 9.8, 4.7, 2.4 Hz, 1H), 1.48 (s, 3H), 1.41 (s, 3H), 1.34 (s, 3H), 1.30 (s, 3H) ppm.
^{13}C-NMR (101 MHz, $CDCl_3$): δ 170.7, 170.3, 169.4, 169.3, 133.3, 117.7, 99.6, 72.9, 72.8, 72.7, 70.0, 61.9, 20.7,20.7, 20.6, 20.5

Benzyl-β-D-glucopyranoside (**415**)

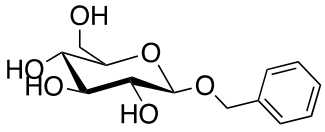

412 (1 g, 2.28 mmol) was dissolved in MeOH (20mL/gram). NaOMe dissolved in MeOH (1 M) was added dropwise until pH was greater than 11 and stirred until complete checking with TLC (4:2 hexanes:EtOAc). The solution was neutralized using Amberlite® IR120 H^+ resin, filtered, and concentrated to produce **415** as white crystals (0.62 g, 92% yield).[7]

^{1}H-NMR (300 MHz, DMSO-d_6): δ 7.41-7.26 (m, 5H), 5.12 (d, J= 4.9 Hz, 1H), 4.95 (dd, J= 17.5, 4.7 Hz, 2H), 4.83 (d, J= 12.2 Hz, 1H), 4.59-4.53 (m, 1H), 4.22 (d, J= 7.7 Hz, 1H), 3.72-3.67 (m, 1H), 3.49-3.44 (m, 1H), 3.17-3.00 (m, 4H)
^{13}C-NMR (101 MHz, DMSO-d_6): δ 138.1, 131.4, 130.1, 120.8, 102.6, 77.5, 77.2, 74.0, 73.9, 70.6, 69.1, 61.6
LRMS (ESI): m/z calcd. For $C_{13}H_{18}NaO_6$ [M+Na]+ 371.0; found, 371.0.

(4-Bromophenyl)methyl-β-D-glucopyranoside (**416**)

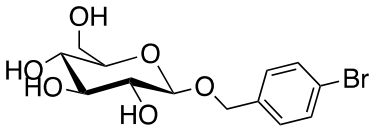

413 (1 g, 1.78 mmol) was dissolved in MeOH (20 mL/gram). NaOMe dissolved in MeOH (1 M) was added dropwise until pH was greater than 11 and stirred until complete, checking with TLC (4:2 hexanes:EtOAc). The solution was neutralized using Amberlite® IR120 H^+ resin, filtered, and concentrated to produce **415** as white crystals (0.57 g, 92% yield).[17]

^{1}H-NMR (300 MHz, DMSO-d_6): δ 7.53 (m, 2H), 7.35 (m, 2H), 5.11 (d, J= 4.8 Hz, 1H), 4.96-4.90 (m, 2H), 4.79 (d, J= 12.6 Hz, 1H), 4.58-4.50 (m, 2H), 4.21 (d, J= 7.7 Hz, 1H), 3.71-3.67 (m, 1H), 3.49-3.42 (m, 1H), 3.16-3.00 (m, 5H)
^{13}C-NMR (101 MHz, DMSO-d_6): δ 138.1, 131.4, 130.1, 120.8, 102.6, 77.5, 77.2, 74.0, 73.9, 70.6, 69.1, 61.6
LRMS (ESI): m/z calcd. For $C_{13}H_{17}NaO_6Br$ [M+Na]+ 371.0,374.0; found, 371.0, 374.0.

Allyl-β-D-glucopyranoside (**417**)

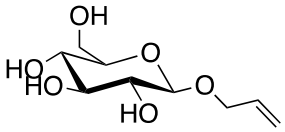

414 (1 g, 2.58 mmol) was dissolved in MeOH (20 mL/gram). NaOMe dissolved in MeOH (1 M) was added dropwise until the pH was greater than 11 and stirred until complete, checking with TLC (4:2 hexanes:EtOAc). The solution was neutralized using Amberlite® IR120 H^+ resin, filtered, and concentrated to produce **417** as white crystals (0.51 g, 90% yield).[8]

^{1}H-NMR (300 MHz, DMSO-d_6): δ 5.90 (ddt, J= 17.3, 10.5, 5.3 Hz, 1H), 5.31 (dq, J= 17.3, 1.8 Hz, 1H), 5.13 (dq, J= 10.5, 2.1 Hz, 1H), 5.06 (d, J= 4.9 Hz, 1H), 4.95 (d, J= 4.7 Hz, 1H), 4.91 (d, J= 4.8 Hz, 1H), 4.50 (t, J= 6.0 Hz, 1H), 4.26 (dt, J= 13.4, 4.9 Hz, 1H), 4.14 (d, J= 7.8 Hz, 1H), 4.03 (ddt, J= 13.3, 5.6, 1.5 Hz, 1H), 3.66 (ddd, J= 11.8, 6.1, 1.7 Hz, 1H), 3.42 (dt, J= 11.6, 5.7 Hz, 1H), 3.17-2.94 (m, 4H)
^{13}C-NMR (101 MHz, DMSO-d_6): δ 138.1, 116.8, 98.4, 86.3, 78.1, 76.1, 74.3, 71.2, 61.5
LRMS (ESI): m/z calcd. For $C_9H_{16}NaO_6$ [M+Na]+ 243.1; found, 243.1.

1,2:5,6-Di-*O*-isopropylidene-α-D-3-*O*-Benzyl-glucofuranose (**403**)

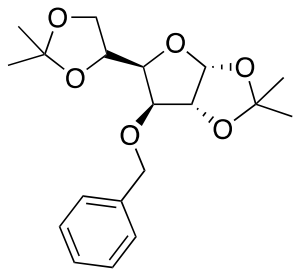

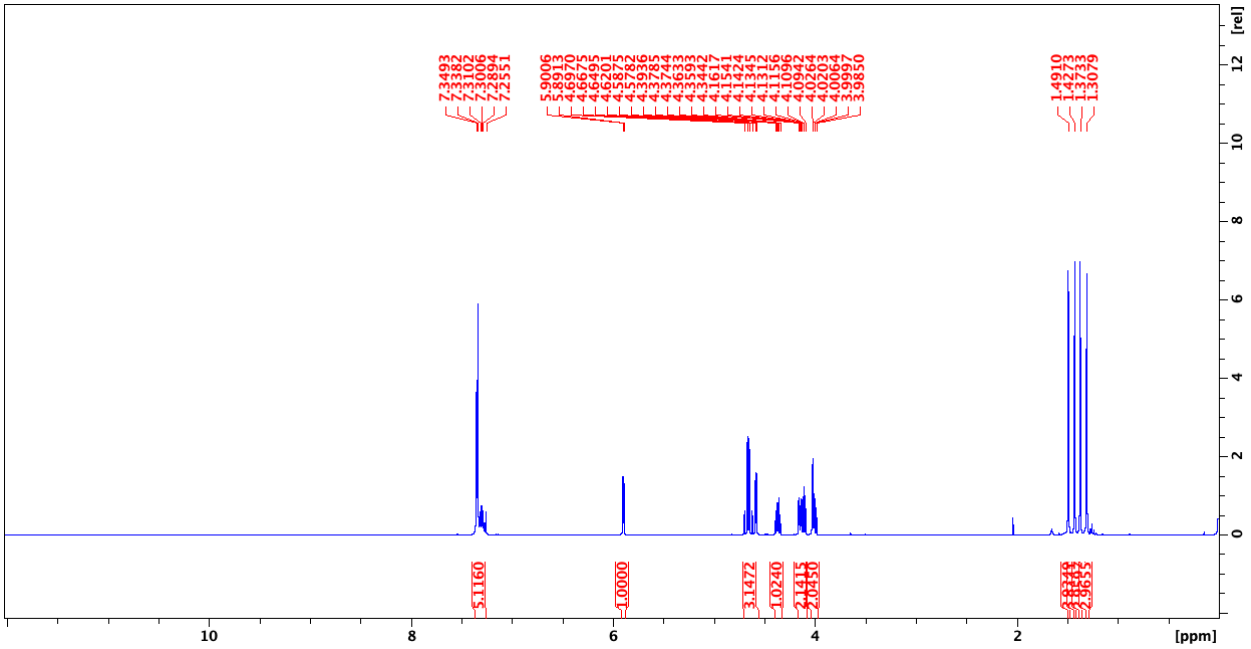

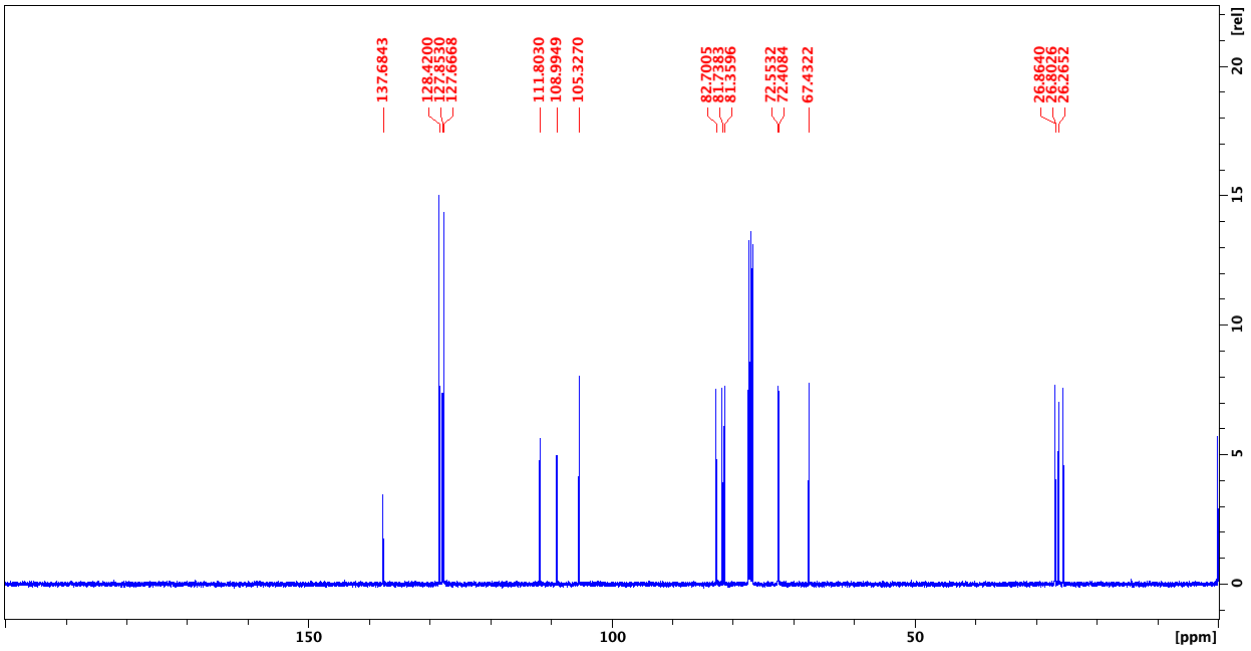

1,2:5,6-Di-*O*-isopropylidene-α-D-3-*O*-Bromobenzyl-glucofuranose (**404**)

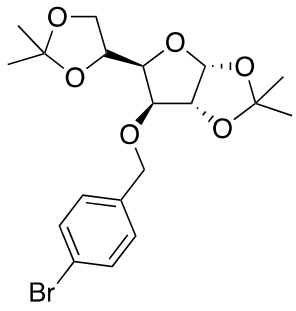

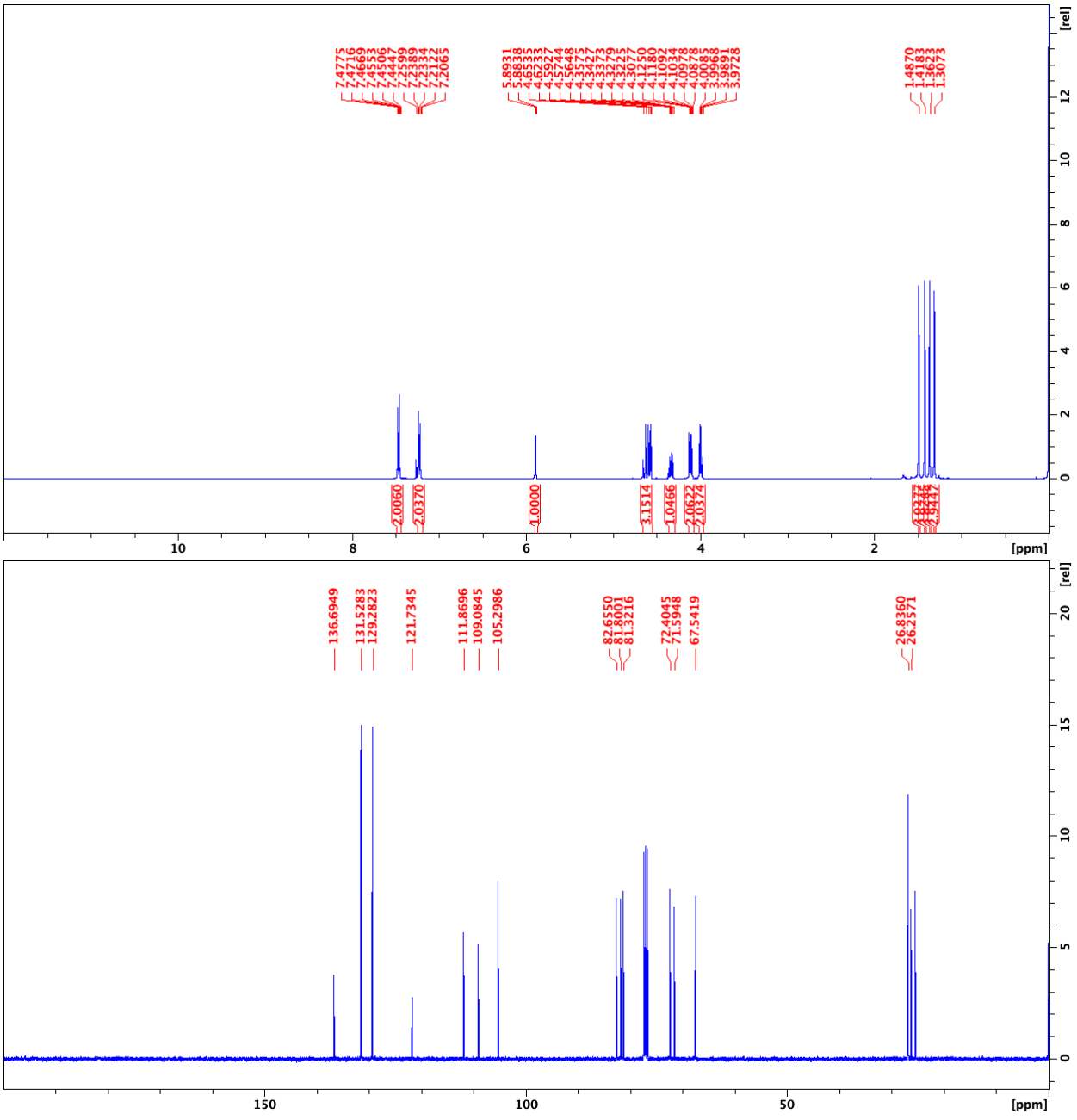

1,2:5,6-Di-*O*-isopropylidene-α-D-3-*O*-Fluorobenzyl-glucofuranose (**405**)

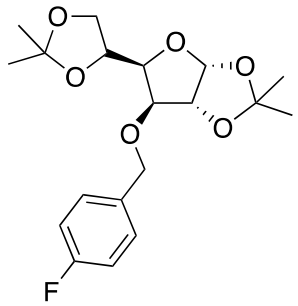

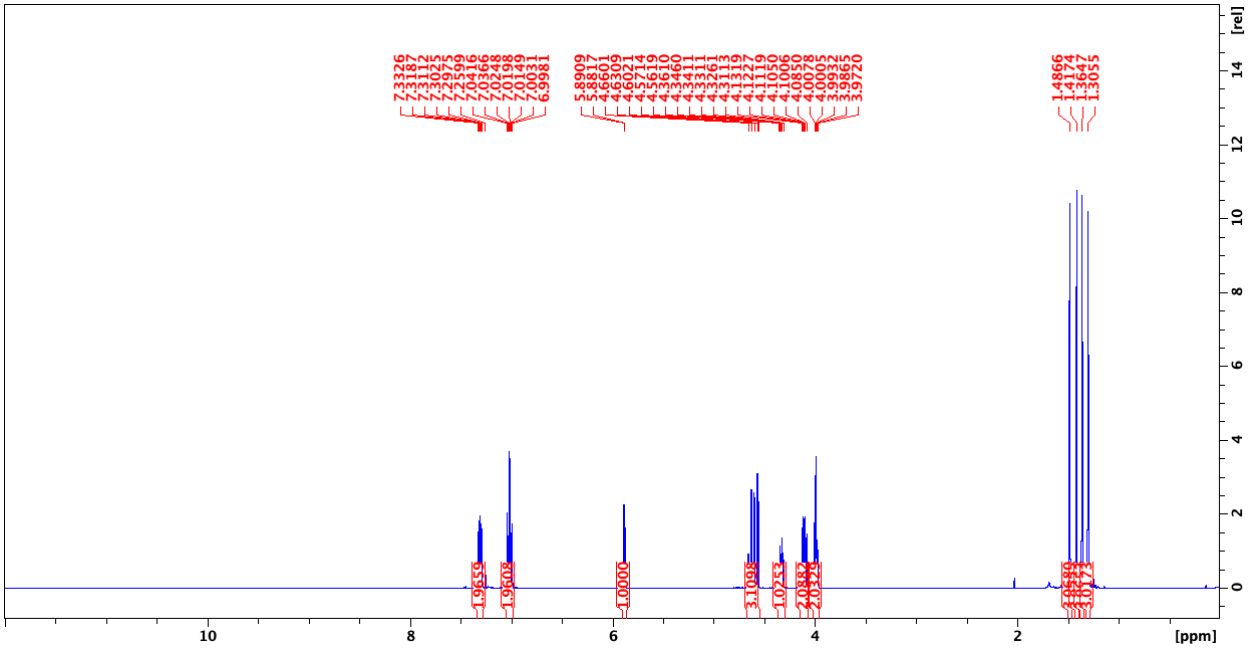

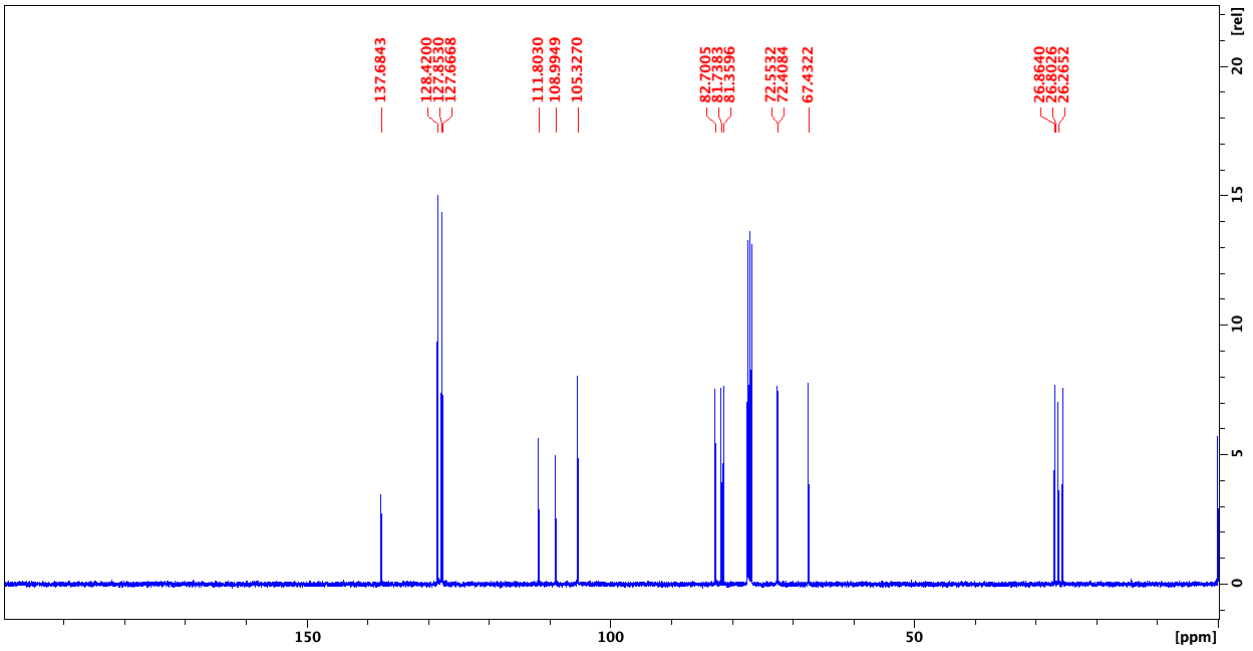

1,2:5,6-Di-*O*-isopropylidene-α-D-3-*O*-allyl-glucofuranose (**406**)

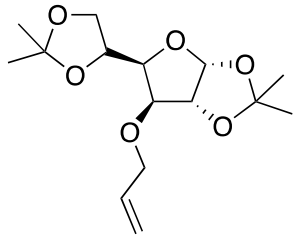

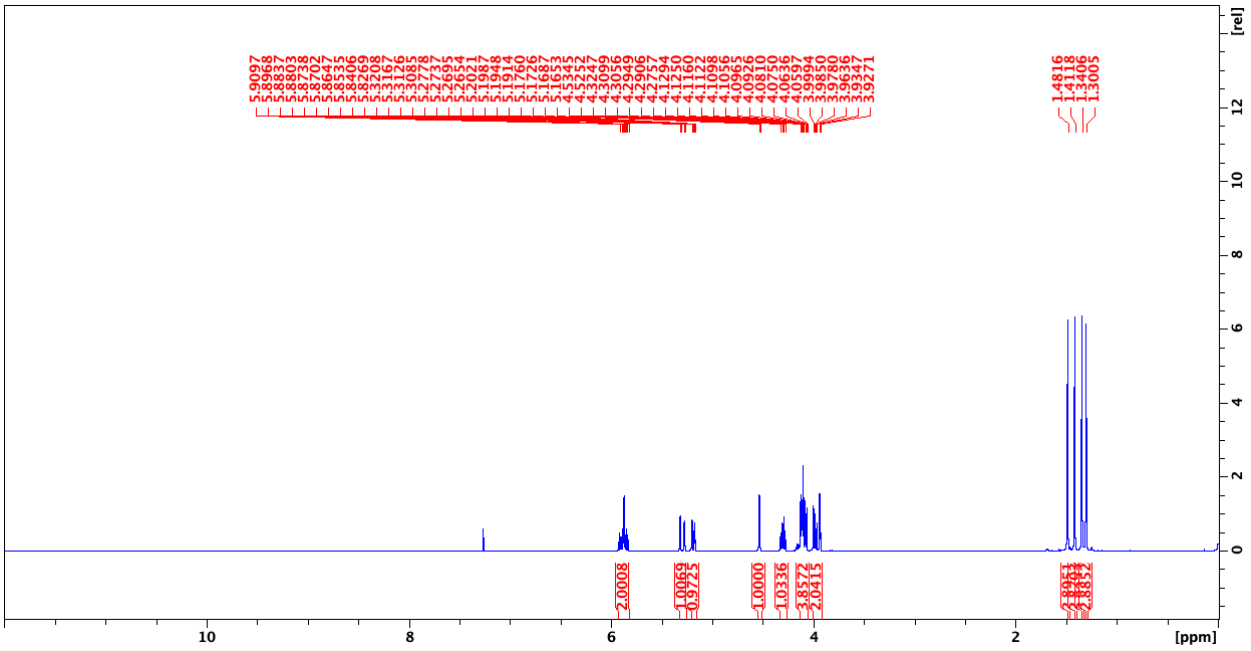

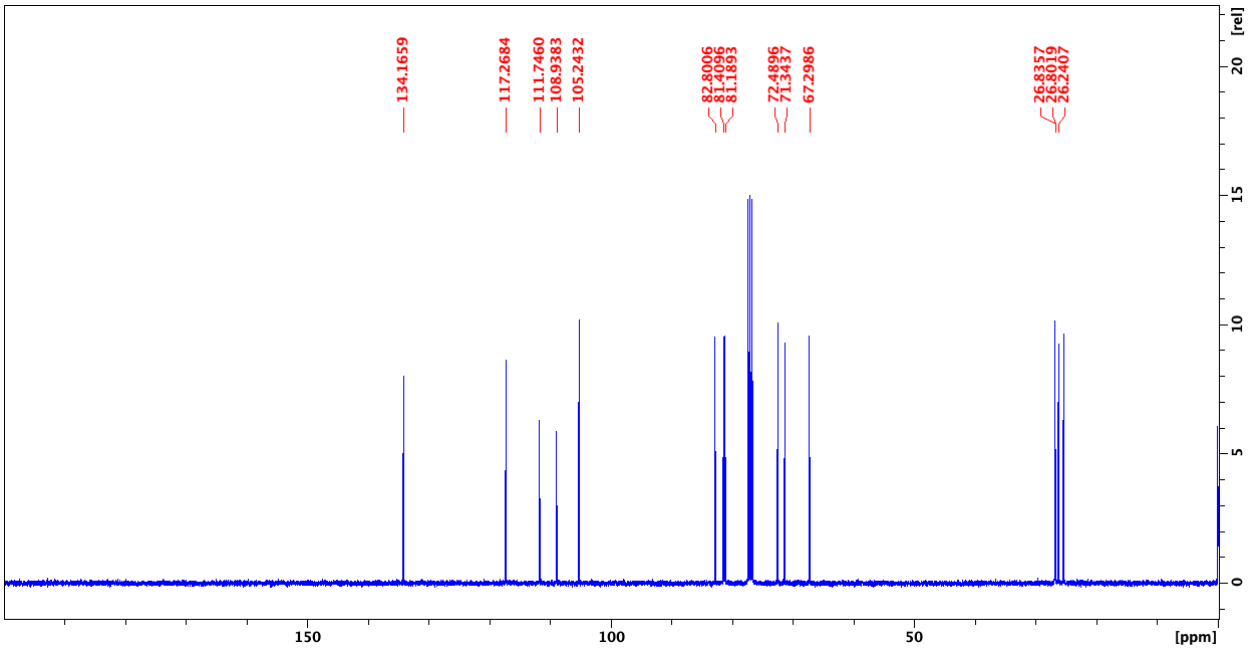

3-*O*-Benzyl-D-glucopyranoside (**407**)

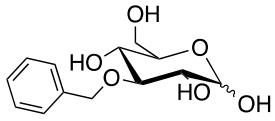

407

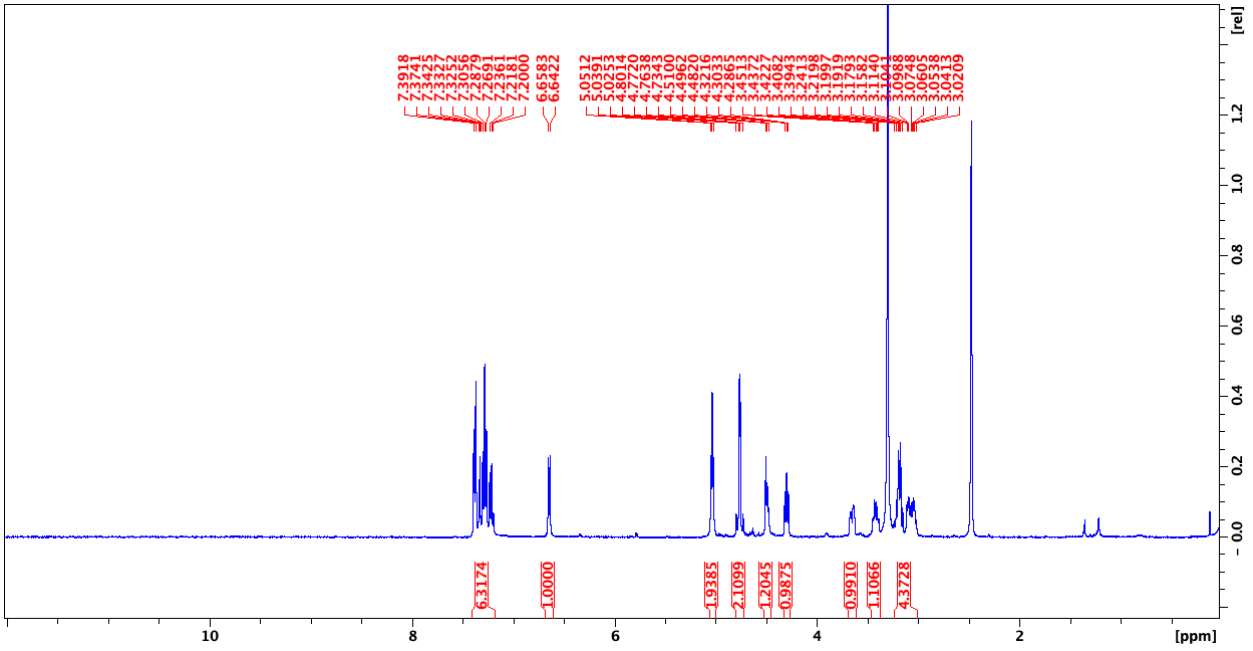

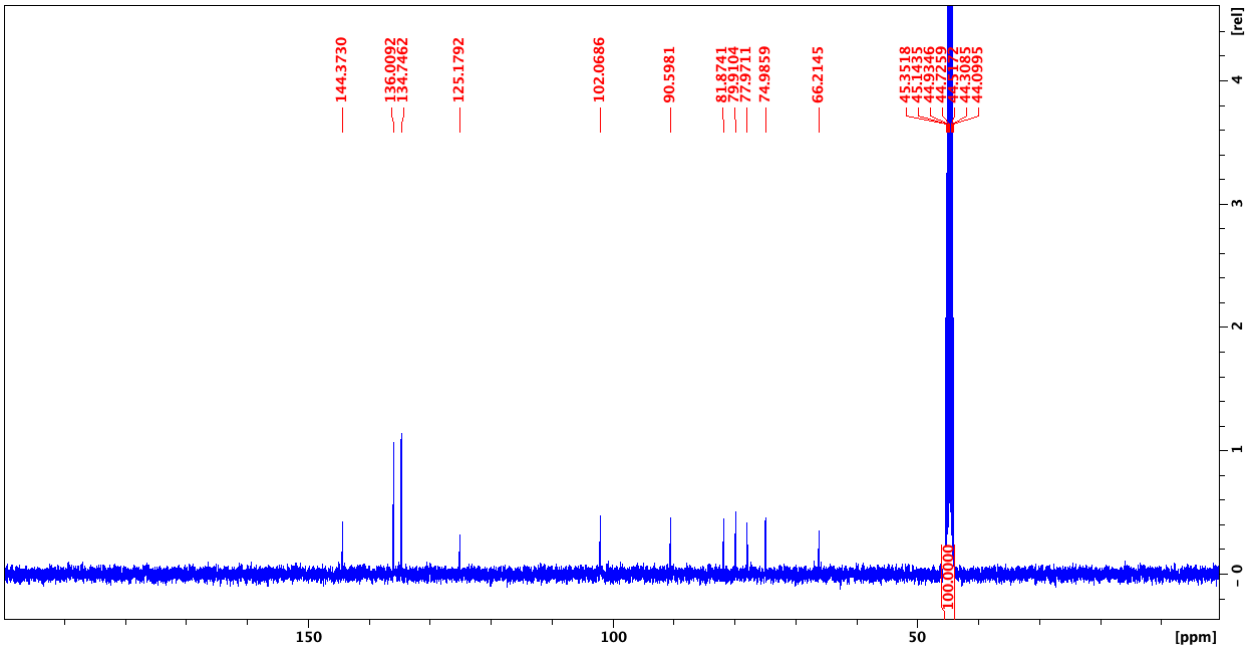

3-*O*-*para*-Bromobenzyl-D-glucopyranoside (**408**)

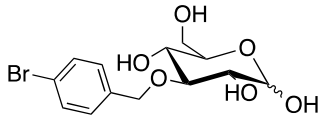

408

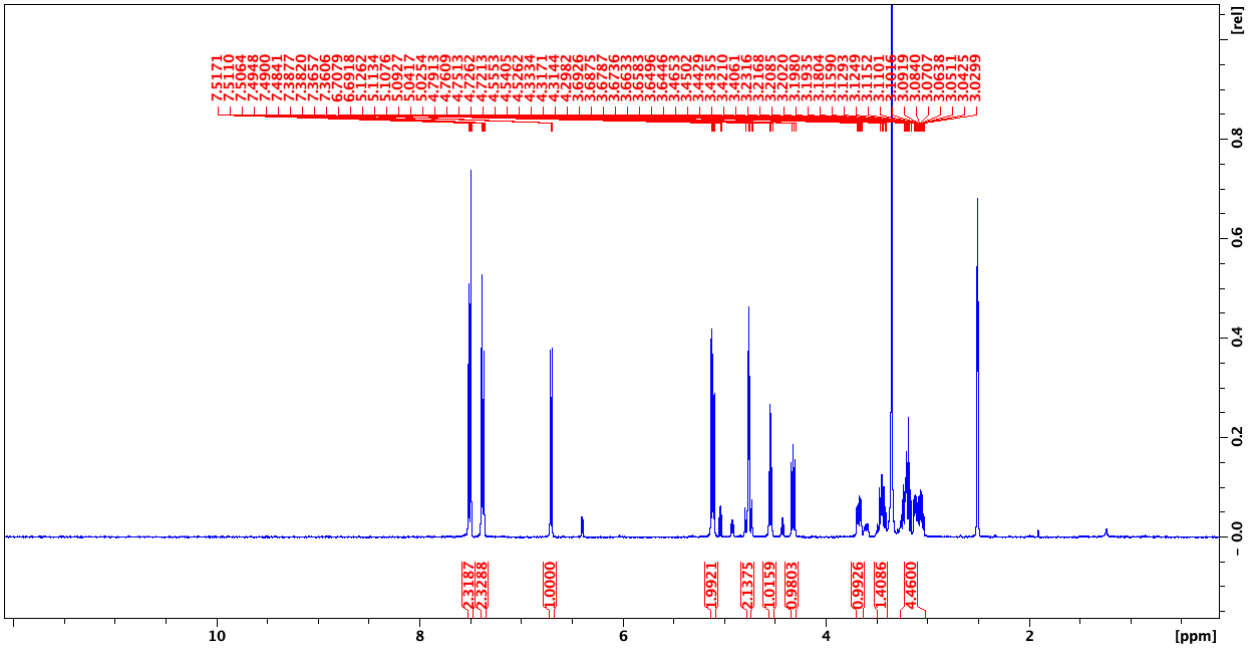

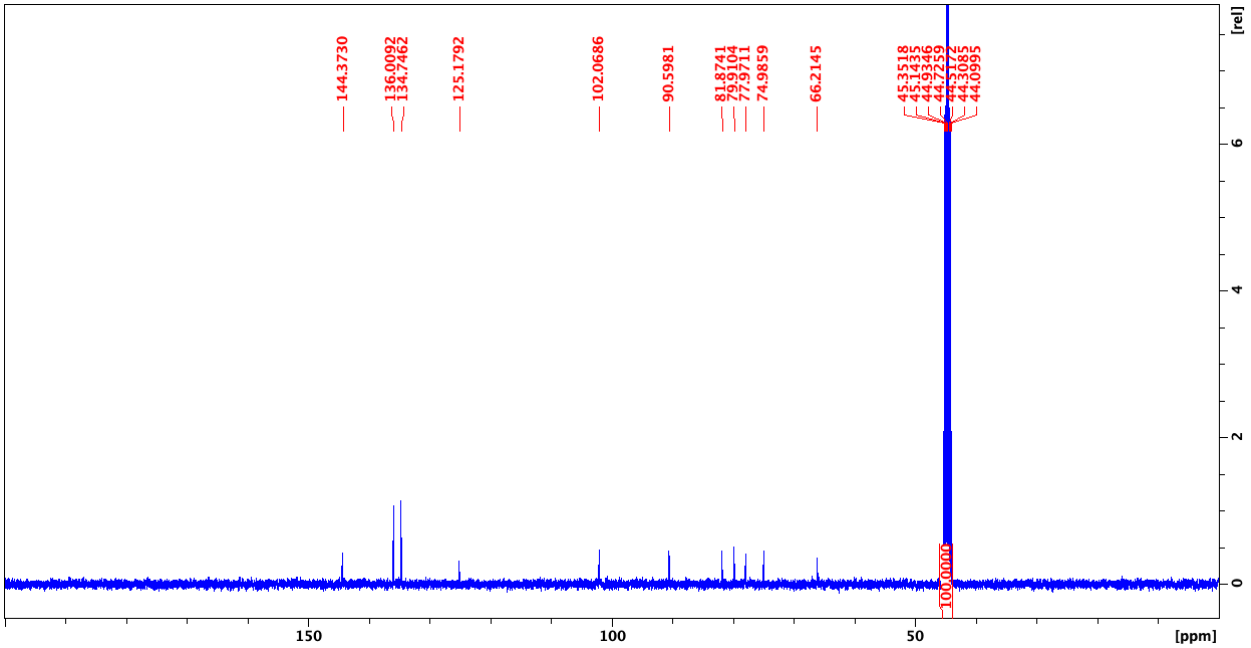

3-*O*-*para*-Fluorobenzyl-D-glucopyranoside (**409**)

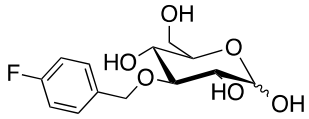

409

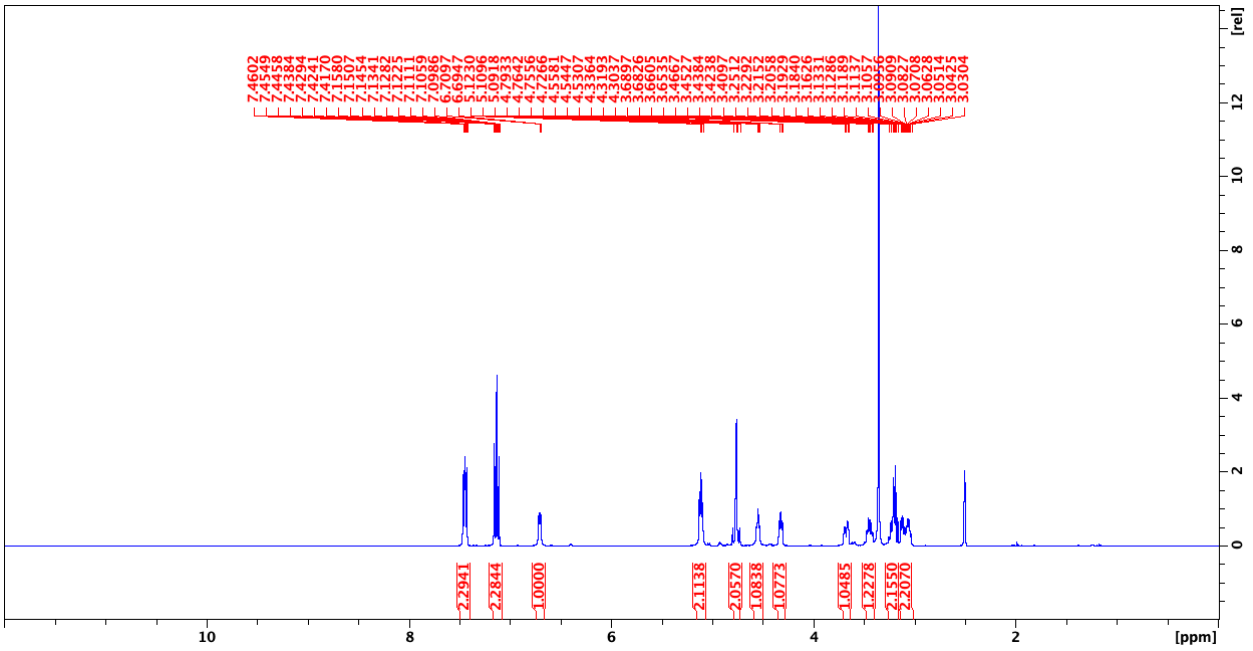

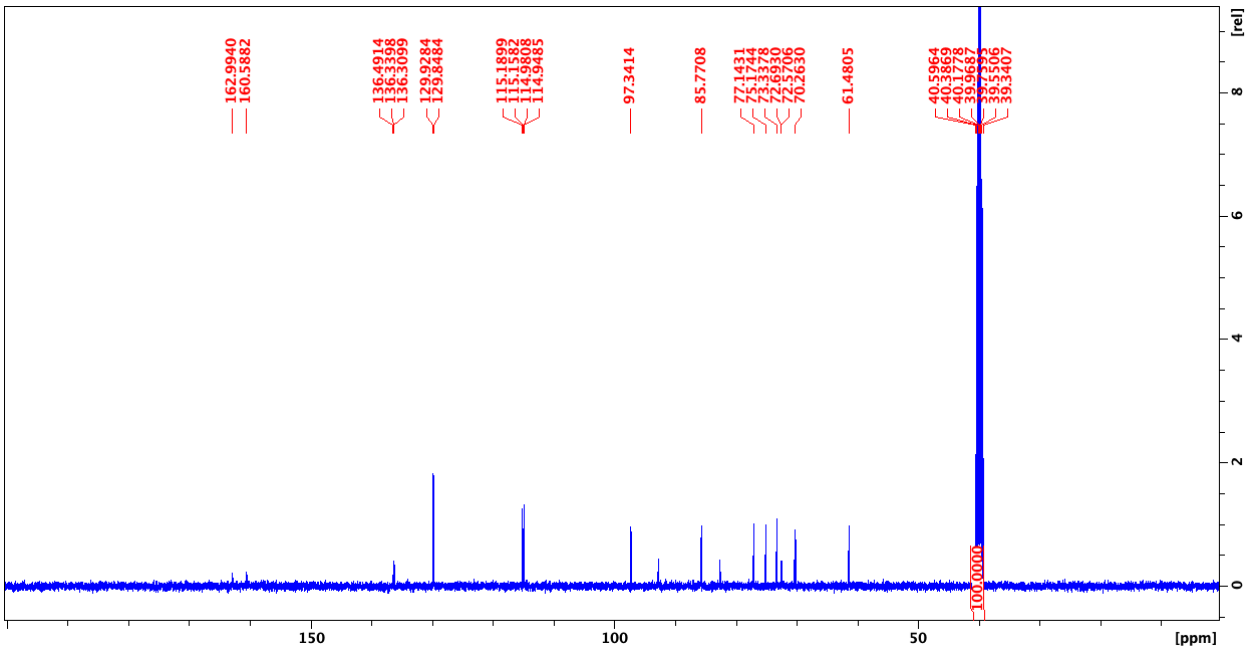

3-*O*-Allyl-D-glucopyranoside (**410**)

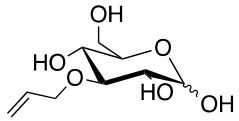

410

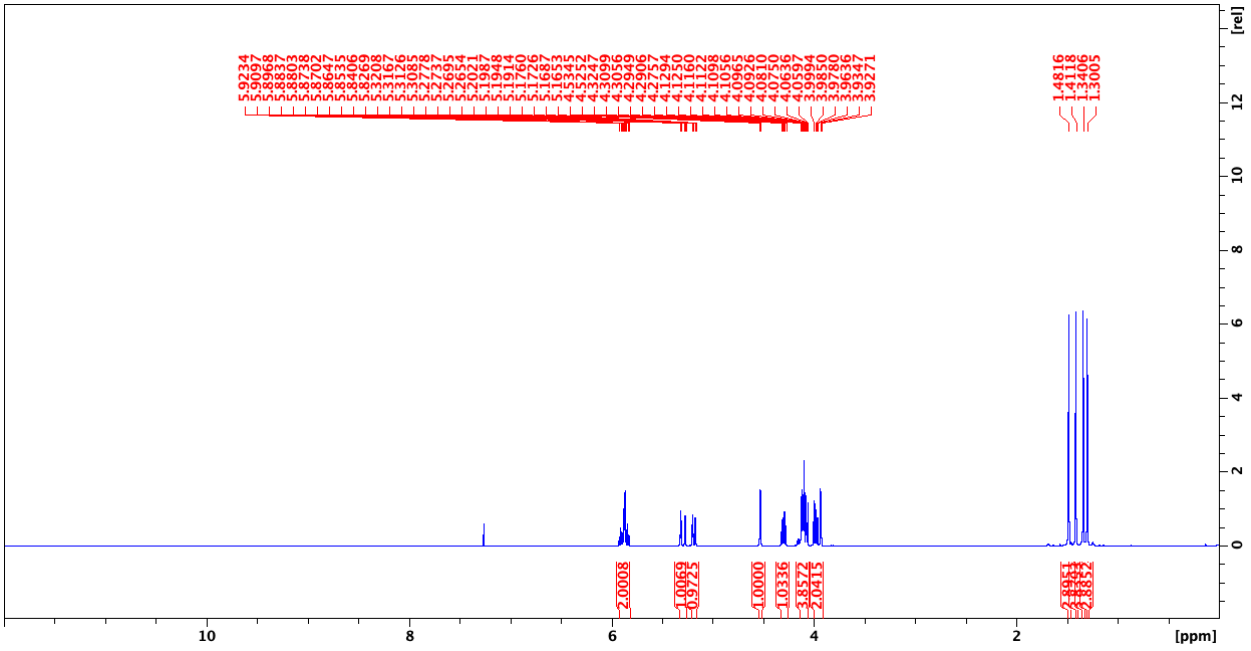

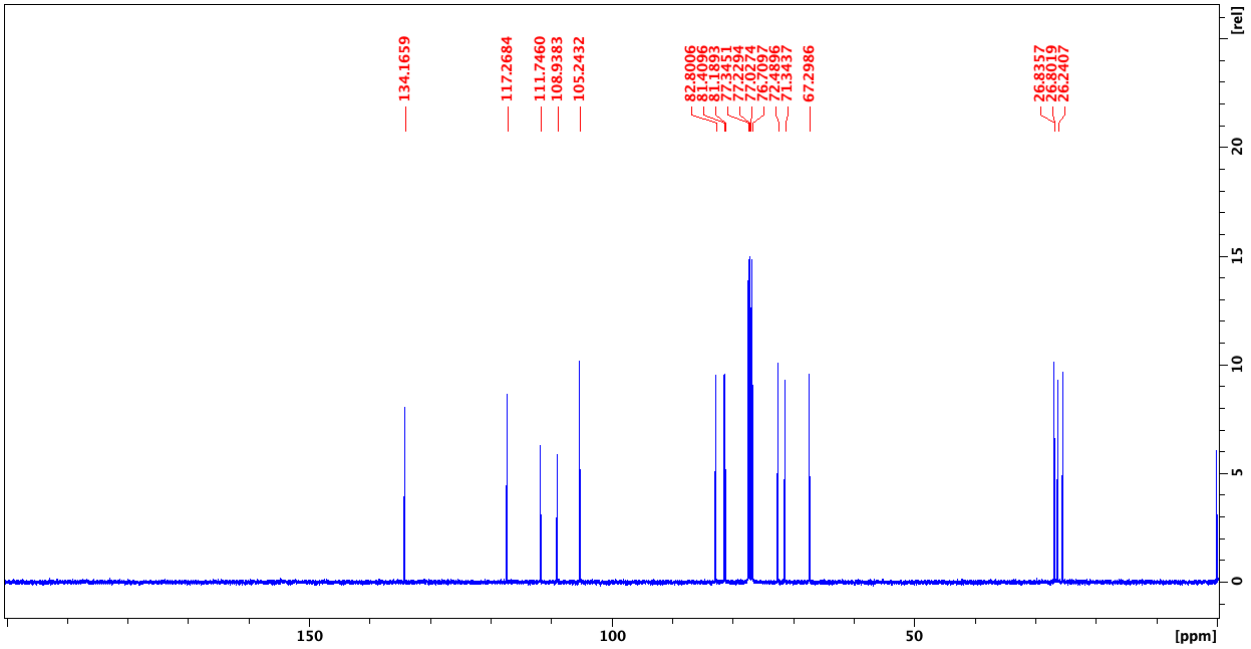

Benzyl -2,3,4,6-tetra-*O*-acetyl-β-D-glucopyranoside (**412**)

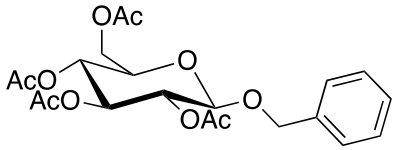

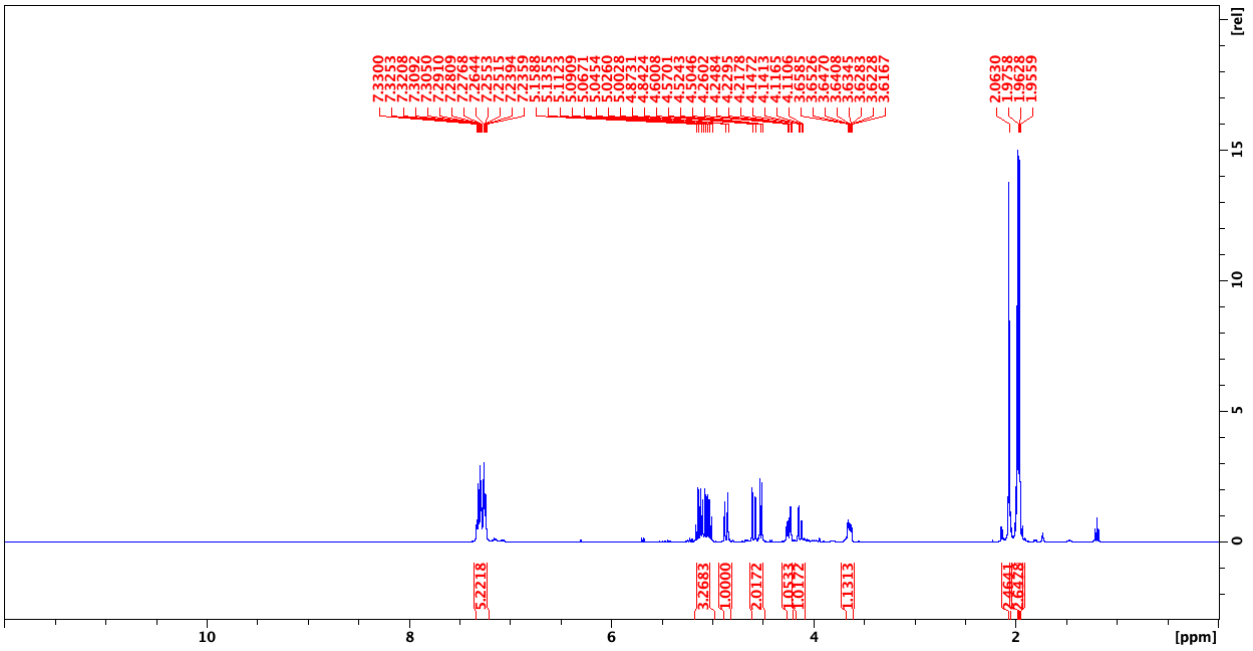

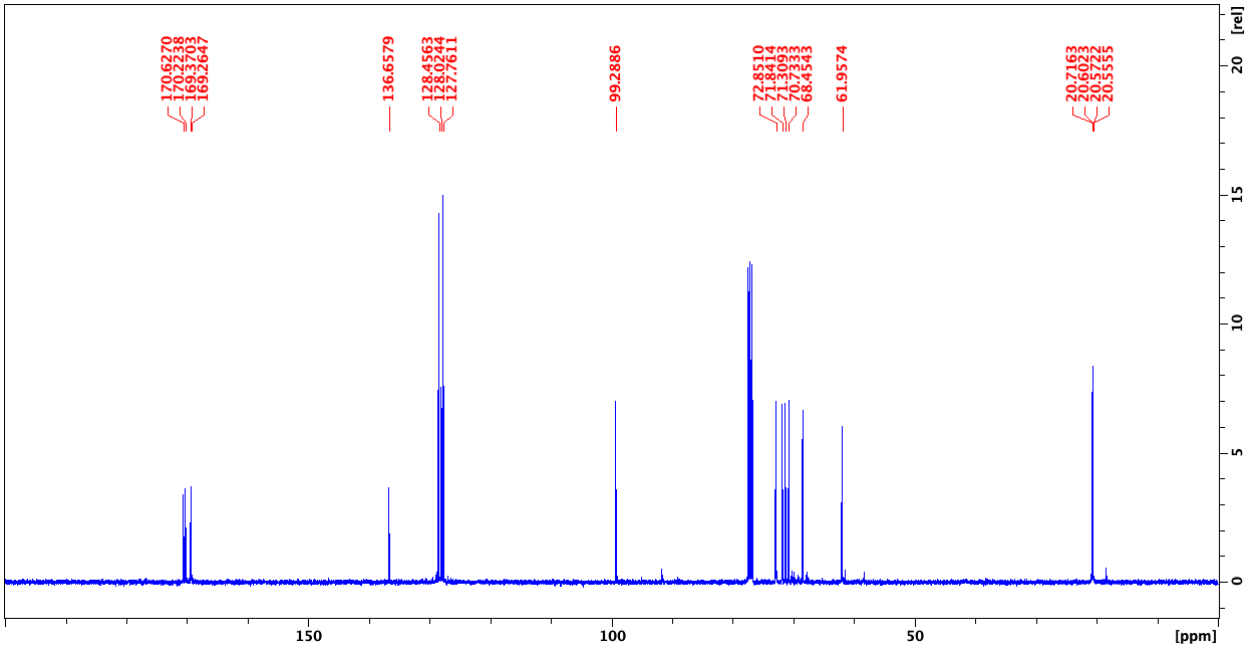

4-Bromobenzyl-2,3,4,6-tetra-*O*-acetyl-β-D-glucopyranoside (**413**)

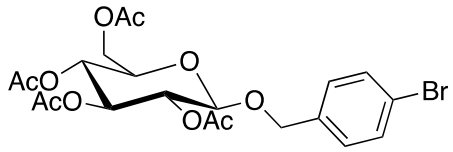

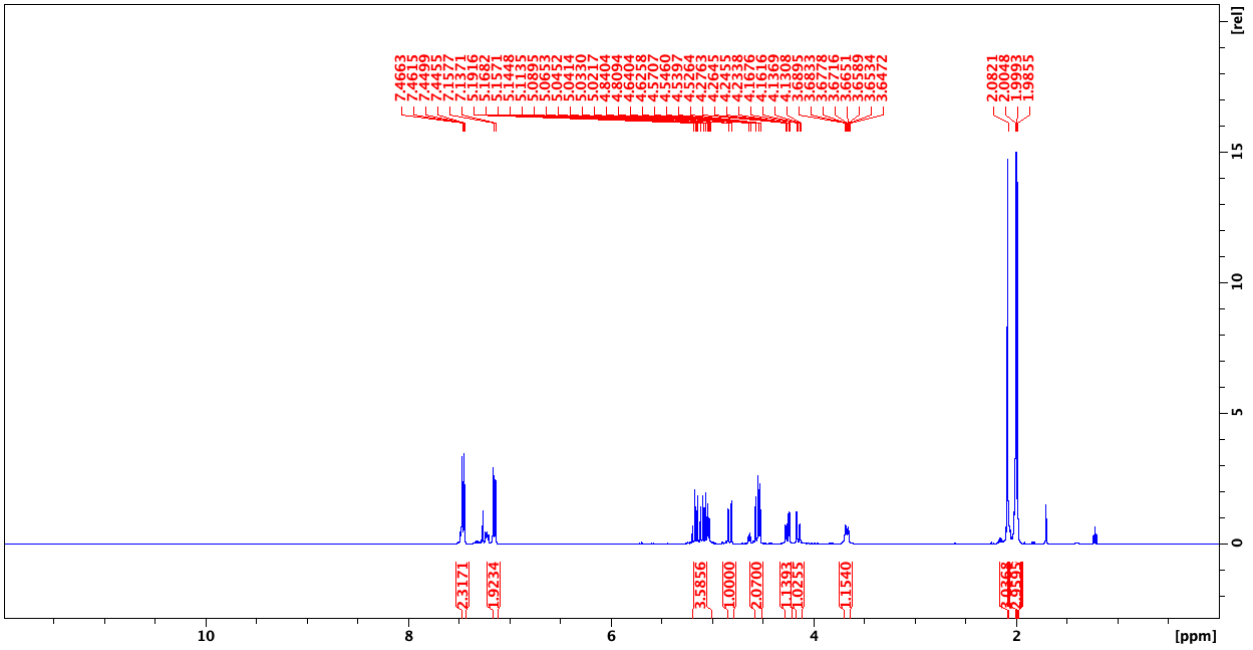

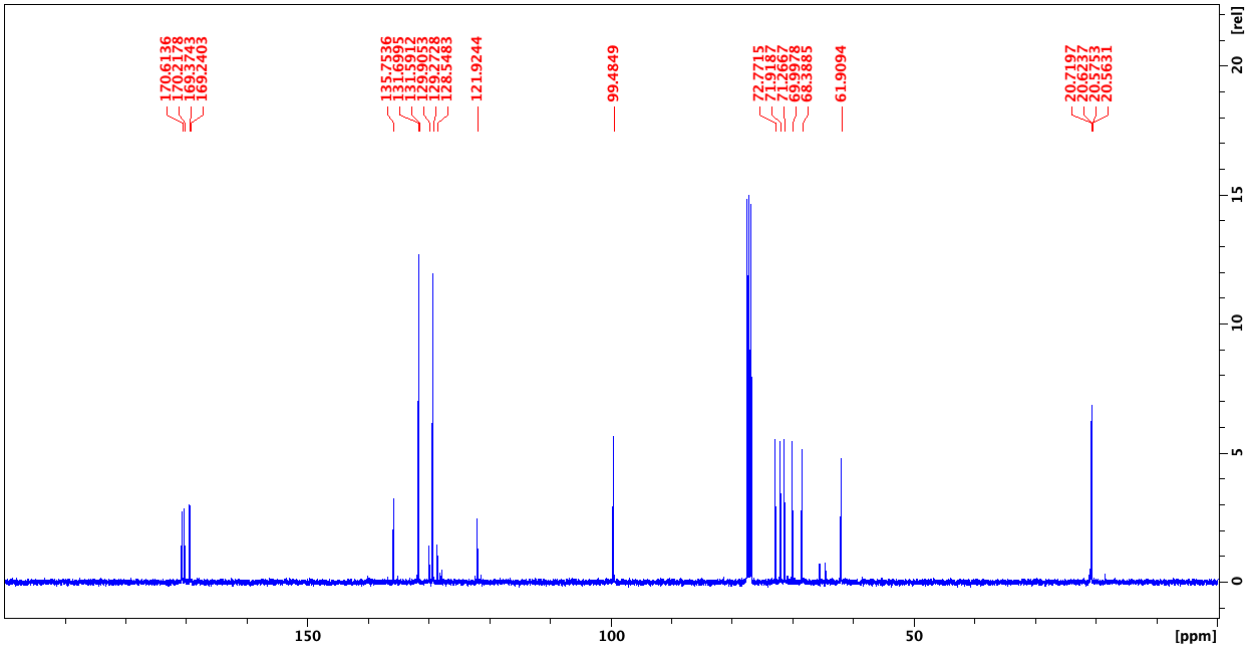

Allyl-2,3,4,6-tetra-O-acetyl-β-D-glucopyranoside (**414**)

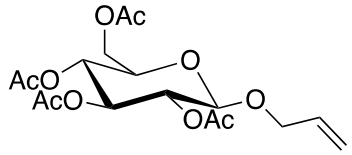

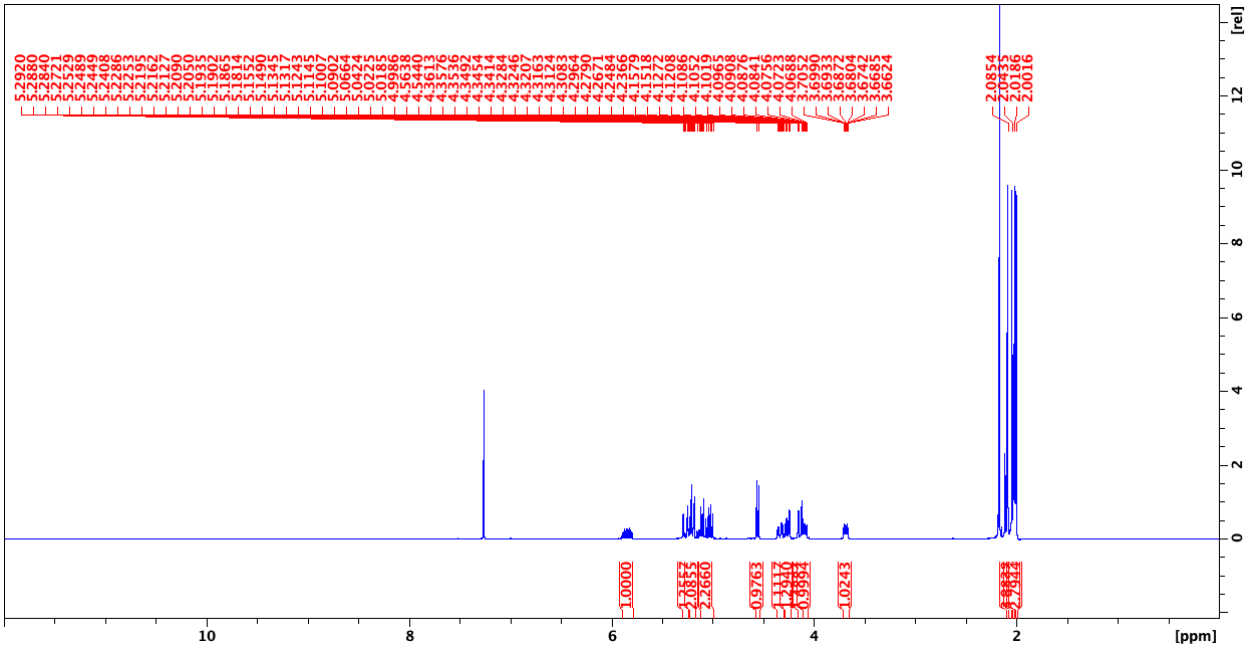

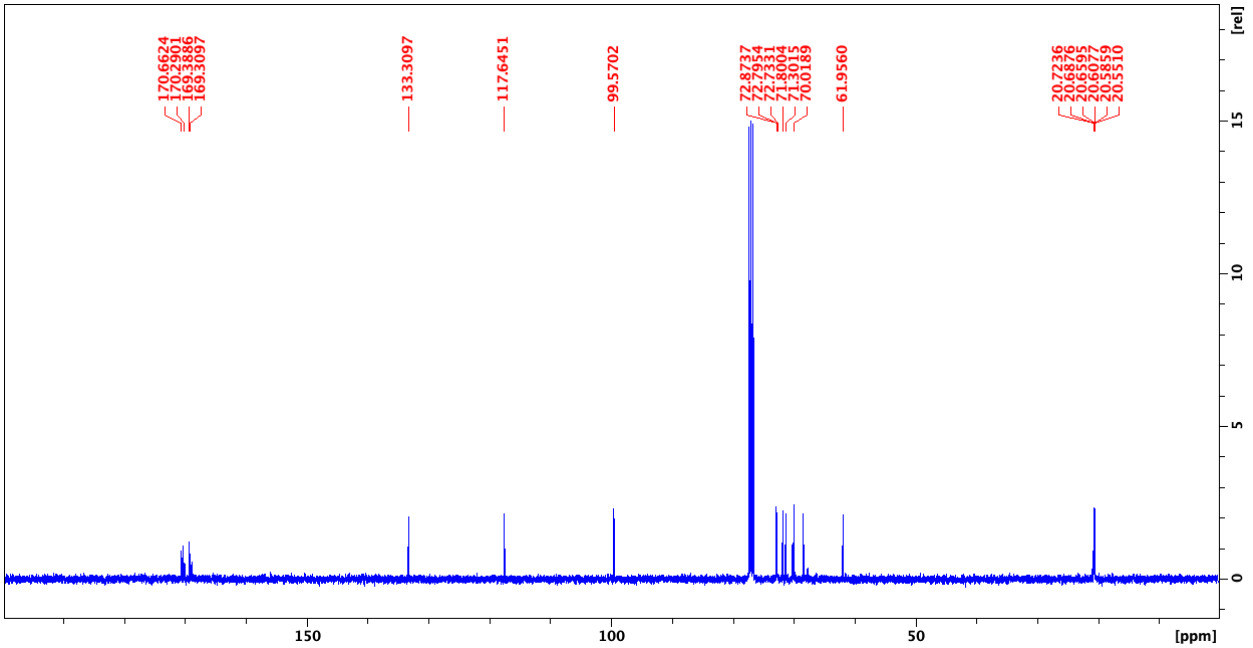

Benzyl-β-D-glucopyranoside (**415**)

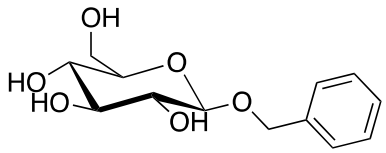

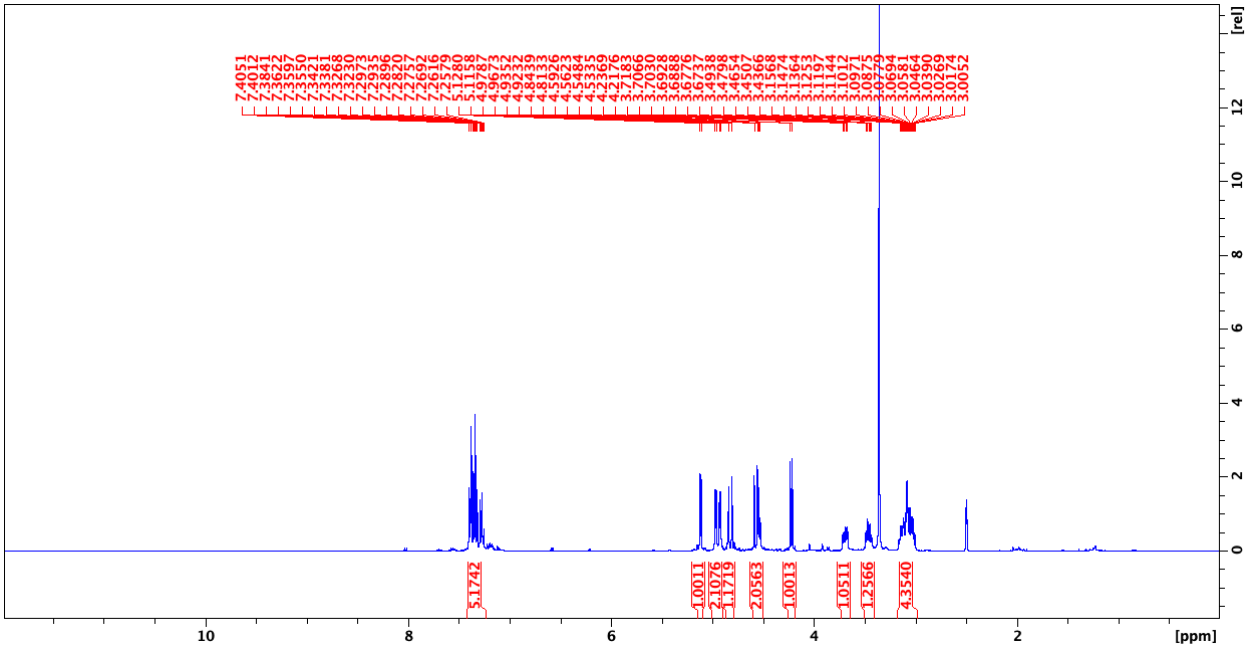

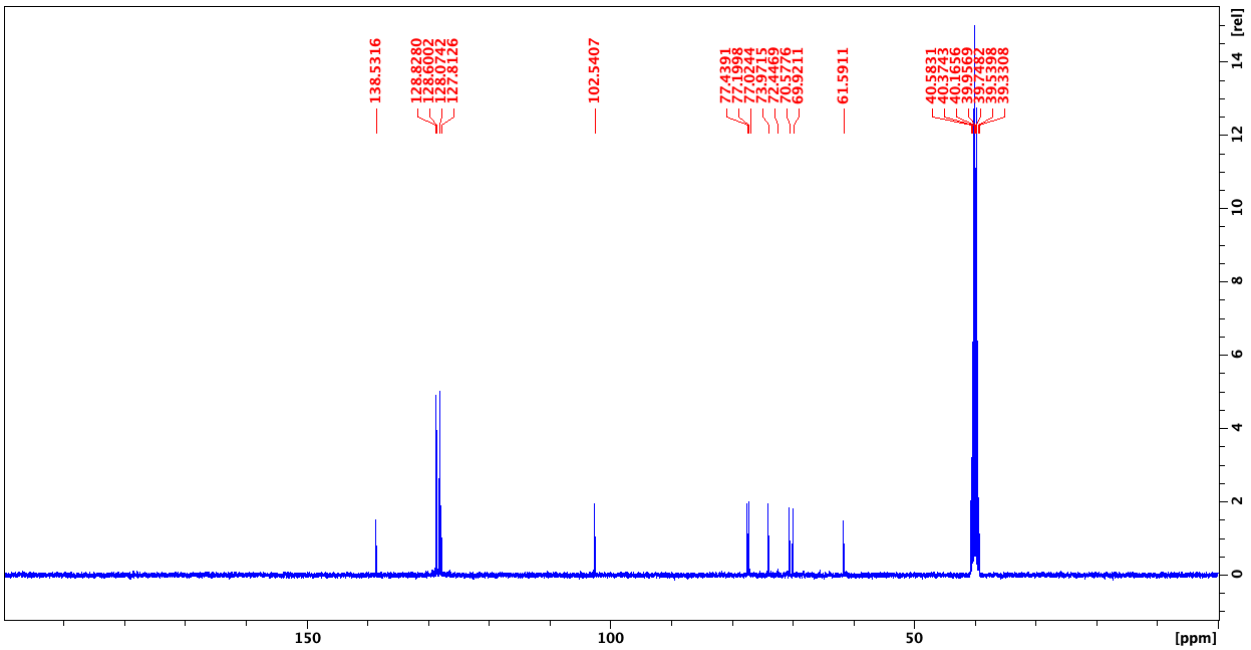

(4-Bromophenyl)methyl-β-D-glucopyranoside (**416**)

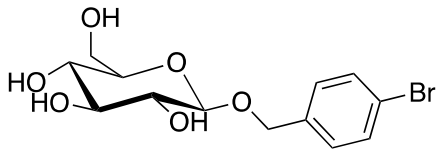

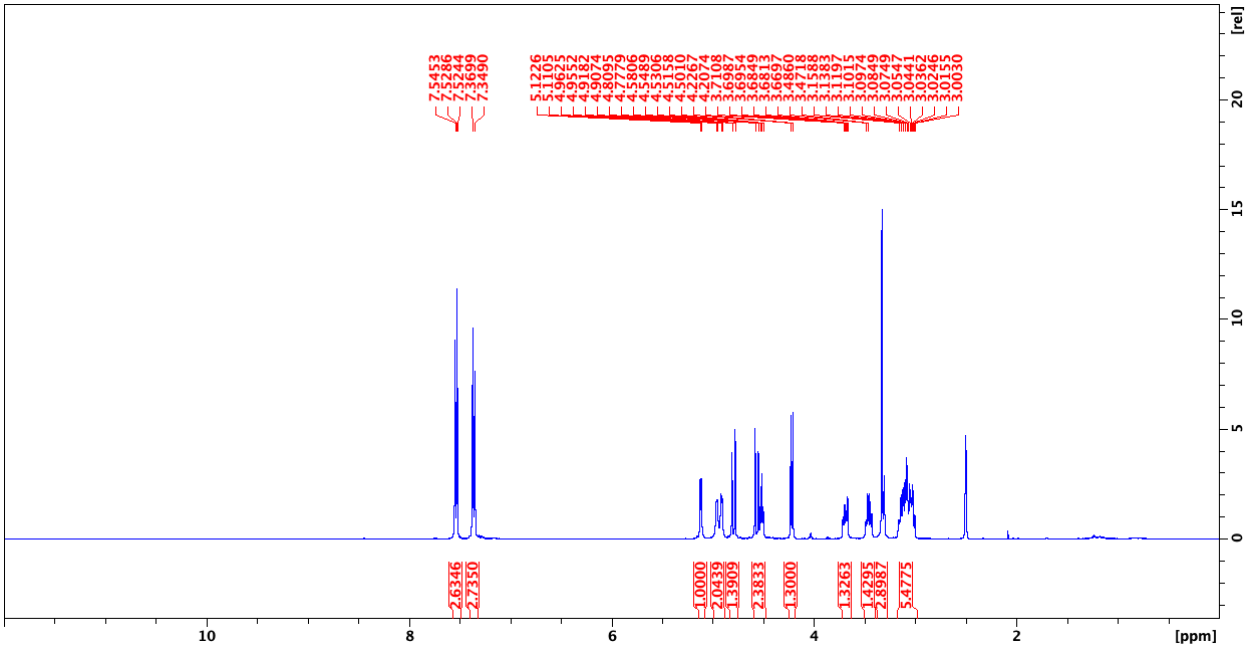

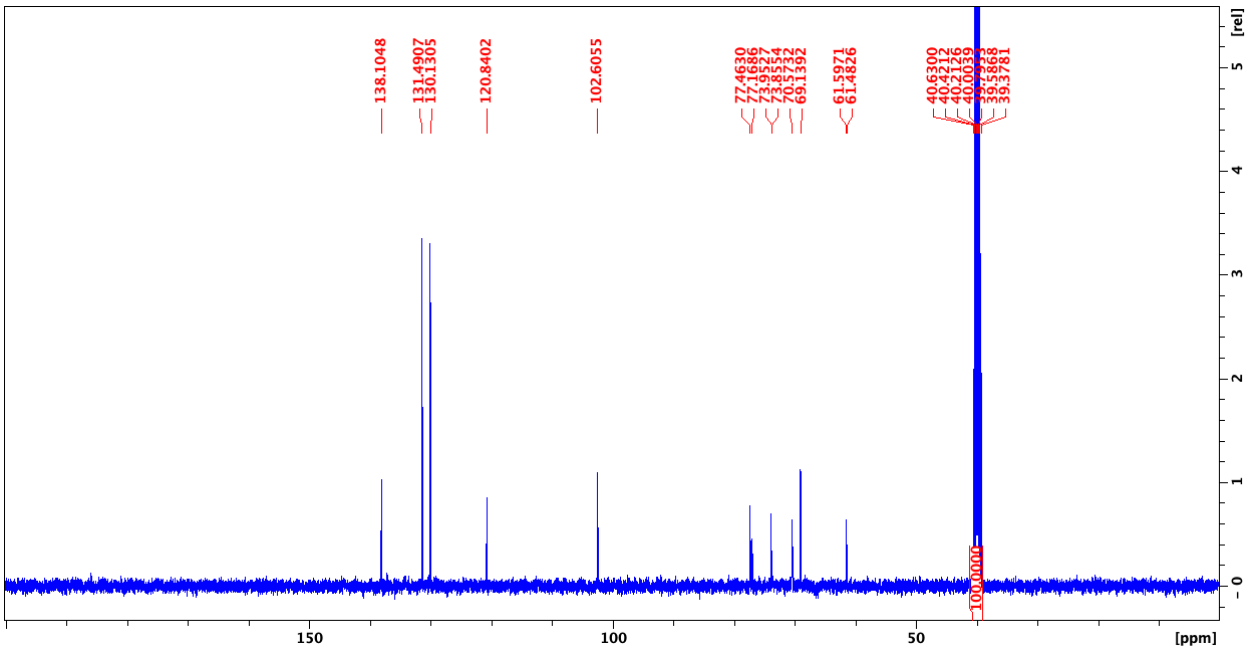

Allyl-β-D-glucopyranoside (**417**)

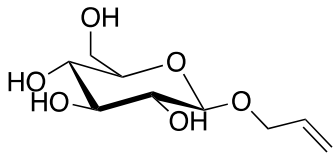

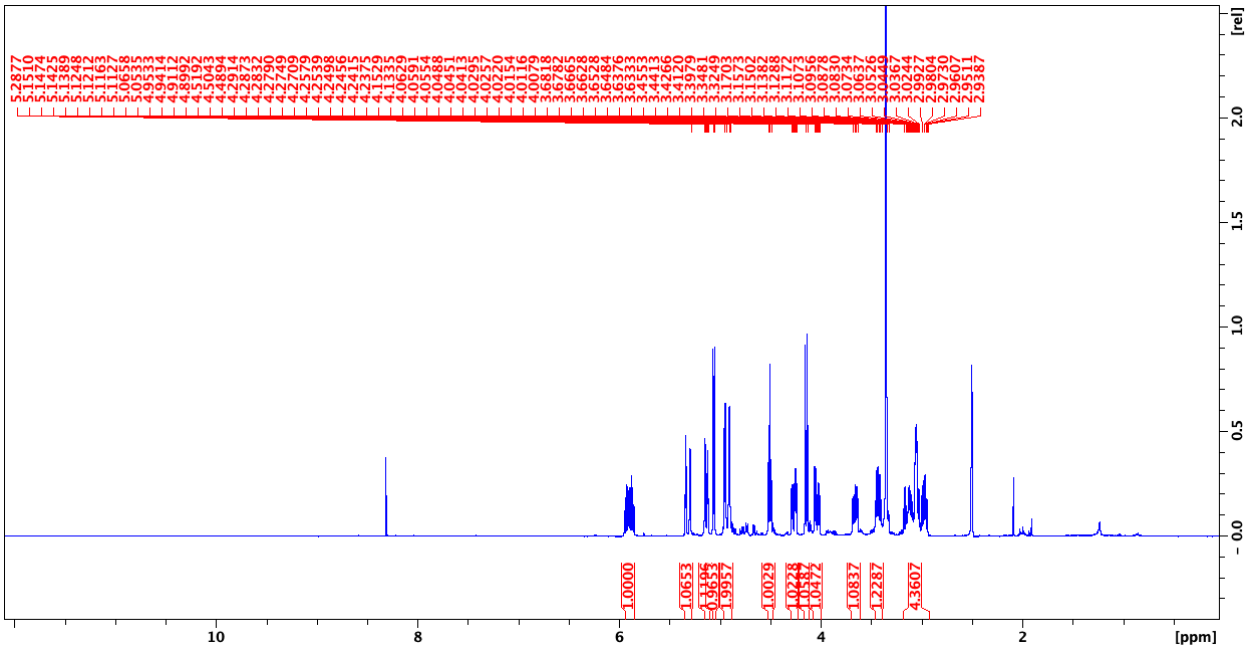

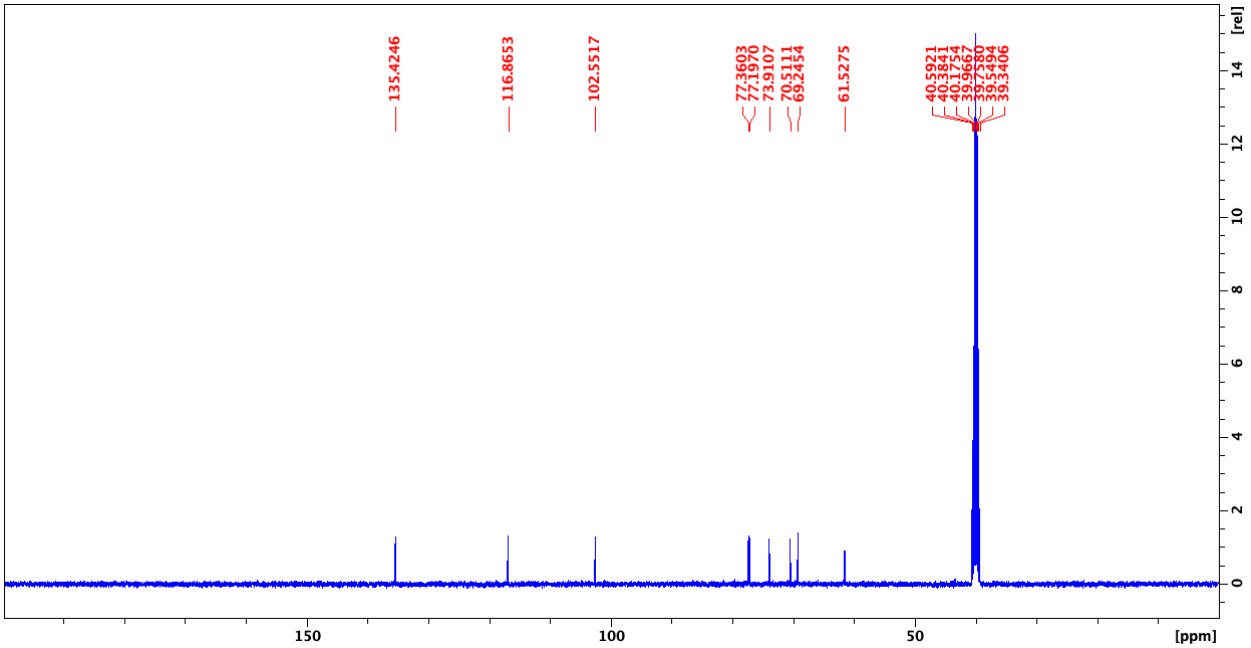

4.3 References

(1) Abraham, S.; Keillor, K.; Capicciotti, C. J.; Perley-Robertson, G. E.; Keillor, J. W.; Ben, R. N. Quantitative Analysis of the Efficacy and Potency of Novel Small Molecule Ice Recrystallization Inhibitors. *Crystal Growth and Design* **2015**, *15* (10), 5034–5039. https://doi.org/10.1021/acs.cgd.5b00995.

(2) Schneider, C. A.; Rasband, W. S.; Eliceiri, K. W. NIH Image to ImageJ: 25 Years of Image Analysis. *Nature Methods* **2012**, *9* (7), 671–675. https://doi.org/10.1038/nmeth.2089.

(3) Swift, M. L. GraphPad Prism, Data Analysis, and Scientific Graphing. *Journal of Chemical Information and Computer Sciences* **1997**, *37* (2), 411–412. https://doi.org/10.1021/ci960402j.

(4) Christensen, S. M.; Hansen, H. F.; Koch, T. Molar-Scale Synthesis of 1,2:5,6-Di- O -Isopropylidene-α- d -Allofuranose: DMSO Oxidation of 1,2:5,6-Di- O -Isopropylidene-α- d -Glucofuranose and Subsequent Sodium Borohydride Reduction. *Organic Process Research & Development* **2004**, *8* (5), 777–780. https://doi.org/10.1021/op049903t.

(5) Yang, H. J. Nonfluorous, Highly CO_2-Soluble Chelating Ligands for ScCO 2 Metal Ion Extraction. *Chemistry Letters* **2006**, *35* (9), 1000–1001. https://doi.org/10.1246/cl.2006.1000.

(6) Takeo, K.; Kitamura, S.; Murata, Y. Synthesis of Nigero-Oligosaccharides. *Carbohydrate Research* **1992**, *224* (C), 111–122. https://doi.org/10.1016/0008-6215(92)84098-D.

(7) Deffieux, D.; Natangelo, A.; Malik, G.; Pouységu, L.; Charris, J.; Quideau, S. First and Biomimetic Total Synthesis of a Member of the C-Glucosidic Subclass of Ellagitannins, 5-O-Desgalloylepipunicacortein A. *Chem. Commun.* **2011**, *47* (5), 1628–1630. https://doi.org/10.1039/C0CC04007J.

(8) Mende, M.; Nieger, M.; Bräse, S. Chemical Synthesis of Modified Hyaluronic Acid Disaccharides. *Chemistry - A European Journal* **2017**, *23* (50), 12283–12296. https://doi.org/10.1002/chem.201701238.